TROPHIC INTERACTIONS OF HYDROMEDUSAE ACROSS MUTIPLE SPATIAL SCALES

by

MARCO VINICIO CORRALES UGALDE

A DISSERTATION

Presented to the Department of Biology
and the Division of Graduate Studies of the University of
Oregon in partial fulfillment of the requirements for the
degree of
Doctor of Philosophy

March 2022

DISSERTATION APPROVAL PAGE

Student: Marco Vinicio Corrales Ugalde

Title: Trophic Interactions of Hydromedusae Across Multiple Spatial Scales

This dissertation has been accepted and approved in partial fulfillment of the requirements for the Doctor of Philosophy degree in the Department of Biology by:

Lauren Hallett	Chairperson
Kelly R. Sutherland	Advisor
Gregory P. Gerbi	Core Member
Alan Shanks	Core Member
David Sutherland	Institutional Representative

and

Krista Chronister	Vice Provost for Graduate Studies

Original approval signatures are on file with the University of Oregon Division of Graduate Studies.

Degree awarded March 2022

DISSERTATION ABSTRACT

Marco Vinicio Corrales Ugalde

Doctor of Philosophy

Department of Biology

March 2022

Title: Trophic interactions of hydromedusae across multiple spatial scales

Cnidarian medusae are predators that structure pelagic ecosystems. Studies on their predatory impact have focused on big cruising scyphomedusae even though hydrozoans represent 60% of all medusan diversity and prey upon a wide range of taxa. It is unclear how hydromedusan feeding behavior relates to their effects on marine food webs. In this dissertation, I present three studies to illustrate how traits of planktonic predators determine food-web level processes. In Chapter II I determined how passive (sinking) and active (swimming) feeding behavior affects pre-encounter responses of prey to the medusae-induced fluid motion. I showed how passive prey were ingested during both feeding behaviors, whereas flow-sensing prey such as copepods escaped the predator's active feeding behavior but were unable to detect the predator's passive sinking behavior and were ingested. Fluid deformation values during passive feeding were below the values that trigger escape responses of copepods.

I explored in Chapter III how the environment mediates trophic interactions through effects on hydromedusan feeding behavior. I quantified in situ turbulent kinetic energy and hydromedusan tentacle length and bell pulsation frequency at two sites in Friday Harbor, Washington: a nearshore site protected from the channel flow and the Friday Harbor Marina, influenced by channel flow. The

protected site presented a shorter range of turbulence compared to the marina. Hydromedusan tentacle length was larger in the protected site and tentacle length was larger in turbulence from 1-5 cm2 s-3, but at higher turbulence tentacle length decreased.

In Chapter IV I collected mesozooplankton from five stations along two cross-shelf transects in the Northern California Current during winter and summer of 2018-2019 to determine prey resource use by hydromedusae and determine temporal shifts in their trophic niche. Hydromedusae fed mostly on copepods, appendicularians, and invertebrate larvae, but their diets showed seasonal shifts in prey resource driven by the abundant species *Clytia gregaria*, which fed mostly on copepod eggs during winter and fed mostly on appendicularians and copepods during summer. Prey selectivity for copepod eggs increased during winter for *C. gregaria* and *Eutonina indicans*.

This dissertation includes both previously published and unpublished coauthored material.

CURRICULUM VITAE

NAME OF AUTHOR: Marco Vinicio Corrales Ugalde

GRADUATE AND UNDERGRADUATE SCHOOLS ATTENDED:

University of Oregon, Eugene, Oregon
Universidad de Costa Rica, San José, Costa Rica

DEGREES AWARDED:

Doctor of Philosophy, Biology, 2022, University of Oregon
Master's in Biology, 2016, University of Oregon
Bachelor of Biology, 2012, Universidad de Costa Rica

AREAS OF SPECIAL INTEREST:

Biological Oceanography
Behavioral Ecology

PROFESSIONAL EXPERIENCE:

Graduate Employee, Department of Biology, University of Oregon, Eugene
September 2014 – March 2022

Research consultant, Fundación Keto, San José, Costa Rica
2012, 2018-2019

Research assistant, Centro de Investigación en Ciencias del Mar y Limnología, Universidad de Costa Rica, San José, Costa Rica
2017-2014

Teaching assistant, Escuela de Biología, Universidad de Costa Rica, San José, Costa Rica
2012-2014

GRANTS, AWARDS, AND HONORS:

FHL Graduate Research Award, University of Washington. 2021

Hill Fund Graduate Award, CAS, University of Oregon. 2019

FHL Graduate Research Award, University of Washington. 2019

Patricia L. Dudley fellowship. FHL University of Washington. 2015

Science Literacy Program Fellow, University of Oregon. 2015

PUBLICATIONS:

Morales-Ramírez, A., I. Till-Ponds, E.J. Alfaro, M. Corrales-Ugalde & C. Sheridan-Rodríguez .2021. Mesozooplankton responses to ocenographic conditions across different scales in Salinas Bay, Northern Pacific coast of Costa Rica during 2011-2013. *Revista de Biología Tropical.* 69(12):142-159

Corrales-Ugalde, M., S. Sponaugle, R.K Cowen & K.R. Sutherland. 2021. Seasonal hydromedusan feeding patterns in an Eastern Boundary Current show consistent predation on primary consumers. *Journal of Plankton Research*. 43(5):712-724

Corrales-Ugalde M. & K.R. Sutherland. 2021. Fluid mechanics of feeding determine the trophic niche of the hydromedusa *Clytia gregaria*. *Limnology and Oceanography.* 66(3):939-953

Zeman S.M., M. Corrales-Ugalde, R.D Brodeur & K.R. Sutherland. 2018. Trophic ecology of the neustonic cnidarian Velella velella in the northern California Current during an extensive bloom year: insights from gut contents and stable isotope analyses. *Marine Biology* 165:150

Morales-Ramírez A., M. Corrales-Ugalde, O.Esquivel-Garrote, Allan Carrillo-Baltodano, Karina Rodríguez-Saenz & Carolina Sheridan. 2018. Marine zooplankton studies in Costa Rica: a review and future perspectives. *Revista de Biología Tropical* 66(1) S24-S41.

Corrales-Ugalde M., I. Castellanos-Osorio & A. Morales- Ramírez. 2018. Dichotomous key for the identification of Appendicularians in the Eastern Tropical Pacific and Inter-American Seas, with a species list for Costa Rica. *Revista de Biología Tropical* 66(1) S108-S122.

Corrales-Ugalde M. & Alvaro Morales-Ramírez. 2017. New record of *Stellamedusa ventana* Raskoff & Matsumoto, 2004 in the Eastern Tropical Pacific. *Marine Biodiversity*. doi 10.1007/s12526-017-0781-5

Corrales-Ugalde M., A.J. Quesada, B. Naranjo-Elizondo & J. Cortés. 2017. New records of gelatinous zooplankton from an oceanic

island in the Eastern Tropical Pacific. *Journal of the Marine Biological Association of the United Kingdom*. doi:10.1017/S0025315417000558

Corrales-Ugalde M., S.P. Colin & K.R. Sutherland. 2017. Nematocyst distribution corresponds to prey capture location in hydromedusae with different predation modes. *Marine Ecology Progress Series.* 568: 101-110

Azofeifa-Solano J.C., M. Corrales-Ugalde, I. Castellanos-Osorio & A. Morales-Ramírez. 2016. Euphausiids (Crustacea: Euphausiacea) from a hotspot of marine biodiversity, Isla del Coco, Costa Rica, Eastern Tropical Pacific. *Revista de Biología Tropical. 64(1): 221-230*

Corrales-Ugalde M. & J. Sibaja-Cordero. 2015. Benthic macrofauna found in sandy beaches from Osa Conservation Area, Puntarenas, southern Pacific coast of Costa Rica. *Revista de Biología Tropical. 63(1): 273-285*

Angulo A., B. Naranjo-Elizondo, M. Corrales-Ugalde & J. Cortés.2014. First record of the genus *Paracaristius* (Perciformes: Caristiidae) from the Pacific of Central America, with comments on their association with the siphonophore *Praya reticulata* (Siphonophorae: Prayidae). *Marine Biodiversity Records* 7(132):1–6.

Morales-Ramírez A., E. Suárez-Morales, M. Corrales-Ugalde & O.E. Garrote. 2014. Diversity of the free-living marine and freshwater Copepoda (Crustacea) in Costa Rica: a review. In: Wehrtmann IS, Bauer RT (Eds) Proceedings of the Summer Meeting of the Crustacean Society and the Latin American Association of Carcinology, July Costa Rica, 2013. *ZooKeys* 457: 15–33.

Castellanos-Osorio, I., R. Hernández-Flores, A. Morales-Ramírez & M. Corrales-Ugalde.2012. Appendicularias (Urochordata) and Chaetognaths (Chaetognatha) of Isla del Coco National Park, Costa Rica. *Revista de Biología Tropical.* 60(3): 243-255.

ACKNOWLEDGEMENTS

"*We all need each other to save ourselves.*
We are not what we are, solitary and alone,
the blood is complete only with another blood
and love, struggle, and hope
are complete with another love, another struggle, another hope."- jorge debravo

It is hard to describe in a couple of pages all the events necessary for a person to complete a work like this. All the interactions with all the people I've known have contributed, one way or another, in my choice to pursue this line of work. Thus, my sincere gratitude goes to whoever I have crossed paths with.

It is necessary to highlight here the most defining aspects and people of my life. First, my higher education in Biology was only possible thanks to the social democratic system of my country of origin, Costa Rica, that for almost a century has heavily invested in accessible education. Together with this, my parents, Marco Corrales Montero and Giselle Ugalde Sanchez, through a lot of sacrifice and hard work, provided the perfect environment for my sister and I to learn about the joy of knowledge and work, and allowed us to freely choose our life paths. I also want to thank Amanda, my sister, since as kids were able to appreciate the delights (and pains) of the natural world. I still remember the time she got stung by a *Pelagia noctiluca* as a kid.

During my undergraduate studies in Costa Rica I met professors and friends that, to this day, serve as mentors and role models. I want to thank Eddy Gomez, Jeffrey Sibaja, Jenaro Acuña, Jorge Cortés and my undergraduate advisor, Álvaro Morales, for providing the material and intellectual support to study oceanography and marine zooplankton ecology. My gratitude goes also to my friends Allan Carrillo, Viktoria Bogantes, Andrés Quesada, Aldo Farah, Beatriz Naranjo and Juan Carlos

Azofeifa for providing so many great advice and moral support. To this day I continue to learn much from them about life and science.

Once I arrived at the United States, I was lucky to meet many people that made me feel welcome and made grad school life fun, with lots of adventures and friendship: Sam Zeman, Keats Conley, Kyle Meyer, Felipe Campos-Cerda, Dan Thomas, Dan Sulak, Dustin Carroll, Dylan Colon, Teresa Findlay, Brooke Hunter, Eli Orland, Suzanne Perdew, Bill Dassenko, Logan Ogden, Jessica Masterman and Joanna Lyle. Some of the people that I met in grad school are also responsible for keeping my sanity throughout this process: Hilarie Sorensen, Aliza Karim, Reyn Yoshioka and Maria Jose Marín Jarrín (aka the Niskin Bottle), thank you for tolerating me all of these years. I also want to highlight the insightful feedback and valuable help that Maria Jose, Reyn, Jessica and Joanna provided throughout the research process of my dissertation.

During my time in the PhD program, I was fortunate to work and teach with incredibly smart biologists and ecologists that had a strong influence in the process of my research: Peter Wetherwax, Laurel Pfeifer-Meister and Brendan Bohannan I want to highlight the excellent work that my dissertation advisory committee did throughout this process. They were able to overlook my innate tendency to chaos in the first stages of my dissertation and provided great guidance throughout this process. My thanks to Allan Shanks, Gregory Gerbi and David Sutherland for helping to solidify my knowledge in oceanography. The help provided by researchers from other institutions was also key for the completion of this dissertation: Robert K. Cowen, Su Sponaugle, Taylor Eaton and Kevin Buch from Oregon State University and Pema Kitaeff from the University of Washington

But the most fortunate aspect of my dissertation is that I had Dr. Kelly R. Sutherland as my advisor. Beyond the countless things that she taught me, I learned with her that (real) professionalism is intrinsically linked to kindness, order, respect, generosity, and love to the work we do. Under her guidance I became the type of scientist that I always wanted to be.

And finally, I want to thank my wife Karla Conejo Barboza. Since we met during our years as biology students, I was captivated by the joy and love she feels when we studied the countless life forms that live on this planet. Without the support she provided me, this dissertation would not be possible. The path that we have built together is stronger than all the distance that kept us apart for so many years, and that same path gives me the strength to see the future not with fear, but with hope.

"Donde yo encuentro poesía mayor es en los libros de ciencia, en la vida del mundo, en el orden del mundo, en el fondo del mar, en la verdad y música del árbol, y su fuerza y amores, en lo alto del cielo, con sus familias de estrellas, -y en la unidad del universo, que encierra tantas cosas diferentes, y es todo uno, y reposa en la luz de la noche del trabajo productivo del día. Es hermoso, asomarse a un colgadizo, y ver vivir al mundo: verlo nacer, crecer, cambiar, mejorar, y aprender en esa majestad continua el gusto de la verdad."-José Martí

To Karla. Your love fills my life with joy, and drives away fear.

TABLE OF CONTENTS

Chapter Page

LIST OF FIGURES

Figure Page

Figure Page

Chapter V

LIST OF TABLES

Table Page
Chapter IV

CHAPTER I

INTRODUCTION

Predator-prey interactions control to a large extent the amount of energy that flows through intermediate levels of the food web, from basal primary production to higher order consumers (Pimm, 1982). In addition, predation pressure can modify the structure of planktonic communities and food webs by consumption and competitive interactions (Ruzicka et al. 2012, 2016; Purcell 2018). However, it is challenging to decipher how the behavioral and morphological traits of predator and prey structure the functioning of marine food webs, given the differences in scales across organismal level processes (millimeters to centimeters) to population and community level processes (>100 meters, Prairie et al. 2012). This work seeks to determine how the feeding behavior, predator-prey dynamics, and environmental variables determine prey ingestion rates of planktonic tentaculate predators.

In marine ecosystems, tentaculate gelatinous predators are key components of planktonic food webs, acting as secondary consumers (Robinson et al. 2014) and as a food source for higher-order carnivores (Hays et al. 2018). Thus, it is crucial to understand the variables that modulate their trophic impact in marine ecosystems. Of the many gelatinous tentaculate predators in pelagic ecosystems, the trophic role of Cnidarian jellyfish has been extensively researched. There is substantial evidence that Cnidarian jellyfish populations have increased in some parts of the world (Purcell et al. 2007, Brotz et al. 2012, Condon et al. 2012), usually as the result of anthropogenic perturbations such as global warming (Richardson et al. 2009), eutrophication (Mills 1995, Tatsuki 2005), addition of hard substrates (Holst & Jarms 2007, Duarte et al.

2012), overfishing (Daskalov 2002, Parsons & Lalli 2002), and non-native species introductions (Santhakumari et al. 1997, Meek et al. 2013, Baumsteiger et al. 2017). Cnidarian medusae have diverse life history and life cycle strategies, including the alternation between sexual and asexual reproduction (Colins 2005). This allows them to exploit abundant but temporary food resources (Boero et al. 2008) and bloom in regions where either climatic or anthropogenic factors produce favorable conditions for their reproduction (Pagés et al. 1996, Purcell et al. 2007). These blooms, however, are hard to predict since they are not recurrent on regular spatial or temporal timescales (CIESM 2001, Kawahara et al. 2006, Miglietta et al. 2008). Moreover, even species-level population dynamics can vary greatly across small spatial and temporal scales (Lucas 2001, Pitt et al. 2004). Blooms can also substantially affect zooplankton community structure by reducing the standing stocks of their prey (Purcell 1989, Purcell & Grover 1990).

Population blooms by cnidarian medusae can be a relevant structuring factor of pelagic communities by affecting the mortality rates of potentially dominant species (Piraino et al. 2002, Hansson et al. 2005). For instance, medusae could reduce the abundance of herring and anchovy by feeding on their eggs and larvae (Purcell 1989, Purcell & Grover 1990, Zeman et al. 2016). In contrast to the extensive information regarding scyphomedusae predation (Graham & Kroutil 2001, Brodeur et al. 2008, D'Ambra et al. 2013, Zeman et al., 2016), the trophic roles of small hydromedusae are not well understood (Colin et al. 2005). More information is needed regarding the factors that structure their feeding impact and their trophic relevance in pelagic communities, since some hydrozoan species are invasive (Mills & Sommer 1995), can control the population

dynamics of primary consumers (Daan 1989) and can act both as grazers and predators (Colin et al. 2005, Morais et al. 2015, Morais et al. 2017).

Early studies on hydromedusan feeding mechanics established two feeding guilds based on the bell fineness ratio *F* (*bell height/bell diameter*, Costello et al. 2008). This metric classifies hydromedusae either as 1) "sit-and-wait" predators, which rely on prey motion to initiate encounters, feed mostly on microcrustaceans and have an $F > 1$. Other hydromedusae are classified as 2) current-feeding predators, which generate a feeding current with each bell pulsation that brings soft bodied planktonic organisms in contact with the feeding structures and have an $F< 1$ (Costello & Colin 2002). This diversity of hydromedusan feeding modes makes them an ideal study system for determining which behaviors are associated to higher prey ingestion rates, and their consequently higher trophic impact in marine food webs.

Ingestion rates of hydromedusae can be theoretically calculated from behavioral parameters of both predator and prey. One of them is the capture and ingestion efficiency of a specific prey type, which can be estimated through sequential steps of the predation process (Holling 1959). In current-feeding cnidarian hydromedusae, swimming and predation are coupled such that swimming also brings prey into contact with feeding structures (Acuña et al. 2011). Fluid mechanical disturbances may initiate escape responses by flow-sensing prey. In Chapter II, I considered how fluid signals define the trophic niche of current-feeding gelatinous predators. I used the hydromedusa *Clytia gregaria* to determine how passive (sinking) and active (swimming) feeding behavior affects pre-encounter responses of prey to the medusae-induced fluid motion, and how prey responses affect the medusae's ingestion efficiencies. Chapter II was published in the

journal *Limnology and Oceanography* (Corrales-Ugalde & Sutherland 2021) with coauthor Dr. Kelly R. Sutherland, who assisted with funding, writing, and served as the principal investigator.

Another crucial variable to determine ingestion rates based on predator and prey behavior is the capacity of said predator to "sample" for prey, referred to as the encounter kernel rate e (L h^{-1}) (Kiørboe 2008). In planktonic tentaculate predators such as hydromedusae, the magnitude of e is determined by the volume entrained by feeding currents (Katija et al. 2011) plus the volume occupied by the predator's capture surfaces (i.e. tentacles, oral lobes, oral arms) and the movement speed of predator and prey (Acuña et al. 2011), which can either be controlled by active swimming or passive drifting (Mills 1981). Environmental fluid motion in estuaries and tidal channels could have significant effects in predator-prey interactions due to their high values of turbulence compared to other marine ecosystems, which disrupt plankton behavioral patterns (Fuchs and Gerbi 2016). In Chapter III I explored how the heterogeneity in fluid disturbances (turbulence) in a tidal channel affects hydromedusan tentacle length and bell pulsation frequency (proxy to swimming speed). This chapter is unpublished but will include Jessica Masterman, who assisted with field work and experimental design, and Dr. Kelly R. Sutherland, who will assist with manuscript preparation, assisted with funding, and served as the principal investigator.

Another strategy to estimate ingestion rates at the ecosystem level is to quantify hydromedusan ingested prey and compare it to prey availability. Given the large diversity of hydromedusan life cycles (Collins 2002) some hydromedusan species are only present

in pelagic environments when resource availability is high, whereas others are present throughout the year, but their abundance increases during high productivity periods (Boero et al. 2008, Miglietta et al. 2008). It is likely that the capability to feed on a variety of food sources might explain the sustained prevalence of hydromedusae even when their main prey is absent (Morais et al. 2015) and thus show seasonal shifts in prey selectivity. In Chapter IV, I collected mesozooplankton from five stations along two cross-shelf transects in the Northern California Current (NCC) during winter and summer of 2018-2019. I analyzed gut contents of 11 hydromedusan species and described the prey community to determine prey resource use by hydromedusae and determine temporal shifts in the trophic niche of hydromedusae in this large marine ecosystem. Chapter IV was published in the *Journal of Plankton Research* (Corrales-Ugalde et al. 2021) with coauthors Dr. Su Sponaugle and Dr. Robert K. Cowen, who served as co-principal investigators in this project together with Dr. Kelly R. Sutherland. All coauthors contributed with funding and with final manuscript preparation. Chapters II and III contribute significantly to our understanding of the relevant behavioral, morphological, and environmental variables that determine predation impact of planktonic predators, which provide a mechanistic explanation to the observed prey selection and ingestion rates of hydromedusae documented in Chapter III.

CHAPTER II

FLUID MECHANICS OF FEEDING DETERMINE THE TROPHIC NICHE OF THE HYDROMEDUSA CLYTIA GREGARIA

From Corrales-Ugalde, M., and K. R. Sutherland. 2021. Fluid mechanics of feeding determine the trophic niche of the hydromedusa *Clytia gregaria*. Limnol. Oceanogr. 66(3):939-953. By permission of Wiley Periodicals LCC under license 5239540007271.

1. INTRODUCTION

Pathways of energy transfer in pelagic ecosystems, from basal primary production to high order carnivores, can only be understood if we consider the trophic interactions of the food web's intermediate levels. A large percentage of these intermediate trophic levels comprise predatory gelatinous zooplankton such as cnidarian medusae (Robison 2004). Defining the parameters that constrain prey resource use of gelatinous predators becomes crucial to understand energy flow through pelagic food webs. These predators do not actively search for prey, but instead rely on feeding currents and prey swimming patterns to capture food (Hansson and Kiørboe 2006; Katija et al. 2011).

Medusae produce vortices that originate at the bell margin with each bell contraction. These vortices entrain ambient fluid from outside the bell (Dabiri et al. 2005) and this entrained fluid brings prey into contact with the tentacles, which capture the prey (Ford et al. 1997). This feeding strategy is associated with high prey clearance rates (Acuña et al. 2011). However, current feeding scyphomedusae feed at low rates on highly abundant prey such as copepods (Suchman & Sullivan 2000). In

laboratory settings, schypomedusae ingest less than 1% of the copepods encountered (Suchman 2000). Avoidance of medusae by copepods is the result of their remarkable sensitivity to fluid deformation rates (Fields & Yen 1997; Buskey et al. 2002) which allows them to detect the predator's feeding current and respond by escaping (Costello and Colin 1994).

Despite predator detection and avoidance, several studies show that copepods are ingested by current-feeding medusae (Daan 1989, Purcell 1992, Ford et al. 1997, Suchman & Sullivan 1998). High ingestion efficiencies of flow-sensing prey are usually the result of predatory feeding behaviors that increase prey capture. For instance, the spatial and temporal complexity of medusae-induced fluid vortices can overwhelm copepods resulting in entrainment by large scyphomedusae feeding currents (Wagner et al. 2020). Other predators create feeding currents with high fluid deformation rates near prey-capture surfaces (Colin et al. 2010). Manipulation of fluid signals in space and time by gelatinous predators is therefore an important feature mediating capture of flow-sensing prey (Costello & Colin 1994).

Predation impact of cnidarian medusae has been inferred mostly from studies focused on large, conspicuous scyphomedusae (Purcell 1997), which do not represent the full array of medusan feeding strategies, and thus misrepresent the trophic role of smaller hydromedusae. Predation by hydromedusae alters the community structure of lower trophic levels (Matsakis & Conover 1991), since hydromedusae appear to selectively consume specific prey types (Madin 1988; Purcell & Mills 1988; Dabiri et al. 2010). This selective predation affects prey populations of holozooplankton and early life stages of invertebrates and fish (Larson 1987; Mills 2001). Previous research

has indicated the importance of fluid mechanics as a defining feature of hydromedusan trophic niches (Costello & Colin 2002; Song et al. 2014). Quantifying animal-fluid interactions of hydromedusae will provide a mechanistic understanding of how pulses in seasonal abundance (Mills 1995) among diverse species of hydromedusae shape pelagic food webs (Purcell 2017).

Two fundamentally distinct feeding strategies have been described for hydromedusae (Costello et al. 2008; Dabiri et al. 2010). "Sit-and-wait" Trachymedusae and Anthomedusae do not generate hydrodynamic disturbances when feeding; instead they rely on prey motion to initiate encounters. Current-feeding Leptomedusae entrain prey in the fluid vortices produced during each swimming cycle of bell contraction and relaxation. Prey are then brought into contact with the predator's feeding structures (Costello & Colin 2002). Gut content analyses on these hydromedusan species have shown that "sit and wait" predators are capable of capturing mechanosensitive prey, such as copepods, whereas current- feeding medusae consume mostly slow swimmers and passive prey, such as other gelatinous taxa and invertebrate eggs (Costello & Colin 2002).

Among coastal hydromedusae, the trophic role of the current feeder *Clytia* spp. has received limited attention despite its ample geographic distribution (Boero et al. 2008) and its seasonal dominance in coastal ecosystems (Mills 1981; Daan 1989; Lucas 1995; Suarez-Morales et al. 1999; Gravili et al. 2008). Its swimming behavior shifts periodically between sinking upside down with its tentacles relaxed, and then turning with asymmetric bell pulsations, to swim rapidly upward with the tentacles extended (Mills 1981). Gut content observations of *C. gregaria* collected from Coos

Bay, Oregon, as well as other studies, confirm that this jellyfish is able to capture flow-sensing copepods (Supplemental Fig. 1, Daan 1989). We hypothesized that fluid deformation rates (strain and shear) generated during predation by *Clytia gregaria* strongly dictate the outcome of the predation process and can ultimately be related to the prey resource use. We 1) quantified *C. gregaria's* predation steps on a natural prey assemblage and, 2) visualized the temporal and spatial variability of the fluid signals produced during feeding to determine whether predator-induced fluid motion mediates trophic niches of tentaculate predators. To determine whether fluid signals determine feeding selectivity more broadly in other current feeding medusae, we also quantified fluid deformations produced by *Aequorea victoria* and *Mitrocoma cellularia.*

2. MATERIALS AND METHODS

2.1 Animal collection and handling

Individuals of *C. gregaria* (Agassiz, 1862) were collected of the Charleston Marina in Coos Bay, Oregon, from June-September 2018 by dip netting from the docks. Jellyfishes were kept individually in 30- and 60-ml plastic container at 12 °C for 24 hours prior to analysis. Prey were obtained from100 µm and 200 µm plankton tows and were maintained in 2 L plastic beakers with seawater and constant rotation (2 rpm). Prey samples were refreshed every day to minimize any damage.

2.2. Predator-prey interaction videos

After being starved for a minimum of 24 hours, *C. gregaria* individuals were placed in 18.5 x11.5x5 cm (1 Liter) glass tank with seawater. Since transfer to the tank caused the medusae to retract their tentacles, each medusa was left for a period of

up to two hours in the tank for acclimation. During this time, the tank was partially submerged in a 12-13 °C sea table (same temperature as the water where the jellyfish were collected). Once tentacle extension was observed, prey were concentrated and collected in a 30 ml aliquot from the 2 L beaker by placing a white light on one side of the beaker. These aliquots were observed under a dissecting microscope to ensure that prey were intact with no broken appendages (relevant for mechanical sensing; Lenz et al. 1995; Hartline et al. 1996). Using this method we obtained a nearshore prey assemblage that was composed of copepods from the species *Centropages abdominalis*, *Acartia* sp., the cladoceran *Evadne* and cirripede nauplius larvae from the genus *Balanus* sp.. Copepod nauplii were not obtained in these aliquots, either because they were not retained by the 100-µm mesh, or because nearshore copepod species were not spawning during the months of the study (Peterson et al. 1977). We were unable to separate invertebrate eggs or other passive prey types from the plankton tows; therefore, passive prey were simulated using *Artemia* nauplii, since they do not show strong escape responses and are readily captured and ingested by medusae (Ford et al. 1997; Corrales-Ugalde et al. 2017).

We added the prey to the glass tanks holding one *C. gregaria* and recorded the predator-prey interactions with a Sony HDR CX900 camcorder for 25 minutes recording at 60 frames s^{-1}, with a 59.3x33.4 mm field of view and a ~4 mm depth of field. Videos were recorded in a dark room with an infrared light source (Yeshizhuanjia LED lamp) and tank temperature varied between 13 °C and 15 °C. The camera was attached to a motion control system (Newmark), which allowed us to

track the hydromedusa as it moved through the tank and interacted with prey. Prey types were distinguished based on their size, morphology, and behavior.

2.3. Predation process analyses

The outcome of each predator-prey interaction was quantified in five different steps of the predation process: interaction, encounter, capture, transfer, and ingestion (Holling 1959; Regula 2009). Interaction was defined as an event that led either to a prey escaping the predator or a prey entering the encounter zone of the predator. Note that the interaction step has not been explicitly acknowledged in previous studies investigating the components of predation (Regula 2009; Wagner et al. 2020); the other four steps (encounter, capture, transfer and ingestion) are more typical. Encounter was defined as prey contacting the tentacles. Capture occurred when a prey item stuck to the tentacles for more than 1 second (Hansson & Kiørboe 2006). Transfer occurred when the tentacle retracted, and the bell margin folded to bring the captured prey in contact with the manubrium. Ingestion occurred when the bell margin moved back to its original unfolded position, and when the prey was fully encapsulated by the lips of the manubrium. Efficiencies of predation processes were calculated as proportions as follows: interactions that result in encounters (no. interactions/ no. encounters), capture efficiency (no. captures/ no. encounters), transfer efficiency (no. ingestions/no. transfers) and ingestion efficiency (no. ingestions/ no. encounters) (Fig. 1). To visualize the effects of early prey escapes on the feeding efficiency of the predator, we also calculated the total ingestions from interactions as (no. ingestions/ no. interactions) (Fig. 1). We excluded from our

analyses predation events that occurred within 1 cm of the surface, bottom, or sides of the tank, and also excluded interactions that occurred outside of the depth of field.

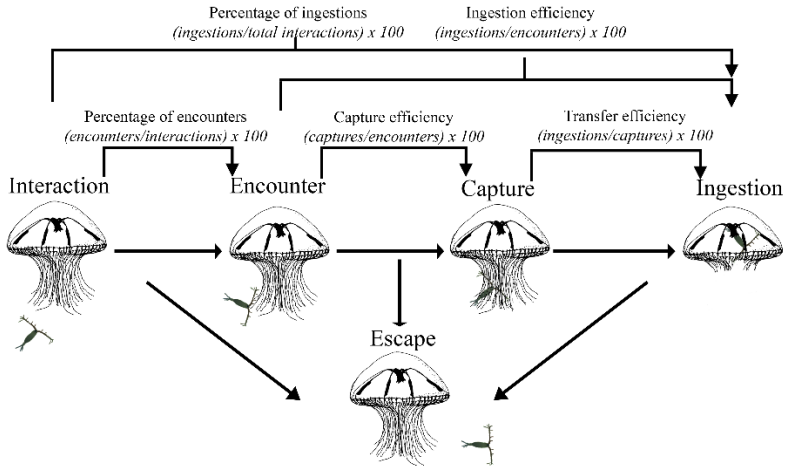

Figure 1. Breakdown of the predation process and calculation of the efficiency of each step (adapted from Regula et al. 2009). The interaction step has not traditionally been quantified in predator-prey interaction studies.

Analyses of the data distribution of the total ingestions from interactions and the ingestion efficiency revealed non-normal skewness and kurtosis values (Supplemental Information). Therefore, we first performed a Kruskal-Wallis (KW) test to compare the ranked means of the total ingestions from interactions and the ingestion efficiency for each prey type (significant differences between rank sums when $p<0.05$). If differences among ranked means were significant, post-hoc comparisons between prey species were made with a Bonferroni-Dunn test (significant differences among rank sums when $p<0.05/2$, Dunn 1964). Second, we used a KW test to compare the ranked means of the total ingestions from interactions and ingestion efficiencies for each feeding behavior of the predator. All analyses were performed in R x64 3.6.0. Data distribution was analyzed with the "fitdistrplus"

package (Delignette-Muller and Dutang 2019). KW and Bonferroni-Dunn test were performed using the "dunn.test" package (Dinno 2016).

2.4. Determination of predator fluid signals

The same individuals used for the predator-prey interaction videos were recorded to quantify fluid deformation rates after a 24-hour recovery period. Organisms were placed in the same tank (18.5 x11.5x5 cm), this time seeded with hollow, neutrally buoyant 10 µm glass beads. After an acclimation period of 2 hours in the tank at 12-13 °C submerged in the sea table, or once the tentacles were extended, an aliquot of the same prey assemblage used for the predator-prey interaction videos was added to the tanks to keep the tank setup consistent, and the medusa was recorded for a period of 10 minutes. Videos were recorded in a dark room and the tank was illuminated by a 1.8 W, 786 nm wavelength (red) laser sheet and images were recorded with a Phantom Miro M 110 Camera (1280 x 800 pixels) recording at 844 frames s^{-1} with a 60.6 x 37.7 mm field of view. Tank temperature varied between 13 °C and 17 °C, which was typical of seawater temperature ranges in the Coos Bay estuary during summer (Roegner & Shanks 2001), and swimming behavior remained normal over this temperature range.

Image pairs were processed using a cross-correlation PIV algorithm with multi-pass processing (DaVis software), where the initial interrogation window was 32x32 pixels (3 iterations) and decreased to a 24x24 window (1 iteration) to obtain the velocity vector map. Processing was limited to the video sequences where the medusae were swimming straight and the laser plane bisected the animal's axisymmetric body. Fluid

structures produced by *C. gregaria*'s swimming were therefore accurately captured with our two-dimensional setup (Gemmell et al. 2015, Dabiri et al. 2010).

2.5. Estimation of fluid signals produced by *C. gregaria* swimming behaviors

Flow-sensing copepod prey respond to both longitudinal and shear fluid deformation rates (Kiørboe et al. 1999). Thus, we quantified four distinct sources of mechanical stimuli within the hydromedusa encounter zone: longitudinal ($\frac{\partial u}{\partial x}$) and shear ($\frac{\partial u}{\partial y}$) deformation rates in the x axis and longitudinal ($\frac{\partial v}{\partial y}$) and shear ($\frac{\partial v}{\partial x}$) deformation rates in the y axis, where *u* and *v* are the fluid velocities in the x and y axis respectively. After obtaining the longitudinal and shear deformation rates for each node in the velocity vector field, the maximum deformation rate (Δ) of each node was obtained following Kiørboe & Visser (1999) (Supplemental Information). This metric also has the advantage of being independent of the coordinate system used. Although approximating a three-dimensional flow from two dimensional DPIV videos can lead to uncertainties in kinetic energy estimates (Dabiri et al. 2010), correct alignment of the medusae's axis with the laser sheet and analysis of video sequences where the medusae was swimming perpendicular to the laser sheet ensured axisymmetry in the wake structures (Gemmel et al. 2015). Thus, our 2D videos were able to accurately quantify the velocity vector fields produced by the swimming medusae, since there was no flow velocity in the unmeasured third dimension (Wagner et al. 2020). Any underestimations of Δ did not affected the qualitative comparisons between the fluid signals produced by the feeding behaviors analyzed in this study.

Planktonic predators tend to capture prey within an encounter zone, which is defined by the tentacle morphology of each hydromedusan species (Madin 1988). However, in current-feeding hydromedusae, prey are mostly captured within 1.5 times the equivalent spherical diameter of the medusa (1.5 ESD) as measured from the bell margin (Corrales-Ugalde et al. 2017). Since medusan feeding currents are unsteady flows, we used two complimentary approaches to describe the temporal and spatial variations in fluid deformation rates within the encounter zone. First, we used a custom MATLAB script to define the encounter zone in the 2D PIV videos as a square with an area of 1.5 ESD^2 and obtained the highest Δ present within that area (Fig. 2a). Second, to quantify spatial changes in the intensity of the fluid deformation rates within the encounter zone, we plotted the deformation rates as a function of distance from the bell diameter (0) up to a distance of 1.5 times the ESD (Fig. 2b). These two approaches for obtaining the fluid deformation rates were done at four stages of the active swimming cycle: (1) during bell contraction, (2) at maximum contraction, (3) during bell expansion, and (4) at maximum bell expansion. During passive sinking, we measured deformation rates at a time when the bell was relaxed, and tentacles trailed behind the swimming bell (Mills 1981).

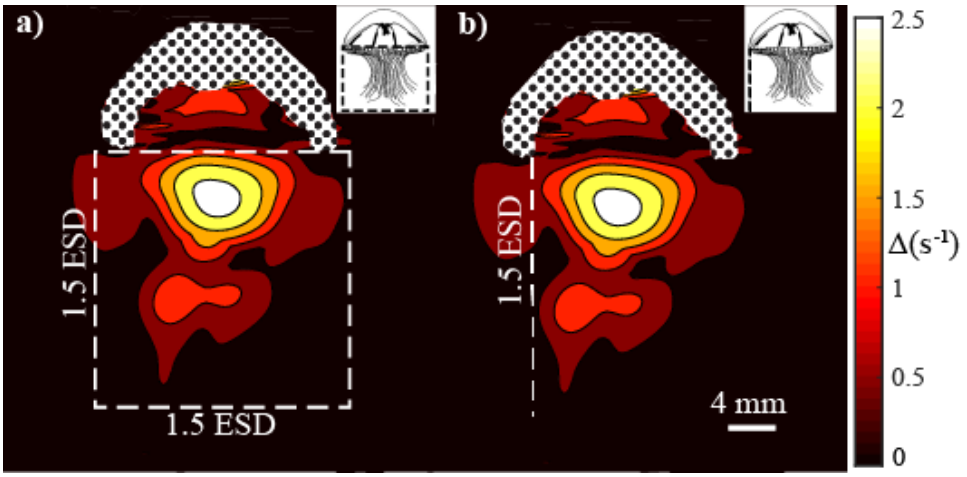

Figure 2. Method for measuring fluid deformation rates produced by *C. gregaria*'s feeding behavior. (a) Maximum deformation rates (Δ) occurring in the encounter zone, defined here as an area of 1.5 ESD^2 (ESD= equivalent spherical diameter), which includes the regions where most of the prey are caught by the tentacles (Madin 1988; Corrales-Ugalde et al. 2017). (b) Deformation rates (Δ) as a function of increasing distance from the bell margin to illustrate the change in deformation rates along the encounter zone. Dotted areas represent the region in the videos that was occupied by the medusae.

To put the fluid mechanics of feeding by *C. gregaria* into a broader context of hydromedusan predation, we compared the magnitude of the maximum deformation rates produced by two other co-occurring Leptomedusae in the Pacific Northwest: *Aequorea victoria* (Murbach & Shearer, 1902) and *Mitrocoma cellularia* (Agassiz, 1862) collected from Friday Harbor, WA in 2013 and 2014. *A. victoria* and *M. cellularia* present similar feeding behaviors to *C. gregaria* (Colin et al. 2003), but do not feed on flow-sensing prey (Costello & Colin 2002). The PIV videos of *A. victoria* and *M. cellularia* that were analyzed only included active swimming sequences. In these videos, a larger (22.5x16.5x7.5 cm, 2.87 Liter) tank was illuminated by a 1.8 W,

786 nm wavelength laser sheet and images were recorded with a Phantom Miro M 110 Camera (1280 x 800 pixels) recording at 500 frames s^{-1} with a 36 x 36 mm field of view for *A.victoria* and a 45x45 mm field of view for *M. cellularia*. Image pairs were processed with the same methods as for the *C. gregaria* videos. We compared the deformation rates produced by the hydromedusae with the lowest known deformation rates from flow field mimics (i.e pipettes with suction flow) that elicited escape responses of *Centropages* sp. and *Acartia* sp. (Kiørboe et al. 1999, Burdick et al. 2007).

2.6. Statistical analyses of fluid deformation rates across species

To determine whether the magnitude of the deformation rates differs among species, we performed a factorial Analysis of Variance (ANOVA) using species as a predictor variable and swimming cycle as a within block factor ($\Delta(s^{-1}) = species + swimming\ cycle + (species \times swimming\ cycle) + \varepsilon$). This design tested whether the swimming cycles differed between species and if any species produced different fluid deformation rates during a given swimming cycle. Larger medusae may be expected to produce higher deformation rates. We addressed this bias by comparing the bell diameter across species (ANOVA), and by testing whether shear rates increase with bell diameter (linear regression). To determine whether swimming behavior in *C. gregaria* affects the magnitude of the velocity gradients produced, we performed a KW test to compare the ranked means of Δ for each of its feeding behaviors (active swimming vs. passive sinking). We performed a non-parametrical test for this comparison due to unequal sample sizes.

3. RESULTS

3.1. *Clytia gregaria* swimming behavior

Starved and acclimated *C. gregaria* performed the same swimming behavior previously observed in much larger tanks (1570-L; Mills 1981). After swimming upward and touching the water's surface, the hydromedusae remained motionless, then with asymmetric bell pulsations reoriented the body upside down (oral surface directed upward, aboral surface down) and then sank due to their negative buoyancy, with the tentacles trailing behind. The individuals analyzed never showed neutral buoyancy. This "passive sinking" behavior was persistent until the medusae touched the bottom of the tank, and then using asymmetric bell pulsations they oriented the aboral side towards the top of the tank and swam back upwards. The hydromedusae tentacles were extended during active swimming and passive sinking, which indicated feeding during both behaviors. To highlight the connection between active swimming and fluid motion, we refer to feeding during this behavior as "current feeding". Interactions with prey occurred mostly when the prey was either located close to the aboral surface of the jellyfish or when the prey entered the encounter zone of the jellyfish (Fig. 3). These interactions occurred every ~1.5 minutes.

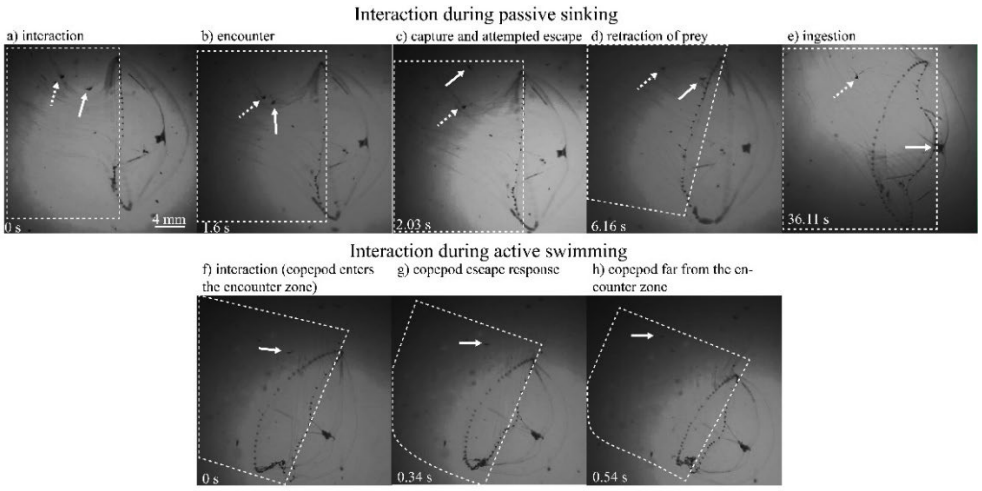

Figure 3. Representative frames of predator-prey interaction videos with steps in the predation process. White dashed squares approximate the encounter zone of *C. gregaria* (1.5 ESD^2). Frames (a-e) show an interaction during passive sinking between the copepod *Acartia tonsa* (solid arow), a barnacle larva (*Balanus* nauplius, dashed arrow) and the hydromedusa *C. gregaria*. During this sequence, the barnacle larva was never ingested by the medusa. The interaction between the copepod and the medusa followed the sequence: (a) initiation of an interaction as the copepod enters the predator's encounter zone, (b) *A. tonsa* encounters the hydromedusa's tentacles, (c) *A. tonsa* is captured by the tentacles and tries to escape (d) the hydromedusa pulls the copepod toward the bell margin and, (e) the bell margin folds toward the mouth to initiate ingestion. Frames (f-h) show an interaction during active swimming between *Centropages abdominalis* and *C.gregaria* that results in an escape.

3.2. Effects of prey type and predator swimming behavior on the predation process

We analyzed a total of 14 videos and 538 predator prey interactions, with an average of 38.4 interactions per video. The observations of *C. gregaria* feeding on a natural prey assemblage (Fig. 3) yielded many more interactions between copepods and *C. gregaria* (n= 387) than interactions with *Balanus* nauplii (n=23) and the

cladoceran *Evadne* (n=6) but not all of these interactions led to ingestions by the hydromedusae. The efficiency of each step of the predation process is included in Table 1. The differences in efficiencies were related to prey-specific behavioral responses to predation. Actively swimming copepods like *C. abdominalis* and *Acartia* sp. either escaped before encountering the predator or tried to escape once they were captured by the tentacles (Fig. 3). *Clytia gregaria* detected the copepod's escape motion once they were stuck to the tentacles, which prompted the medusa to retract its tentacles and bend the swimming bell to bring the prey into contact with the manubrium (Fig. 3e). This fast ingestion response of *C. gregaria* resulted in high capture efficiencies of copepods (Table 1). *Balanus* nauplii and the cladoceran *Evadne* were encountered with high efficiencies (Table 1, Fig. 4a) but were never ingested since they were poorly retained by the tentacles (see Regula et al. 2009, Table 1, Fig. 4b-c). Both *Evadne* and *Balanus* ceased to move their appendages when encountering *C. gregaria*'s tentacles; this opossum-like behavior might have allowed them to remain undetected by the hydromedusae.

Table 1. Average efficiencies in each step of the predation process for different prey types interacting with the hydromedusa *Clytia gregaria*. Values in parentheses are standard errors.

Prey taxa	Encounter efficiency (Encounters/Interactions)		Capture efficiency (Captures/Encounters)		Transfer efficiency (Ingestions/Captures)		(Ingestions/Interactions)		Ingestion efficiency (Ingestions/Encounters)	
	Active swimming	Passive sinking	Active swimming	Passive sinking	Active swimming	Passive sinking	Active swimming	Passive sinking	Active swimming	Passive sinking
Centropages abdominalis (active prey)	7.2(2.12)	61(13.6)	61.1(16.2)	49(15.5)	38.9(16.2)	47.2(16.9)	2.8(1.6)	31(13.1)	33.3(14.4)	43.6(16.4)
Acartia tonsa (active prey)	8.8(4.8)	51.2(13.8)	9.2(6.3)	39.6(16)	22.2(14.7)	50(18.9)	3(2)	23.8(9.6)	9.25(6.3)	39.6(16)
Barnacle nauplii (*Balanus* sp.)	100(0)	100(0)	40(24.5)	81.9(11.7)	0(0)	16.7(9.6)	0(0)	11.4(5.9)	0(0)	11.4(5.9)
Cladoceran (*Evadne* sp.)	100(0)	100(0)	50(28.9)	100(0)	0(0)	0(0)	0(0)	0(0)	0(0)	0(0)
Artemia salina (passive prey)	100(0)	100(0)	67.9(11.7)	90(10)	93.4(3.1)	96(4)	63.5(10.7)	88(12)	63.5(10.7)	88(12)

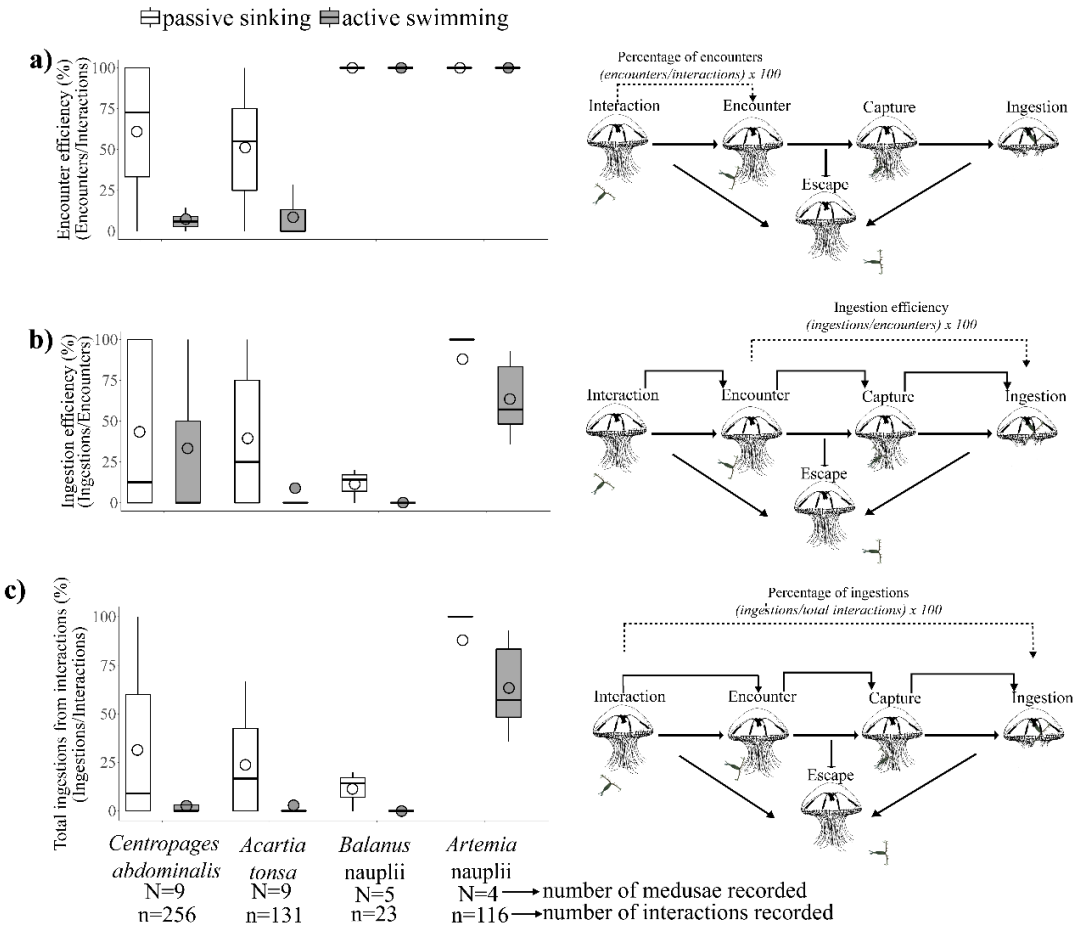

Figure 4. Summary of the predation outcomes for each prey type during *C. gregaria's* feeding behaviors: passive sinking (white) and active swimming (gray). Circles represent means, bars represent the 25th and 75th quantiles, and whiskers represent 95% confidence intervals. (a) Encounter efficiency (b) Ingestion efficiency and (c) Total ingestions from interactions. The predation process diagram to the right of each plot to highlights the relevant steps.

Overall, ingestion efficiencies of copepod prey were much higher when early detection of the predator by the prey—i.e. the interaction step—was not considered (Table 1). This early detection effect is represented by the encounter efficiency (encounters/interactions). When *C. gregaria* was actively swimming most

interactions did not result in encounters (Fig. 4a). Therefore, the total ingestions from the total number of interactions for actively swimming *C. abdominalis* was low (ingestions/interactions x100= 2.8±1.6%, Fig. 4a,b). Ingestion efficiencies for *C. abdominalis* that, by definition, did not account for the interaction step were about ten-fold higher (ingestions/encounters x100= 33.3±14.4%, Fig. 4b, c). Passive prey (nauplii larvae and cladocerans), on the other hand, had uniformly high post-interaction encounter efficiencies with the hydromedusae (Fig. 4a).

Including early detection of predator by the prey (encounter efficiencies) as part of the predation process can drastically change the calculated ingestion efficiencies of different prey types (Fig. 5, Table 1, Table 2). When pooling the observations during passive sinking and active swimming, there were a low number of interactions of the predator with copepods that resulted in ingestions. The no.ingestions/no. interactions x 100 for *Centropages abdominalis* was 17.06±7.27% (mean±standard error) and for *Acartia tonsa* was 12.75±5.16% (KW $X^2 = 26.97$, df=4, $p < 0.001$, Fig. 5a). Some interactions with *C. abdominalis* resulted in encounters, however, and this led to higher ingestion efficiencies (no.ingestions/no. encounters x 100) of 38.50±10.7% (KW $X^2 = 19.8246$, df=4, $p < 0.001$, Table 1, Fig. 5b). Interactions across prey types were more likely to result in ingestions during passive sinking (no.ingestions/no. interactions x 100 =35.06±7.53%, KW $X^2 = 6.1606$, df=1, $p = 0.013$, Table 1 , Fig. 5c). Ingestion efficiencies were also higher during passive sinking (no.ingestions/no. encounters x 100 = 43.83±8.76%, KW $X^2 = 4.6916$, df=1, $p = 0.030$, Fig. 5d).

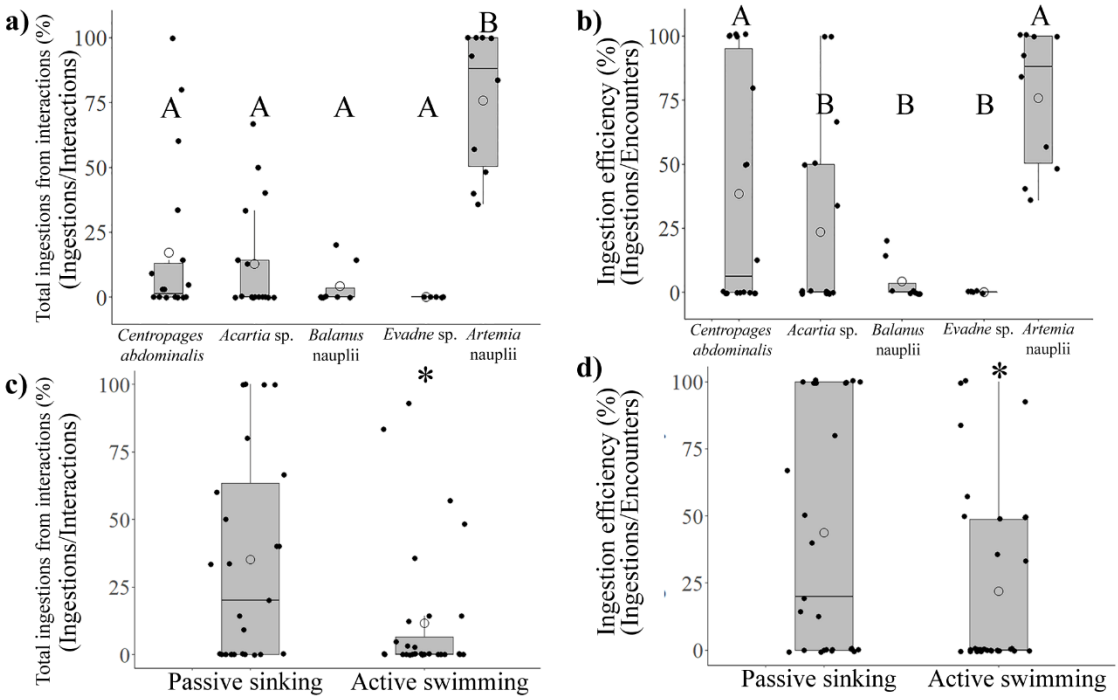

Figure 5. Encounter and ingestion efficiency of *C. gregaria*, shown for each prey type (a, b) and for each feeding behavior (c, d). Different letters above boxplots represent significant differences across multiple comparisons of rank means (Bonferroni-Dunn test, Supplemental Table 2 and 3). Asterisks represent significant differences across rank means.

Table 2. Comparisons of the pairwise Bonferroni-Dunn test results on the predation efficiencies of different prey types. The fraction (ingestions/interactions) represents an ingestion efficiency calculation that considers early detection of the predator by the prey (encounter efficiencies, see Fig. 4). Rank sums between groups are different when probability ≤ 0.05/2 (bold numbers). Ingestion efficiencies of *C. abdominalis* and *Artemia* nauplii are different only when encounter efficiencies are considered (underlined values).

Prey pairs	Dunn's Z		Probability (p)	
	Ingestions/ interactions	Ingestions/ encounters	Ingestions/ interactions	Ingestions/ encounters
Centropages- *Acartia*	-0.59	-1.05	1.000	1.000
Centropages - *Balanus* nauplii	-1.03	-1.68	1.000	0.457
Centropages - *Evadne*	1.72	2.13	0.425	0.166
Centropages – *Artemia* nauplii	3.67	2.36	**<u>0.0012</u>**	<u>0.089</u>
Acartia- *Balanus* nauplii	0.56	0.84	1.000	1.000
Acartia- *Evadne*	1.29	1.37	0.984	0.86
Acartia – *Artemia* nauplii	-4.13	-3.23	**0.0002**	**0.006**
Balanus nauplii- *Evadne*	0.69	0.53	1.000	1.000
Balanus nauplii – *Artemia* nauplii	3.97	3.48	**0.0004**	**0.0025**
Evadne - *Artemia* nauplii	4.37	3.75	**0.0001**	**0.0009**

3.3. Spatial and temporal variation of fluid deformation rates during *C. gregaria*'s feeding behaviors

Analysis of the spatial changes of Δ (s^{-1}) along a transect for each phase of the active swimming behavior revealed that shear rates were lower than the detection thresholds of both *Acartia* sp. (0.45 s^{-1}) and *Centropages* sp. (1.4 s^{-1}) at ~1xESD from the bell margin (Fig. 6 a-d). This explains why copepods can be captured even during active swimming, which we corroborated with some of the predator-prey interaction videos. The highest shear rates were observed closer to the bell margin (0-0.6xESD, Fig. 6 a-d). The magnitude of the shear rates along the transect also changed in each phase of the swimming cycle: during bell contraction, shear rates were below the detection threshold of *Centropages* sp. (Fig. 6a) and exceeded the detection threshold of *Acartia* sp. only at 0-0.5xESD. As the swimming vortex was shed from the bell margin when fully contracted, it generated high shear rates between 0-0.8xESD (Fig. 6b). The highest shear rates were produced during bell expansion, when the surrounding fluid entered the oral surface, between 0-0.6xESD (Fig. 6c). When the bell was fully expanded, shear rates were higher than the detection threshold of *Acartia* sp.—between 0-0.7xESD—but were lower than the detection threshold of *Centropages* sp. throughout the length of the ESD. Throughout the swimming cycle however, there was always a region (~1-1.5x ESD) that had shear rates lower than the detection threshold of both copepod species. During passive sinking, however, shear rates were below the detection threshold of copepod prey throughout the length of the ESD (Fig. 6e).

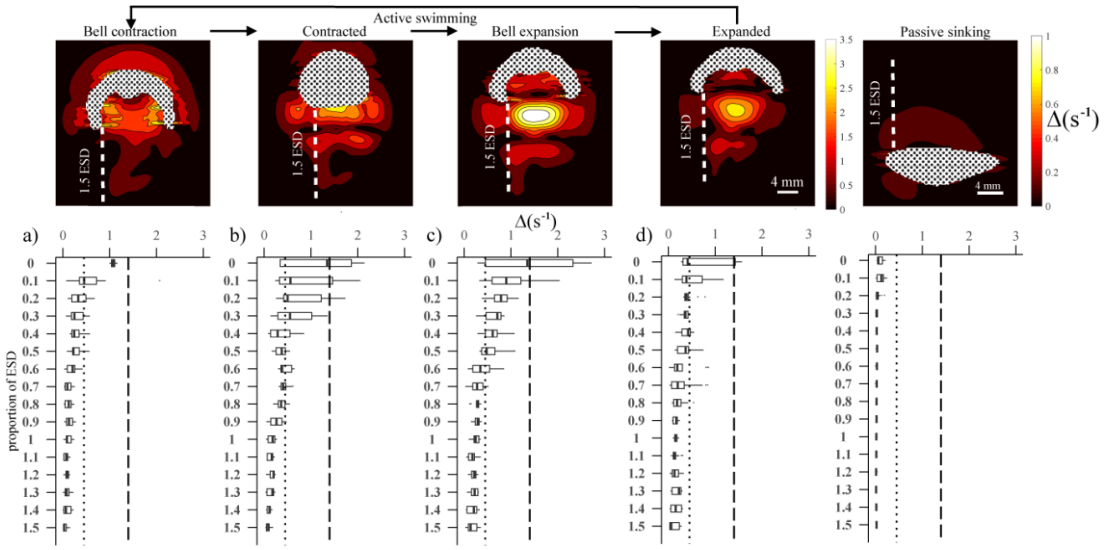

Figure 6. Spatial and temporal variation in maximum deformation rates $\Delta(s^{-1})$ produced by *C. gregaria's* active current-feeding behavior and passive sinking behavior. Δ was calculated from the velocity vector fields along a transect from the bell margin to 1.5 times the Equivalent Spherical Diameter (ESD, white line in panels). During active swimming (a-d), deformation rates exceed the detection threshold of *Acartia* sp. (dotted lines, ~0.45 s^{-1}) and *Centropages* sp. (dashed lines, ~1.4 s^{-1}), whereas the deformation rates produced during passive sinking (e) are below the detection levels of these species. Dotted areas represent the region in the videos that was occupied by the medusae.

3.4. Shear deformation rates in *C.gregaria*'s encounter volume

Figure 7 shows the highest maximum shear rate (Δ) measured in an area equivalent to the encounter zone (encounter zone=1.5 ESD^2) for each hydromedusae species analyzed and for each of *C. gregaria's* feeding behaviors. Fluid deformation rates measured from the 2D PIV videos showed that during active swimming, *C. gregaria* produced maximum fluid deformation rates within the encounter zone that were two orders of magnitude larger than when the hydromedusae were passively sinking in the water column (KW $X^2 = 24.407$, df=1, p = <0.0001). These rates were also higher than the minimum deformation rates that produce escape responses in

Acartia sp. and *Centropages* sp (Fig. 7). We also noticed that a lot of copepod escape responses were occurring at the aboral surface of the hydromedusa when it was actively swimming. Rowing medusae entrain fluid located upstream into the animal's wake (Peng & Dabiri 2009, Katija et al. 2011) thus, the maximum deformation rates occurring in a transect equal to the bell diameter of each hydromedusae are presented in Supplemental Fig. 2.

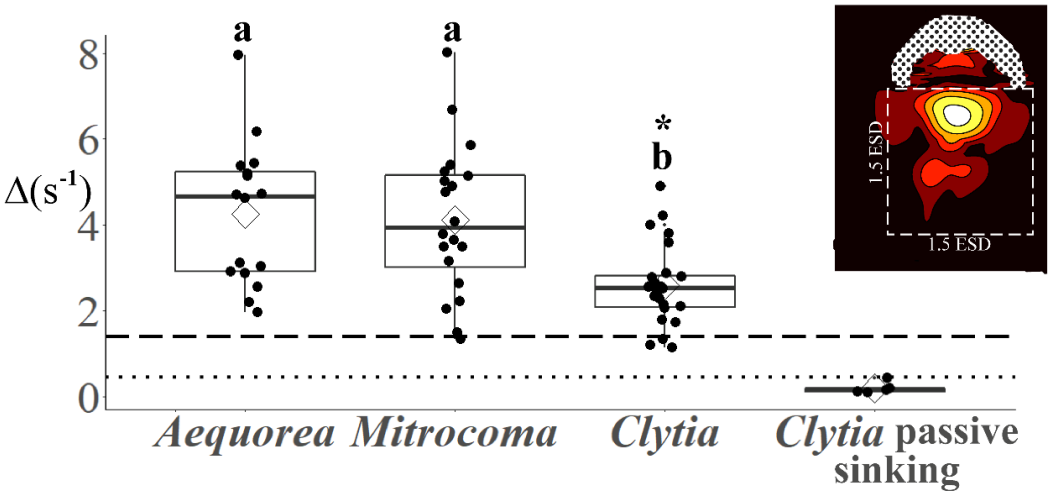

Figure 7. Maximum deformation rate (Δ) produced by *A.victoria*, *M. cellularia* and *C. gregaria*. *C. gregaria* produces lower deformation rates when swimming, compared to the larger Leptomedusae, *A. victoria* and *M. cellularia* (two-way ANOVA, $F(2,52) = 5.532$, $p = 0.0070$). Letters above boxplots indicate significant differences across means (Post-Hoc Tukey test, Supplemental Table 4). The asterisk indicates significant differences across rank means of the comparison between swimming behaviors (KW X^2 (1 df) = 12, p =0.0005). Detection threshold of *Acartia* sp. corresponds to the dotted line (~0.45 s^{-1}) and detection threshold of *Centropages* sp. corresponds to the dashed lines (~1.4 s^{-1}). Dotted areas represent the region in the videos that was occupied by the medusa.

3.5. Comparison of fluid signals produced by three Leptomedusae during active swimming

Comparisons between the PIV videos of the three medusae included only sequences when the medusae were actively swimming upwards. *Clytia gregaria's* active swimming behavior produced lower deformation rates (Δ=2.57±0.18 s^{-1}, mean± standard error) than *A. victoria* (Δ=4.02±0.44 s^{-1}) and *M. cellularia's* (Δ=3.83±0.49 s^{-1}) swimming behaviors (two-way ANOVA, $F_{2, 52} = 5.532$, $p = 0.0070$, Table 3, Supplemental Table 4, Fig. 7). There was no interaction between the hydromedusae species and swimming cycle (two-way ANOVA, $F_{6,52} = 0.559$, $p = 0.7608$, Supplemental Fig. 3). Across species, maximum deformation rates were higher during bell relaxation compared to bell contraction (two-way ANOVA, $F_{3, 52}= 5.008$, $p = 0.0042$, Supplemental Fig. 4, Supplemental Table 2). Bell diameter did not differ across the individuals of each species (ANOVA, $F_3= 2.292$, $p = 0.12$) and there was no significant correlation between bell diameter and the maximum deformation rate (Δ) produced during swimming ($R^2= -0.01631$, $F_{1,58}=0.05311$, $p=0.8185$; Supplemental Fig. 5).

Table 3. Average bell diameter, bell height, equivalent spherical diameter (ESD) and maximum deformation rate produced by the hydromedusae. N=sample size, numbers between parentheses are standard errors.

Hydromedusa species	Bell diameter (mm)	Bell height (mm)	ESD (mm)	$\Delta(s^{-1})$
Aequorea victoria (N=5)	26.1(2.84)	14.60(1.20)	21.48(2.14)	4.02(0.44)
Mitrocoma cellularia (N=5)	20.56(4.38)	12.52(2.64)	16.87(3.28)	3.83(0.49)
Clytia gregaria (active swimming) (N=5)	17.21(0.64)	7.69(0.85)	12.52(0.44)	2.57(0.18)
Clytia gregaria (passive sinking) (N=4)	17.02(0.86)	5.34(0.75)	11.89(1.08)	0.17(0.06)

4. DISCUSSION

Alternation between passive sinking and active swimming by the hydromedusa *Clytia gregaria* allows it to capture flow-sensing and passive prey types, effectively expanding its trophic niche. The capacity of *C. gregaria* to capture flow-sensing copepods is explained by (1) the low fluid deformation rates produced at certain regions of the encounter zone during current active swimming and (2) the overall decrease in fluid deformation rates within the encounter zone during passive sinking (Fig. 6). Pre-encounter prey escape during the "interaction" phase of the predation process is a crucial step mediating predation efficiency (Fig. 5; Wagner et al. 2020). We propose that the magnitude of the fluid deformation rates produced by current-feeding medusae can be considered a relevant phenotypic feature that defines prey resource use. *Aequorea victoria* and *M. cellularia* produce higher shear values

during swimming than *C. gregaria* (Fig. 7), which likely explains the absence of copepods in their guts (Costello & Colin 2002).

4.1. Morphological and behavioral determinants of prey selection

Prey selectivity is determined by a series of morphological and behavioral features of both prey and predator that determine the outcome of each step in the predation process (Holling 1959). This approach, however, does not consider the effects of early detection of the predator by the prey. Encounter between predator and prey is typically considered the first step in predator-prey interactions and is defined as an actual contact between the prey and the medusa tentacles (Regula et al. 2009). Copepods can sense predators that produce a "fluid shadow" around their body and food collecting structures (Suchman 2000, Gemmell et al. 2013) and avoid predation completely. During *C. gregaria's* active swimming behavior (i.e. producing a feeding current), maximum deformation rates within the encounter zone were 1-4 s^{-1} at a distance of 0 to 0.7 ESD from the bell diameter (Fig. 6a-d). These values were higher than detection thresholds previously estimated for both *Acartia* sp. (0.45 s^{-1}) and *C. abdominalis* (1.4 s^{-1}) (Kiørboe et al. 1999; Burdick et al. 2007). Therefore, very few interactions became encounters during active swimming compared to slow moving prey such as *Balanus* nauplii and *Artemia* nauplii (Fig. 4a). Overall, the total number of ingestions when the predator was actively swimming was <10% of the total number of interactions (Fig. 5c). When *C. gregaria* stopped rowing, and passively sank through the water column, it reduced the magnitude of fluid shear around its body by an order of magnitude (Fig. 7), and thus increased the number of ingestions to ~30% of the interactions (Fig. 5c).

Prey characteristics such as setal sensitivity and developmental stage can explain the large variability observed in the encounter efficiencies of copepod prey (Figs. 4 and 5; Robinson et al. 2019). Copepods react to mechanical stimuli when fluid velocity gradients bend the mechanosensory setae in their antennules (Yen et al. 1992). Two types of setae are involved in copepod mechanoreception: mixed modality mechano/chemosensory setae distributed in the proximal and middle portions of the antennae and specialized mechanosensory setae restricted to the distal parts of the antennule (Lenz et al. 1996). Distal mechanosensory setae are likely the predominant system of predator detection and avoidance, since they are outside of the copepod's feeding current, and are highly sensitive to high frequency stimuli (Lenz & Yen 1993). Evasive responses of copepods are more likely if the distal sections of the antennae are the first to encounter the fluid structures generated by the feeding medusae. In addition, the center of mass in large adult copepods is further apart from the sensors in the antennae compared to smaller juvenile copepodites. This size difference implies that a lower deformation rate is needed to bend the mechanosensory setae in large copepods, making them more sensitive to mechanical stimuli compared to smaller copepodites (Kiørboe & Visser 1999, Bradley et al. 2013).

Differences in capture efficiencies are attributed to the predator's behavior once prey have contacted the tentacles (Hansson & Kiørboe 2006, Regula et al. 2009), but post-capture prey behavior is also relevant in defining capture efficiencies. Copepods initiated strong escape responses when adhered to the hydromedusae's tentacles. This allowed for ~50% of captured copepods to avoid ingestions (inverse of

transfer efficiency, Table 3). Jerking action by copepods on the tentacles might stimulate the nematocysts to fire, thus increasing prey adhesion. Struggling by the copepods also prompted *C. gregaria* to retract the tentacle and bend it toward the manubrium to ingest the prey (Fig. 3). This prey recognition, and subsequent reaction by the predator, produced a high capture and handling efficiency of both copepod species (Fig. 5 d-e).

Passive prey like *Balanus* nauplii, the cladoceran *Evadne* and *Artemia* nauplii did not exhibit escape responses when contacting the tentacles and thus were unable to evade capture (Fig. 5d) but were able to evade ingestion (Fig. 5e). Low handling efficiencies can be explained by the inability of *C. gregaria* to recognize that prey was stuck to the tentacles (Pastorok 1981) since both *Balanu*s and *Evadne* stopped moving when encountering the medusae. In addition, this and other studies have highlighted the lack of adherence between barnacle nauplii and hydromedusae tentacles (Colin et al. 2005, Hansson & Kiørboe 2006, Regula et al. 2009). *Clytia gregaria*'s nematocysts are microbasic mastigophores, which can penetrate and adhere to copepod exoskeletons and invertebrate eggs (Purcell & Mills 1988). It is possible that by refraining from moving once captured, both *Evadne* and *Balanus* nauplii prevent triggering the nematocysts on *C. gregaria*'s tentacles (Suchman & Sullivan 1998), thus reducing adherence forces. Other passive prey like copepod eggs and *Artemia* nauplii are readily ingested by *C. gregaria*: mastigophores likely penetrate their soft bodies, resulting in increased adherence and ingestion efficiency of these prey types.

4.2. Energetic advantages of alternative feeding behaviors

The alternation of active swimming behavior with passive sinking in *C. gregaria* potentially maximizes the energetic return from foraging by increasing the ingestion efficiency (Fig. 5d) and by broadening its usable prey spectrum. In coastal environments, *C. gregaria* spends ~80% of the time swimming and only 20% drifting, but its tentacles remain extended during both periods (Colin et al. 2003). Active swimming is an efficient mechanism to maximize contact rates with passive prey (Acuña et al. 2011) such as invertebrate and copepod eggs (Colin & Costello 2002), but it makes the predator easily detectable by rheotactic prey such as large calanoid copepods (Fields & Yen 1997). These large copepods represent a desirable prey over small invertebrate eggs: it can take up to 31 *Acartia* eggs (0.104 µg C) to equal the carbon content of one malnourished adult *Acartia* (3.21 µg C) (data from Kiørboe et al. 1985; Durbin & Durbin 1996). Maximizing energy intake is crucial for an ephemeral hydromedusa, which is under strong selective pressure to generate and release gametes in a short period of time. Complementary feeding behaviors may increase fitness by allowing it to feed efficiently on whatever prey is available at any given time in the water column.

4.3. Ecological implications of complementary feeding mechanics in *C. gregaria*

The ecological impact of zooplanktivores is determined by the rate at which they ingest prey. The first step in obtaining ingestion rates is to estimate the encounter kernel rate ($E=\pi D^2(V^2+W^2)^{0.5}$), which represents the volume sampled by the predator for prey per unit time, and is proportional to the detection distance (D), the velocity of

the predator (V) and the velocity of the prey (W) (Kiørboe 2008). The capture efficiency (a) is another key variable that determines the maximum clearance rates (F) of the predator ($F=aE$). The maximum clearance rate determines how many of the encountered prey per unit volume are ingested. These two parameters are intrinsic to each predator and are mostly defined by their feeding behavior. Predatory behaviors that result in high clearance rates can have dramatic effects on marine plankton communities (Colin et al. 2010).

Alternation between different feeding behaviors in hydromedusae can have a marked effect in energy transfer routes within pelagic food webs if their feeding behavior results in high clearance rates. Table 1 shows the theoretical maximum clearance rates for passive and active prey (*Artemia, Acartia* sp. and *Centropages* sp. respectively) during each of *C. gregaria's* feeding behaviors (active swimming and passive sinking). Despite higher encounter kernel rates during active swimming (i.e. current feeding), the maximum clearance rates of copepods during this behavior were three times lower for *Acartia* sp. and four times lower for *Centropages* sp. compared to the clearance rates when the medusa is passively sinking (Table 4).

Table 4. Theoretical encounter kernel rates ($E=\pi(1.5\ ESD)^2(V^2+W^2)^{0.5}$) and maximum clearance rates ($F=aE$) of *C. gregaria*. 1.5 times the equivalent spherical diameter (average ESD=12.55 mm) was used as a proxy for the detection distance. *C. gregaria*'s swimming velocities (v) and the percentage of ingestions from total interactions between predator and prey were used as a proxy for retention efficiency (a). Swimming velocity data from Garaventa et al. (2010), Mauchline (1998) and this study. Encounter rate kernels and maximum clearance rates were calculated based on Kiørboe (2008) and Colin et al. (2010). Ingestion rates for the copepod genera were calculated from maximum clearance rates and previously recorded copepod abundances in Oregon's coastal waters (Morgan et al. 2003).

Species	Swimming speed (mm s^{-1})		Ingestions /interactions		Encounter kernel rate (L h^{-1})		Maximum clearance rate (L ind^{-1} h^{-1})		Theoretical ingestion rates (ind h^{-1})	
	Active swimming	Passive sinking	Active swimming	Passive sinking	Active swimming	Passive sinking	Active swimming	Passive sinking	Active swimming	Passive sinking
Clytia gregaria (predator)	10.5	3.5	-	-	-	-	-	-	-	-
Centropages sp. (active prey)	3.0		0.028	0.314	43.74	18.47	1.22	5.8	0.66	3.13
Acartia tonsa (active prey)	2.0		0.03	0.237	42.81	18.6	1.28	4.41	0.25	0.88
Artemia salina (passive prey)	3.05		0.64	0.88	43.77	18.58	28.0	16.35	-	-

If we consider nearshore copepod abundances in coastal Oregon (0.199 ind L^{-1} for *A. longiermis* and 0.54 ind L^{-1} for *C. abdominalis*, obtained from Morgan et al. 2003), and multiply these abundances by the maximum clearance rates, we calculate that *C. gregaria* could ingest a higher percentage of *C. abdominalis* than *Acartia* sp. (Table 4), which matches with the higher percentage of *C. abdominalis* found in the gut contents of *C. gregaria* (Supplemental Fig. 1). By multiplying the minimum (3.21 µg C) and maximum (7.75 µg C) carbon content of *Acartia* adults (Durbin & Durbin 1996) by these ingestion rates, we calculate that actively swimming *C. gregaria* would only acquire between 0.8-1.94 µg C hr^{-1} of copepod prey. Passive sinking *C. gregaria* would acquire 2.82-6.82 µg C hr^{-1}. Given that a single *C. gregaria* is capable of ingesting ~20 µg C $hour^{-1}$ in laboratory conditions with natural prey concentrations (Matsakis & Nival 1989, Marshalonis & Pinkney 2008), feeding during passive sinking could help *C. gregaria* achieve its carbon ingestion requirements by supplementing the ingestion of passive prey types (i.e. copepod eggs) with active copepod prey.

These theoretical clearance and ingestion rates might be underestimations if we consider the significant differences between hydromedusan behavior observed in tanks compared to in situ behavior (Mills 1981). Our observations were constrained by the 1 Liter tanks we used (required for good videography), since hydromedusan tentacles reach much larger lengths in natural environments (Ohman 2019) and hydromedusae might capture prey along the full tentacle length. Moreover, swimming and sinking velocities observed in this study are much slower than other tank observations for *C.*

gregaria (~20 mm s^{-1}, see Mills 1981; Colin & Costello 2002); however, previous observations lacked the acclimation period, and the tanks did not contain prey. Higher swimming speeds might produce higher magnitudes of fluid deformation rates and make the medusae easily detectable by prey, but also imply a higher encounter rate kernel since the predator samples more volume per unit time. Future feeding experiments could be conducted in situ or in ~2 Liter tanks (based on container volume to medusa-volume of 2500:1; Purcell 2009) to improve estimates of prey ingestion rates.

CHAPTER III

DOES ENVIRONMENTAL FLUID MOTION INFLUENCE FEEDING BEHAVIOR OF TENTACULATE GELATINOUS PREDATORS

This work will include coauthors Jessica Masterman as contributor to data collection and experimental design and Dr. Kelly R. Sutherland as principal investigator and contributor to the final manuscript preparation. Otherwise, I am the sole contributor of this work to date.

1. INTRODUCTION

Predator-prey interactions control to a large extent the amount of energy that flows through intermediate levels of the food web, from basal primary production to higher order consumers (Pimm, 1982). In addition, predation pressure can modify the structure of planktonic communities and food webs by consumption and competitive interactions (Ruzicka et al. 2012, 2016; Purcell 2018). In marine ecosystems, tentaculate gelatinous predators are key components of planktonic food webs, acting as secondary consumers and as food source for higher-order carnivores (Hays et al. 2018). Thus, it is crucial to understand the variables that modulate their trophic impact in marine ecosystems.

Environmental fluid motion in estuaries and tidal channels could have significant effects on predator prey interactions due to their high values of turbulence compared to other marine ecosystems, which disrupt plankton behavioral patterns (Fuchs and Gerbi 2016). The complex interaction between tidal currents, bottom topography and basin shape can result in areas with either turbulent or sluggish flow (Amoroso and Gagliardini 2010). Such patterns of circulation are known to advect planktonic organisms and

influence recruitment and connectivity of marine populations (Kritzer and Sale 2006). However, it is unknown if species interactions such as predation can be affected by the heterogeneity of flow conditions in these systems.

The fluid dynamics of marine ecosystems act as mechanical stimuli that alter the feeding behavior of planktonic animals. For instance, ambient fluid motion in the form of turbulence can increase copepod feeding efforts (Hwang et al. 1994) and decrease their sensitivity to fluid mechanical signals. Gelatinous predators avoid the upper layers of the water during increases in wind driven turbulence (Jaspers et al. 2018) likely due to the erosion of feeding currents produced by environmental water motion (Katija et al. 2011; Sutherland et al. 2014). However, most of the knowledge we have on turbulence effects on plankton feeding mechanics comes from studies at the organismal scale, and we have not yet measured how environmental turbulence and water acceleration at the organism scale alter the feeding behaviors of gelatinous zooplankton's populations.

Cnidarian hydromedusae with a benthic life stage are one of the most abundant and diverse gelatinous predators of coastal marine environments (Bouillon et al. 2006). Hydromedusae act as secondary consumers of coastal pelagic food webs (Marshalonis and Pinckney 2008; Corrales-Ugalde et al. 2021) and can substantially alter the population dynamics of their prey (Daan 1989; Purcell 2018). Thus, in situ analysis of hydromedusan feeding behavior in natural conditions of background fluid motion will determine if physical drivers of water motion can alter prey consumption by these ubiquitous predators.

The magnitude of prey consumption by a predator is directly determined by the capacity of said predator to "sample" for prey, referred to as the encounter kernel rate *e*

(Liters x hour^{-1}) (Kiørboe 2008). In planktonic tentaculate predators such as hydromedusae, the magnitude of *e* is determined by the volume entrained by feeding currents (Katija et al. 2011) plus the volume occupied by the predator's capture surfaces (i.e. tentacles, oral lobes, oral arms) and the movement speed (Acuña et al. 2011) which can either be controlled by active swimming (i.e. periodical bell contractions) or passive drifting (Mills 1981; Corrales-Ugalde et al. 2021; Mills). Both larger capture surfaces and faster movement speeds increase contact rates with prey (Kiørboe 2008). Thus, any change in these features produced by environmental fluid motion will then modify the capacity of these predators to encounter prey.

In this study, we deployed *in situ* imaging systems in two coastal sites in San Juan Island, Washington, United States to (1) quantify the environmental fluid conditions at an organismal scale at the sites and (2) quantify the behavioral and morphological traits related to feeding (swimming speed, tentacle length) in hydromedusae. We hypothesize that given the differences between the site location (an exposed dock and a nearshore protected cove) turbulence will be higher in the exposed site. We also hypothesize that, with increasing turbulence, hydromedusae will present shorter tentacles and higher pulsation frequencies.

2. METHODS

2.1.Site description

In situ videos of background environmental flow were performed at two sites (Fig. 1) at Friday Harbor, Washington, USA from May 25 to June 12, 2021: a cove (48°32'46.1'' N, 123°0'36.7'' W) referred to throughout as the "protected" site and at the Friday Harbor Marina (48°32'42.4''° N, 123°0'42.9''W) referred to throughout as

the“exposed” site. The exposed site is further offshore than the nearshore protected site, which exposes this site to the strong tidal currents that control circulation around the islands (Zamon 2002). The “protected” site is surrounded to the east and west by rocky shore outcroppings that deflect the flooding and ebbing flows southward and create sluggish flow inside the cove. The videos were recorded after dusk to increase the contrast during videography.

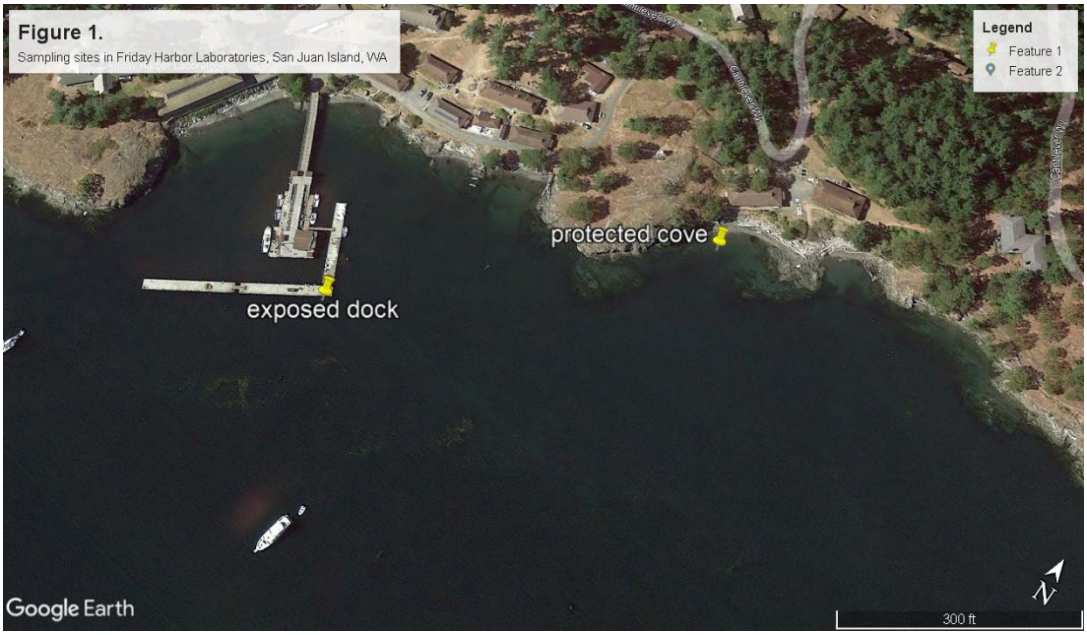

Figure 1. Sampling sites in Friday Harbor Laboratories, San Juan Islands, WA, United States. Friday Harbor Marina (“exposed” site 48°32’46.1’’ N, 123°0’36.7’’ W) and a cove in Friday Harbor Laboratories (“protected” site, 48°32’42.4’’° N, 123°0’42.9’’W).

2.2.In situ observations of environmentally induced fluid motion with PIV

Particle Image Velocimetry (PIV) videos were obtained using a self-contained underwater velocimetry apparatus (SCUVA, Katija and Dabiri 2008). A Canon EOS 5D Mark II camera was used to record videos at 30 fps with a resolution of 1920x1080 pixels, and with a field of view of 197x111 mm. A 660 mn Laserglow Orion laser with a plano-concave lens was used to generate the laser sheet. Videos were recorded on each

sampling event in two orientations: one parallel to the main flow and one perpendicular to the main flow (~30 seconds per video). The SCUVA system was always placed downstream from the main flow to prevent the system from creating artificial fluid disturbances. At the protected site, the SCUVA system was deployed with a tripod attached to the bottom at a depth of 0.6 m. At the exposed site, the camera was manually deployed by an operator. The SCUVA system was deployed on the outer side of the dock, at 0.6 m depth, as far as possible from the dock structure. To consider the changes in fluid motion that might happen between the initial and final times of the brightfield recordings, PIV videos were recorded before and after the brightfield videos, for a total of four PIV videos per recording session.

2.3. Hydromedusan swimming behavior and morphology determined from in situ brightfield imaging

In situ videos of gelatinous zooplankton were recorded with a Sony 4K XAVC-S AVCHD handycam recording at 30 fps with a resolution of 3840x2160 pixels and in a time interval from 20-30 minutes. To achieve brightfield illumination, a rail extended from the camera housing towards the field of view, and at 390 mm from the camera lens, a white-light LED panel was placed on the rail. On the same rail, a plastic diffuser sheet was placed 250 mm from the camera lens. This setup produced a homogeneous brightfield field of view at a focal length of 190 mm from the camera lens (Fig. 2). A screw with known dimensions in the field of view provided scale and a constant focal plane. At the protected site, snorkelers captured images of hydromedusae with the in situ brightfield system near the location where the SCUVA system was deployed. At the exposed site, the camera was held by an operator with arms extended into the water and

recorded organisms far from the pier structure, in the same orientation as the "parallel-to-flow" position of the SCUVA system.

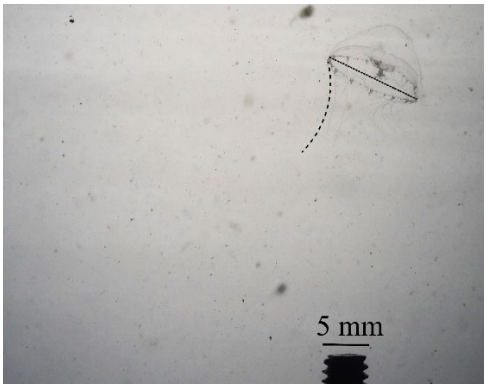

Figure 2. Representative frame with the hydromedusa *Aequorea victoria* recorded by the *in situ* brightfield imaging system. The dashed line shows the tentacle length, and the dotted line shows the bell diameter. The screw that works as a scale is present at the bottom of the image.

2.4.Morphological and behavioral analysis of hydromedusae

Clips lasting from 1-60 seconds containing individual hydromedusae were generated from the full video, and bell diameter, tentacle length and bell pulsation frequency were obtained from each clip. In a video sequence with a recorded individual, the maximum tentacle length observed in the video sequence was recorded. Individuals that were damaged were not analyzed. Since hydromedusan jellyfish include multiple genera of different bell shapes and sizes, we standardized the tentacle length by dividing it by the equivalent spherical diameter (ESD) of each hydromedusan bell to obtain a dimensionless ratio $\left(\frac{tentacle\ legth\ (mm)}{ESD}\right)$. ESD is defined as the diameter of a sphere with the same volume of an animal (Pitt et al. 2013). For medusae, the swimming bell volume can be estimated as half the volume of a hemi-ellipsoid$\left[\left(\frac{4}{3}\pi hr^2\right) \div 2\right]$ where h is the bell height and r is the bell radius.

In situ brightfield videos allowed us to determine the percentage of hydromedusae at each site that presented optimal morphology and behavior for prey capture. Hydromedusae capture most prey at a distance from the bell margin of 1.5xESD (Corrales-Ugalde et al. 2017) therefore, we determined the percentage of hydromedusae at each site that had tentacle lengths equal or higher than 1.5xESD (i.e. number of individuals with $\frac{tentacle\ legth\ (mm)}{ESD} \geq 1.5$). In addition, active swimming by the hydromedusae, characterized by cycles of bell contraction and relaxation, increases medusan swimming speeds (Colin and Costello 2002), which theoretically leads to larger contact rates of the medusae with its prey (Kiørboe 2008). The we determined the proportion of hydromedusae in each site that were actively swimming.

2.5.Determination of velocity fields, fluid signals and turbulent kinetic energy dissipation rates.

Image pairs were processed using a cross-correlation PIV algorithm with multi-pass processing (DaVis software 8.4.0), where the initial interrogation window was 128x128 pixels (3 iterations) and decreased to a 64x64 window (1 iteration) to obtain the velocity vector map (Colin et al. 2010, Sutherland et al. 2014, Jaspers et al. 2017). Turbulence dissipation rate (ε) from PIV videos was calculated from the u and w velocity vectors following de Jong et al. (2009)

$$\varepsilon = 4v\left[\left\langle\left(\frac{\partial u}{\partial x}\right)^2\right\rangle + \left\langle\left(\frac{\partial w}{\partial z}\right)^2\right\rangle + \left\langle\frac{\partial u}{\partial x}\frac{\partial w}{\partial z}\right\rangle + \frac{3}{4}\left\langle\left(\frac{\partial u}{\partial x}\frac{\partial w}{\partial z}\right)^2\right\rangle\right]$$

where v is the seawater kinematic viscosity (1.3 x 10^{-2} cm^2s^{-1} at 10°C), *u* and *w* are the velocity components in the orthogonal coordinates *x* and *z.* A correction that isolates noise from DPIV measurements by estimating dissipation rate using different interrogation window sizes was used to address random measurement errors (Tanaka and

Eaton 2007). In addition, a custom-made MATLAB script was used to exclude dissipation rate estimates that were influenced by animals swimming through the laser sheet. This same script was used to extract the maximum ε that occurred during the 15 seconds of video that were analyzed. For each recording session, only the maximum ε from the four PIV videos was reported.

2.6. Correlation of turbulent dissipation rates with large scale drivers of fluid signals.

To relate the turbulent dissipation rates with drivers of circulation in the San Juan Islands, wind and tidal height data were obtained for the sampling dates from the NOAA weather station No. 9449880 (48°32'42'' N, 123°0'48'' W). Tidal current velocity was obtained from the NOAA current predictions service for west of Point George, WA (48°33'24.12'' N, 122°59'54.6'' W) at 16 m depth. Linear regressions were done between the magnitude of these circulation drivers as predictor variables and turbulence dissipation rates as response variables. These analyses were done in R version 4.0.3

2.7. Comparisons of tentacle lengths and swimming frequencies across sites

Unequal sample sizes and unequal variances between sites justified our use of a Kruskal-Wallis (KW) test to compare the ranked means of the tentacle lengths and bell pulsation frequencies in each sampling site. To determine the effect of turbulent dissipation rate on tentacle length and pulsation frequency, a linear regression was performed using $\log(\varepsilon)$ as a predictor variable and standardized tentacle length $\left(\frac{mm}{ESD}\right)$, and bell pulsation frequency (Hz) as response variables. In addition, turbulent dissipation rate was binned into four categories of turbulence, using the range of 0-1$cm^2\ s^{-3}$ as a control for "no turbulence" and comparing the tentacle length and pulsation frequency of hydromedusae at this range to increasing levels of turbulence, using a KW test

(significant differences between rank sums when $p<0.05$). If differences among ranked means were significant, post-hoc comparisons between tentacle lengths and pulsation frequencies across different categories of turbulence were made with a Bonferroni-Dunn test (significant differences among rank sums when $p<0.05/2$, Dunn 1964). All analyses were performed in R version 3.6.0. KW and Bonferroni-Dunn test were performed using the "dunn.test" package (Dinno 2016).

3. RESULTS

3.1. Correlation of turbulent kinetic energy differences between sites and correlation with flow forcing

Turbulence dissipation rates were similar between sites (KW X^2 (1 df) = 1.352, p = 0.2449). However, the largest range and the maximum values of turbulence measured occurred at the exposed site (Fig. 3).

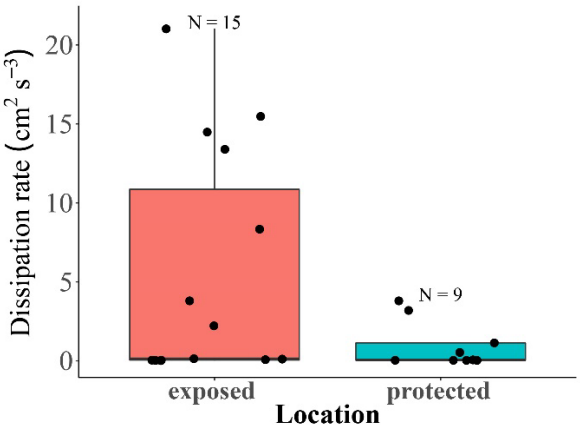

Figure 3. Turbulence dissipation rates obtained from 2D in- situ particle image velocimetry measured in the Friday Harbor Marina ("exposed") and the cove ("protected") (KW X^2 (1 df) = 1.352, p= 0.2449). N= number of videos analyzed, dots represent individual data points, bars represent the 25th and 75th quantiles, and whiskers represent 95% confidence intervals.

The linear relationships between current speed and tidal height with the turbulence dissipation rate were different for the exposed site and the protected site (Fig. 4).

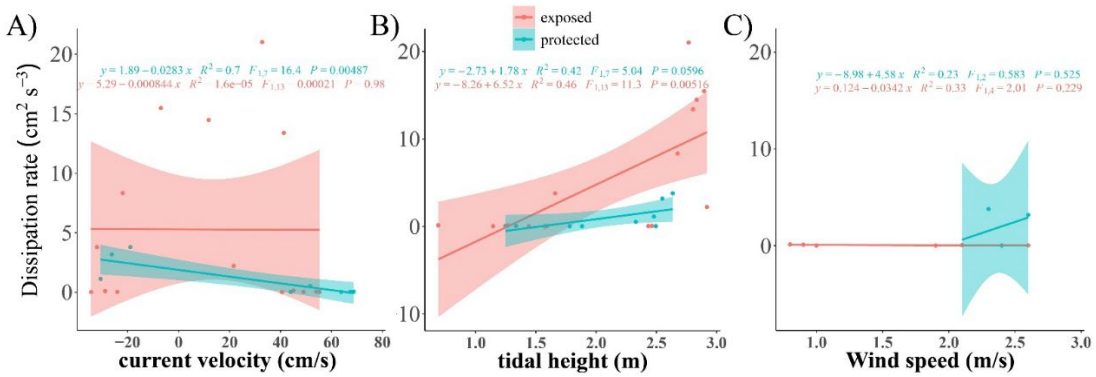

Figure 4. Linear regressions of turbulent kinetic energy dissipation rate (ε) as a function of (A) modelled current velocity in the San Juan Channel (48°33'24.12'' N, 122°59'54.6'' W), (B) tidal height and (C) wind speed in the two sampling sites: the Friday Harbor Marina ("exposed", red, 48°32'46.1'' N, 123°0'36.7'' W) and a cove in Friday Harbor Laboratories ("protected", blue, 48°32'42.4'' N, 123°0'42.9''W). A significant correlation in the protected site was found between ε with current velocity (R^2=0.7, p=0.00487), whereas in the exposed site ε was correlated only with tidal height (R^2=0.46, p=0.00516). NOAA's weather station No. 9449880 has an incomplete wind speed record from 6/2-4/2021 which reduced the number of data points in panel C.

3.2.Differences of hydromedusan tentacle length and bell pulsation frequencies across sites

Ten species of hydromedusae were recorded in the brightfield videos: 181 individuals in the exposed site and 67 in the protected site. In both sites, the most recorded hydromeduse were *Clytia gregaria,* followed by *Aglantha digitale and Mitrocoma cellularia* (Fig. 5).

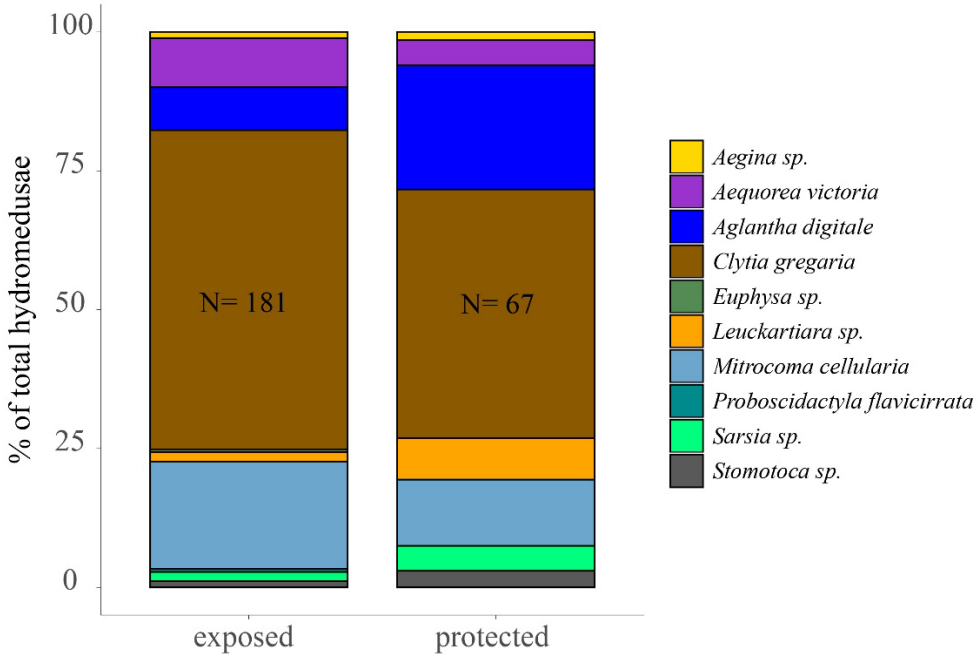

Figure 5. Percentage of each hydromedusan predator from the total of hydromedusae recorded (N) in the Friday Harbor Marina ("exposed", 48°32'46.1'' N, 123°0'36.7'' W) and the cove ("protected", 48°32'42.4'' N, 123°0'42.9''W) sites in Friday Harbor, WA.

The standardized tentacle lengths recorded in the protected site were longer compared to the ones recorded in the exposed site (KW X^2 (1 df) = 75.146, $p < 0.001$, Fig. 6a). However, bell pulsation frequencies were similar between these sites (KW X^2 (1 df) = 0.015337, p = 0.9014, Fig. 6b).

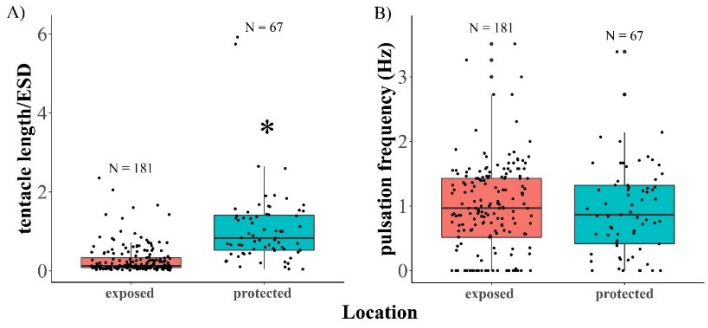

Figure 6. Tentacle lengths (A) and bell pulsation frequency (B) recorded by the in- situ brightfield imaging system. The asterisk indicates significant differences between the tentacle lengths of hydromedusae recorded in the Friday Harbor Marina ("exposed") and the cove ("protected") (KW X^2 (1 df) = 75.146, $p < 0.001$, Fig. 6a). N= number of hydromedusae recorded, dots represent individual data points, bars represent the 25th and 75th quantiles, and whiskers represent 95% confidence intervals.

The hydromedusan community in the protected site had a higher percentage of individuals with tentacle extensions > 1.5 x$\frac{mm}{ESD}$ (95.8 ± 2.1%, mean ±SE) compared to the exposed dock (59.1 ± 7.1%). The percentage of medusae actively swimming (i.e. observable bell contraction) was also higher in the protected site (92.8 ± 11.4 %) compared to the exposed site (75.7 ± 15.2 %, Fig. 7).

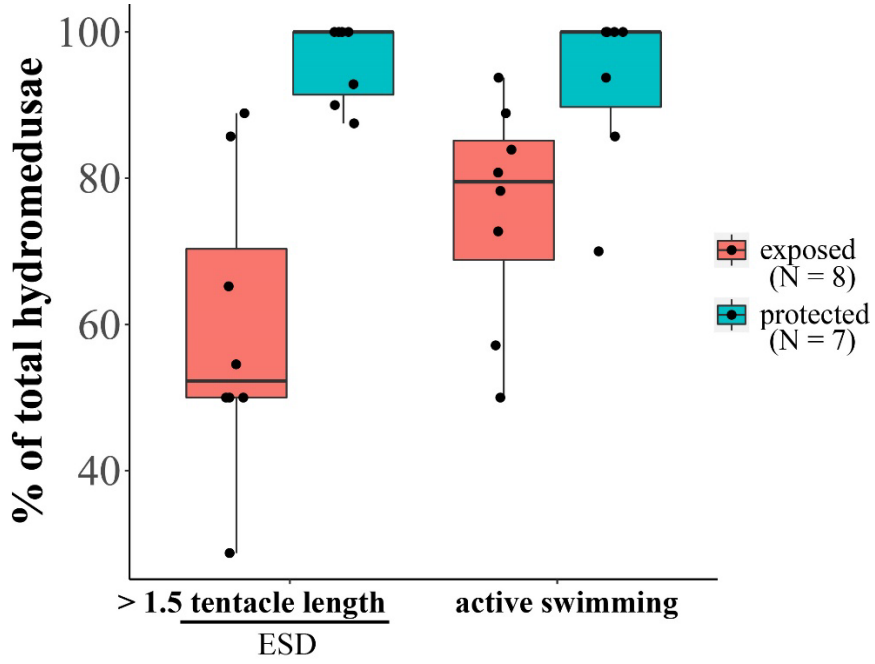

Figure 7. Percentage of the total hydromedusae during each recording time and in each location that had a tentacle length >1.5 x standardized tentacle length $\left(\frac{mm}{ESD}\right)$ and the percentage of

hydromedusae that were actively swimming. N= number of recording times. dots represent individual data points, bars represent the 25th and 75th quantiles, and whiskers represent 95% confidence intervals.

3.3. Effects of turbulence on tentacle length and pulsation frequency

Instantaneous turbulent dissipation rate did not have any effect on the standardized tentacle length (R^2= 0.037, F (1,227)=8.82, p=0.0033; Fig. 8a) or on the bell pulsation frequency (R^2= 0.00076, F(1,227)=0.0173, p=0.896; Fig. 8b).

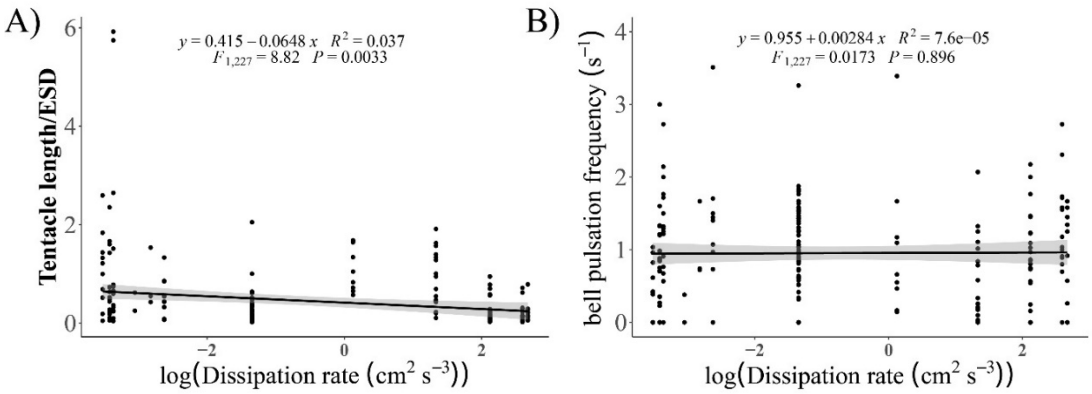

Figure 8. Linear regressions of the logarithm of turbulent dissipation rates and standardized tentacle length (A) and bell pulsation frequency (B). Solid lines represent the linear fit between the variables, grey area represents the 95% confidence interval for the linear fit, and dots represent individual data points.

Standardized tentacle lengths were different across the different categories of increasing turbulence (KW X^2 (3 df) = 32.5727 p < 0.001, Fig. 9a), with the hydromedusae experiencing ε=1-5 $cm^2 s^{-3}$ presenting the highest tentacle lengths. However, bell pulsation frequencies remained similar across all levels of turbulence (KW X^2 (3 df) = 6.9 p =0.08, Fig. 9b).

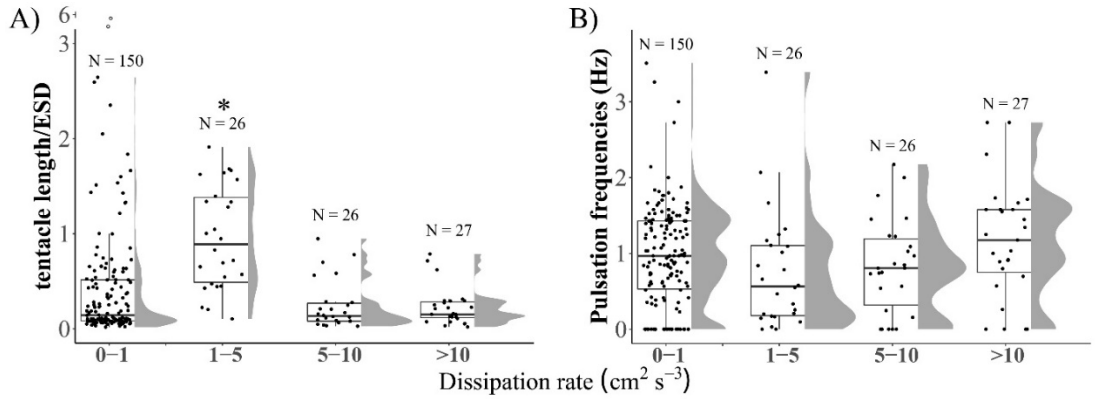

Figure 9. Tentacle lengths (A) and bell pulsation frequency (B) of all hydromedusae, observed in increasing ranges of turbulence dissipation rates. The asterisk above boxplots represent significant differences across multiple comparisons of rank means (Bonferroni-Dunn test, Table I). N= number of hydromedusae recorded, dots represent individual data points, bars represent the 25th and 75th quantiles, and whiskers represent 95% confidence intervals. The grey area is the probability density function of the data. Open circles in panel A align with the "6" tick on the y axis.

Table 1. Comparisons of the pairwise Bonferroni-Dunn test results on the standardized tentacle length ($\frac{tentacle\ length\ (mm)}{Equivalent\ spherical\ diameter\ (mm)}$) and the bell pulsation frequency across increasing ranges of turbulence dissipation rates ($\frac{cm^2}{s^3}$) in Friday Harbor, WA. Rank sums between groups are different when probability ≤ 0.05/2 (underlined numbers).

Turbulence ranges comparisons	Dunn's Z		Probability (p)	
	Std. Tentacle length	Pulsation frequencies	Std. Tentacle length	Pulsation frequencies
0-1 & 1-5	-5.29	1.81	<u>≤0.0001</u>	0.2113
0-1 & 5-10	1.04	1.06	0.903	0.865
0-1 & >10	-0.532	1.32	1.00	0.562
1-5 & 5-10	4.84	-0.573	<u>≤0.0001</u>	1.00
1-5 & >10	-4.49	2.40	<u>≤0.0001</u>	0.049
5-10 & >10	0.395	1.82	1.00	0.205

4. DISCUSSION

In this study we have shown that ambient turbulence experienced at the organismal scale (cm to mm) influences the feeding behavior of hydromedusae. Coastal areas with low turbulence can present optimal conditions for gelatinous tentaculate predators such as hydromedusae to increase prey capture (Fig. 6a, Fig. 7). However, turbulence effects on hydromedusan predatory behavior might not follow a linear relationship: we observed longer tentacle lengths at intermediate levels of turbulence (ε=1-5 $cm^2\ s^3$, Fig 9a) compared to ranges of low turbulence (ε=0-1 $cm^2\ s^3$) and high turbulence (ε>1-5 $cm^2\ s^3$). These results suggest that the spatial heterogeneity of turbulence in marine coastal systems influences the predatory behavior of hydromedusae through modifications of their prey sampling rates.

4.1. Patterns of circulation in the San Juan Islands

The San Juan Island Archipelago presents strong tidal currents that are the major drivers of water circulation in this system (Thompson 1981). Despite the numerous modelling studies regarding circulation patterns in the Salish Sea (Sutherland et al. 2011; Khangaonkar et al. 2011), data on circulation patterns around the San Juan Islands, and specifically around Friday Harbor are scarce. Current velocity data has been collected along two transects close to our sampling sites: one at the northern edge of the junction of San Juan Channel and Friday Harbor (Banas et al. unpubl. data) and one to the south, from Turn Island State Park toward Shaw Island (SJ transect in Yang et al. 2021). Both datasets suggest that flow velocity is highest along the middle and eastern parts of the San Juan Channel, and slower flows are found with decreasing depth. However, Banas et al. (unpubl. data) found that during flood tides, the presence of Reid rock and greater bottom

depths on the west side of the channel produce strong eastward and westward flows, that could potentially influence flow velocities in the Friday Harbor Marina. Local high-resolution descriptions of nearshore circulation are needed to determine the influence of large-scale circulation with nearshore processes.

Tidal patterns in the San Juan Islands are known to affect the food web structure of this ecosystem, by determining the distribution of intermediate levels in the food web such as planktivorous fish and copepods (Zamon 2001, 2002). For instance, during flood tides, copepod abundances increase in the main tidal current of the San Juan Channel, due to the advection of copepod communities from deep layers of the strait of Juan de Fuca (Zamon 2002). This process could also advect the hydromedusan communities from systems outside the San Juan islands, which explains the presence of oceanic Trachymedusae (i.e., *Aglantha digitale*) and Narcomedusae (i.e., *Aegina sp.*) in nearshore systems. These tidal currents can then transport these jellyfish to optimal foraging conditions such as locations outside the main channels during slack water, where prey densities remain constant (Zamon 2002) and ambient turbulence remains low independent of the tidal cycle (i.e. "protected" site, Fig. 4b).

4.2. Turbulence effects on hydromedusan prey sampling rates

At an individual level, the effect of turbulence on medusan predatory behavior can be assessed through calculations of the encounter kernel rate ($E=\pi D^2(V^2+W^2)^{0.5}$), which represents the volume sampled by the predator for prey per unit time, and is proportional to the detection distance (D), the velocity of the predator (V) and the velocity of the prey (W) (Kiørboe 2008). In tentaculate predators, the volume in which prey can be encountered is defined by the pattern of tentacle deployment (Madin 1988). To illustrate

the effects of the location (protected vs. exposed) on hydromedusan encounter kernel rates, we used the tentacle lengths of the leptomedusa *Clytia gregaria* as the detection distance and used previously published data on prey speed (*Acartia tonsa*, *W*= 2.0 mm s^{-1}, Mauchline 1999), and predator active feeding speed (10.5 mm s^{-1}, Corrales-Ugalde & Sutherland 2021). For these calculations, we assume that swimming speed in both sites is similar given the similar bell pulsation frequencies across sites (Fig. 6b). For the sake of simplicity (and since we are focusing on turbulence effects on behavior) we do not consider the acceleration imparted by turbulence on predator and prey swimming velocities, which theoretically increases contact rates (Rothschild & Osborn 1988). Encounter kernel rates in the protected site can be up to one order of magnitude larger (10.63 ± 1.6 L hr^{-1}) compared to the exposed dock site (1.47 ± 0.48 L hr^{-1}, Fig. 10). These differences in encounter kernel rates are solely attributed to differences in tentacle lengths between the sites. Given the relevance of a species like *Clytia gregaria* on grazer population dynamics (Daan 1989) and on food web structuring (Francis et al. 2012; Corrales-Ugalde et al. 2021), location-driven changes in its feeding behavior can produce spatial heterogeneity of its predation impact and affect local food web dynamics.

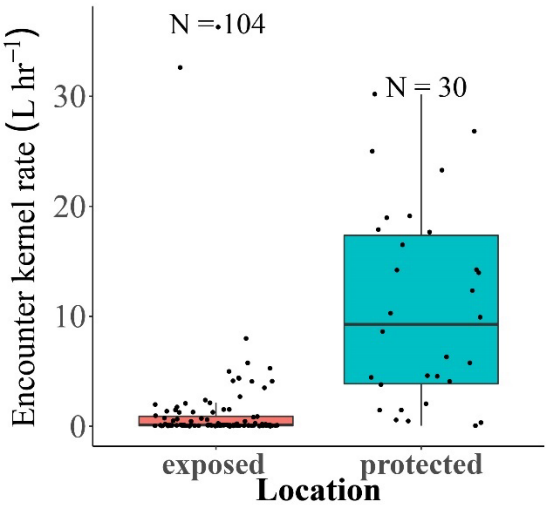

Figure 10. Theoretical encounter rates of the hydromedusa *Clytia gregaria* in the protected site and the exposed site (Friday Harbor Marina). Swimming velocity data from Mauchline (1998) and Corrales-Ugalde & Sutherland (2021). Encounter rate kernels and maximum clearance rates were calculated based on Kiørboe (2008) and Colin et al. (2010).

4.3. Mechanical sensing of cnidarian jellyfish and behavioral responses to flow

In hydromedusae, tilting of the bell induced by fluid rotation can be detected by gravity sensing organs such as statocysts (Mackie 1980). These organs can detect changes in body orientation through the motion of a calcareous stone (statolith) within a fluid filled chamber, which acts upon ciliated sensory cells that cover the inside walls of the chamber (Horridge 1969; Singla 1983). Such structures can be found in the bell margins of all the hydromedusan species found in this study (Bouillon et al. 2006) and are likely to be the sensory organs that allow scyphomedusae to maintain a defined body orientation in response to shear flow (Rakow and Graham 2006).

Body orientation is a crucial component of swimming and feeding behavior in hydromedusae. For instance, the cyclical "swim-and-sink" behavior of *Aglantha digitale* and *Clytia gregaria* includes a distinct phase of upward swimming (aboral side up) and downward sinking (aboral side down, Mackie 1980, Mills 1981). This cyclical behavior increases prey capture efficiencies: active swimming allows the medusae to search or remain in prey patches (Arai 1992) and, in the case of *C. gregaria*, vortices around the bell margin produced during swimming move prey into the tentacles (Colin & Costello 2002), with the caveat of generating fluid disturbances that can be detected by flow

sensing prey (Corrales-Ugalde & Sutherland 2021). During passive sinking, the fluid deformation rates around the tentacles of the hydromedusae fall below the detection thresholds of said prey, which approach the undetectable medusae and get entangled in its tentacles (Corrales-Ugalde and Sutherland 2021). Increased shear and vorticity in fluid parcels under turbulent flow could change the bell orientation of the medusae and interrupt hydromedusae feeding behavior, in particular, the relative time spent swimming vs. sinking could be altered.

4.4. Predator-prey dynamics in turbulent flow

Theoretical models suggest that contact rates between predator and prey increase with increasing turbulence due to the added displacement velocity of the predator, which allows them to "sample" for more prey per time (Rothschild and Osborn 1988). Hydromedusan prey such as copepods are known to swim faster and perform more "relocation jumps" at even low turbulence values (ε=0.05-0.5 $cm^2\ s^{-3}$, Saiz and Alcaraz 1992; Michalec et al. 2015). These ranges correspond to the low turbulence values where we observed the largest hydromedusan tentacle extensions (Fig. 9a), and even if at higher turbulence values (ε=1-5 $cm^2\ s^{-3}$) copepod swimming behavior is greatly hindered by environmental flow, the combination of larger displacement velocities of both predator and prey together with larger predator contact surfaces could lead to enhanced prey captures rates for hydromedusae in intermediate turbulent flows.

However, such enhancement of prey capture is likely to decrease as hydromedusan tentacle length decreases at ε >5-10 $cm^2\ s^{-3}$. Reduced tentacle length yields a reduced encounter volume, which decreases prey capture rates. In addition, some hydromedusae initiate ingestion behavior once they detect tentacle "jerking" produced by

the escape behavior of motile prey after they get entangled in the medusan tentacles (Colin et al. 2005; Corrales-Ugalde and Sutherland 2021). This entanglement requires prolonged contact between the tentacle and the prey, and advective processes (i.e., medusan swimming behavior or ambient turbulence) might detach prey from the medusae's tentacles. Laboratory experiments might allow for isolation of these key modifiers of the predation process (prey behavior, predator tentacle extension, advection by turbulence) to determine how the interactions of these variables affect tentaculate predation efficiency.

4.5. Other factors affecting in situ hydromedusan behavior

The large variability of hydromedusan behavior implies that factors other than turbulence contribute to their *in situ* swimming behavior and tentacle extension. For instance, fully starved individuals present the maximum extended tentacle postures (Mills 1981), which potentially explains the presence of outlier medusae with very long tentacle extensions across all ranges of turbulence (Fig. 9a). However, many hydromedusae had short tentacle extensions in the lowest range of the measured turbulence (ε=0-1 cm^2 s^{-3}). It is likely that enhanced predation by hydromedusae in lower turbulence will result in multiple individuals reaching satiation (i.e., gut fullness). Since indigestible material is excreted through the mouth, and since hydromedusae can only ingest one prey at a time, ingestion rates quickly reach a maximum value in optimal foraging conditions (Colin et al. 2005; Hansson and Kiørboe 2006). It has been suggested that satiated hydromedusae retract the tentacles to prevent prey captures that cannot lead to ingestion (Mills 1981) but the relationships between feeding behavior and gut fullness have not been explored in detail.

In addition to satiation, other biological interactions between planktonic organisms can modify the *in situ* behavior of hydromedusae, such as phoresis, parasitism and predation pressure (Ohtsuka et al. 2009). Phoresis by pandalid shrimp, or "piggyback riding" reduces the tentacle length of hydromedusae (Marliave and Mills 1993) and this association was observed several times in the brightfield videos. Parasitic-induced behavior has only been reported to affect scyphomedusan vertical distributions (Chiaverano et al. 2015), and may also affect feeding and swimming behavior of hydromedusae. Symbiosis with hyperiid amphipods was observed in the recorded individuals, however, the nature of such symbiosis can range from phoresis to complete predation of the host by the amphipod (Vader 1972; Laval 1980). Repetitive contact between these parasites and the feeding structures of the hydromedusae, either during kleptoparasitism or consumption of the hydromedusan tissues, is likely to change normal hydromedusan feeding behavior.

In this study, we have shown that, first, turbulence intensity can vary at very small spatial scales within a tidal channel and, second, turbulence modifies the feeding behavior of tentaculate predators such as hydromedusae. Thus, the presence of "protected " parcels of water shielded from the main circulation within a system (Amoroso and Gagliardini 2010) could imply the presence of optimal "feeding grounds" for tentaculate predators. In such locations, low levels of ambient turbulence increase prey motility while not affecting the patterns of feeding behavior and tentacle deployment of hydromedusae, effectively increasing the encounter rates between these predators and their prey. By performing *in situ* measurements of ambient turbulence coupled with *in situ* observations on feeding behavior, this study complements the

results of abundant laboratory studies that have shown the effects of turbulence on zooplankton biology and behavior.

CHAPTER IV

SEASONAL HYDROMEDUSAN FEEDING PATTERNS IN AN EASTERN BOUNDARY CURRENT SHOW CONSISTENT PREDATION ON PRIMARY CONSUMERS

From Corrales-Ugalde, M., Sponaugle, S., Cowen, R.K, and Sutherland, K.R. (2021). Seasonal hydromedusan feeding patterns in an Eastern Boundary Current show consistent predation on primary consumers. *J. Plankton Res*. 43(5):712-724. By permission of Oxford University under license 5239530078668.

1. INTRODUCTION

Cnidarian jellyfish predation has been highlighted as a key process in structuring the food webs of highly productive Eastern Boundary Current (EBC) upwelling zones (Suchman et al., 2008; Ruzicka et al., 2012, Zeman et al., 2016; Hays et al., 2018). These studies have focused on large, conspicuous scyphomedusae and ignore the potential trophic role of small hydromedusae in EBCs. Hydromedusae comprise 80% of all medusan diversity (Costello et al., 2008), are present in many coastal systems with seasonal upwelling (Buecher and Gibbons, 2003; Miglietta et al., 2008; Rodriguez et al., 2017,) and multiple species can simultaneously increase in abundance during upwelling (Hosia and Båmstedt, 2007; Miglietta et al., 2008; Luo et al., 2014). Such increases in hydromedusan abundance imply an enhanced predation pressure on prey populations. Highly selective feeding by hydromedusae can alter the community composition of lower trophic levels, by reducing the standing stock of planktonic invertebrates (Larson, 1987;

Daan, 1989; Matsakis and Conover, 1991) and fish eggs and larvae (Purcell et al., 1987; Purcell and Grover, 1990). Given the importance of EBCs for maintaining some of the world's largest fisheries, it is necessary to understand the cumulative effects of multiple hydromedusan predation pressures on EBCs plankton community structure.

Hydromedusae prey resource use can be determined by taxon-specific feeding strategies. All hydromedusae use tentacles and oral lips to capture prey, but differences in nematocyst type (Purcell and Mills, 1988) and feeding behavior (Costello and Colin, 2002) define their feeding guilds. "Sit-and-wait" Trachymedusae (i.e. *Aglantha* spp.) and Anthomedusae (i.e. *Leuckartiara* spp., *Proboscydactyla* spp.) rely on prey motion to initiate encounters, and are capable of capturing active, hard-bodied prey such as copepods and crustacean nauplii larvae (Hansson and Kiørboe, 2006; Regula et al., 2009). "Current-feeding" Leptomedusae (i.e. *Clytia* spp., *Eutonina* spp. *Mitrocoma* spp.) entrain prey in the fluid vortices produced during their swimming behavior and consume mostly slow swimmers and passive prey such as other gelatinous taxa and invertebrate eggs (Purcell and Grover, 1990; Costello and Colin, 2002). However, medusan prey selection patterns and predation impact are not fixed, and temporal shifts in hydromedusan prey resource use and ingestion rates have been documented in coastal ecosystems (Hansson et al., 2005; Marques et al., 2015; Morais et al., 2017). It is unclear if these shifts in prey resource use indicate optimal feeding periods for these medusae and to what extent their trophic impact can vary across seasons and environmental conditions.

Although feeding strategies limit the types of organisms that hydromedusae capture, prey abundance and community composition ultimately control what predators consume (Miller et al., 2010). In the Northern California Current (NCC), temporal

variation in climate can lead to changes in the community structure of zooplankton (Bi et al., 2011; Suchman et al., 2012), which result in shifts between species interactions (Francis et al., 2012) and food web structure (Ruzicka et al., 2012). For example, studies focusing on larval fish predation have shown that temporal shifts in planktonic prey composition can modify the trophic level and niche of larval fishes (Brodeur and Pearcy, 1992). During warm and low-productivity years of the NCC, there is high species richness and a low abundance of planktonic prey. This causes a decrease in the dietary overlap of larval fishes and an increase in their trophic position. During cold, high productivity years of the NCC, the reverse scenario occurs and a low species richness coupled with high abundance of prey in low trophic levels cause an increase in larval fish diet overlap and a decrease in their trophic position, since the fish are feeding on prey that occupy lower positions in the food web (Brodeur and Pearcy, 1992).

In contrast to vertebrate carnivores such as fish, hydromedusan effects on the NCC food web are poorly understood. Although time-series studies show a negative correlation between hydromedusa abundance and krill egg abundance in the NCC (Francis et al., 2012), this correlation is limited to one hydromedusan species (*Clytia* sp.), and does not discern the biological interactions (competition, predation, etc.) that link hydromedusan abundance in the NCC to zooplankton community structure.

The goal of this study was to quantify the seasonal variation of hydromedusan trophic interactions in an EBC upwelling zone. We analyzed the gut contents of individual hydromedusae and background prey along two longitudinal transects in the NCC during summer and winter of 2018 -2019. The data were used to determine whether prey

consumption patterns and prey selection of co-occurring hydromedusan species shift between seasons with distinct productivity regimes and patterns of prey availability.

2. METHODS

2.1. Field sampling

During winter (Mar. 2-14, 2019) and summer (Jul 3-12, 2018 and Jul, 14-27, 2019), we collected mesozooplankton from five stations along two cross-shelf transects located in the NCC: the Newport Hydrographic line (NH) and the Trinidad Head line (TR) (Table SI). Stations along the TR transect were closer to each other due to the narrower shelf and more pronounced shelf slope in this location (Fig. 1). Mesozooplankton was sampled at fixed locations during the day with the use of a coupled multiple opening-closing net and environmental sensing system with different opening and mesh sizes (MOCNESS; MOC 1= 1 m^2 aperture, 333 μm mesh, MOC 2= 4 m^2 aperture, 1-mm mesh; Guigand et al., 2005).

After the nets were recovered, samples were placed in a chilled petri dish for selection of hydromedusae. Hydromedusae were picked from the surface depth stratum (0-25 m) since the animals spent less time in the net (~10 min) thus decreasing the chances of gut evacuation. We obtained as many hydromedusae as possible, and we selected individuals for gut content analysis that did not have any visible damage on their swimming bells and tentacles. Selected individuals were rapidly fixed in a solution of formalin in seawater (~4% v/v). Subsequently, hydromedusa guts were inspected under a dissecting microscope. Prey were extracted from the gastrovascular cavity and from the radial canals. To quantify the background prey community, a ring-net (0.2 m^2 aperture,

100 µm mesh) was towed vertically from 0-25 m at the same stations where hydromedusae were collected (Fig. 1). Samples were processed in the lab following Postel et al. (2000). Subsamples (1-5 ml) with >200 planktonic organisms were taken with a Stempel pipette. The organisms in the subsample were enumerated and identified to the lowest possible taxonomic level.

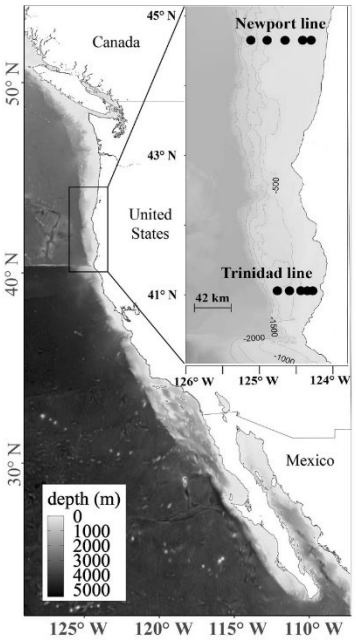

Fig. 1. Sampling stations (black points) in the Northern California Current where hydromedusae and available prey were collected during summer (July 3-12, 2018 and July 14-27, 2019) and winter (March 2-14, 2019). Coordinates for each station are given in Table S1.

After the nets were recovered, samples were placed in a chilled petri dish for selection of hydromedusae. Hydromedusae were picked from the surface depth stratum (0-25 m) since the animals spent less time in the net (~10 min) thus decreasing the chances of gut evacuation. We obtained as many hydromedusae as possible, and we selected individuals for gut content analysis that did not have any visible damage on their swimming bells and tentacles. Selected individuals were rapidly fixed in a solution of formalin in seawater (~4% v/v). Subsequently, hydromedusa guts were inspected under a

dissecting microscope. Prey were extracted from the gastrovascular cavity and from the radial canals. To quantify the background prey community, a ring-net (0.2 m^2 aperture, 100 μm mesh) was towed vertically from 0-25 m at the same stations where hydromedusae were collected (Fig. 1). Samples were processed in the lab following Postel et al. (2000). Subsamples (1-5 ml) with >200 planktonic organisms were taken with a Stempel pipette. The organisms in the subsample were enumerated and identified to the lowest possible taxonomic level.

2.2. Gut content processing and quantification

To reduce errors in the gut content data due to net feeding and gut emptying (Miller et al., 2010) we quantified only the items that were found inside the gastrovascular cavity of the medusae. Prey found in the aliquot containing the preserved medusae, medusae with damaged feeding structures and prey captured but not ingested were not quantified. Net feeding does not alter hydromedusan gut content measurements, since hydromedusae retract their tentacles and do not capture prey when disturbed (Costello and Colin, 2002).

The number of prey of type i inside the guts (a_i) was corrected by prey digestion rates (Sullivan et al., 1997). Species-specific digestion rates were obtained from the literature when available and extrapolated from similar prey types when unavailable (Table I). Digestion rates of invertebrate eggs by hydromedusae were obtained by feeding single *Centropages abdominalis* and *Oithona* sp. eggs to *Clytia gregaria* in the laboratory and noting the time until the ingested eggs were not visible in the gastrovascular cavity. Since digestion rates are affected by temperature (Martinussen and Bamstedt, 2001), these feeding experiments were done at constant 12ºC, which is the same temperature as

the water from which the hydromedusae were collected. This temperature is also within the range of the sea surface temperature reported in Oregon and California during winter and summer of 2018-2019 (Thompson et al., 2019). For each prey type in the gut, the normalized number of prey (N_{ai}) was calculated as $N_{a_i} = \frac{a_i}{digestion\ time}$. The sum of all normalized number of prey (N_d) was obtained by $N_d = \sum_{i=n}^{n} N_{a_i}$. A conversion factor (CF) was then estimated by $CF = \frac{d}{N_d}$, where d was the total number of prey in the guts. The corrected number of prey of type i (a_{di}) was then obtained by $a_{di} = N_{a_i} \times CF$. Subsequent analysis used a_d as the accurate estimation of ingested prey, with units of $\frac{\#prey}{individual}$ (Sullivan et al., 1997; Costello and Colin, 2002).

2.3. Shifts in prey seasonal abundance and consumption patterns of the hydromedusan community

One-way Permutational Analysis of Variance (PERMANOVA) based on a Bray-Curtis similarity index was performed with environmental prey abundance data and gut content data to determine whether prey composition changed in the water column and in the hydromedusan guts in winter vs. summer. In addition, Welch's t-tests were performed to compare the mean prey abundances in winter vs. summer. Non-metric multidimensional scaling (NMDS) was used to visualize seasonal shifts of prey assemblages in the environment and in the hydromedusan guts. These analyses were performed using the "vegan" package (ver. 2.5-7, Oksanen et al., 2020) in the R statistical software (ver. 4.0.3). Since gut content data for *Clytia gregaria* and *Eutonina indicans* had a large sample size (n=103 and n=36, respectively) and were collected during both

seasons, we focused our subsequent analysis of prey selectivity and trophic niche on these species (Fig. 2).

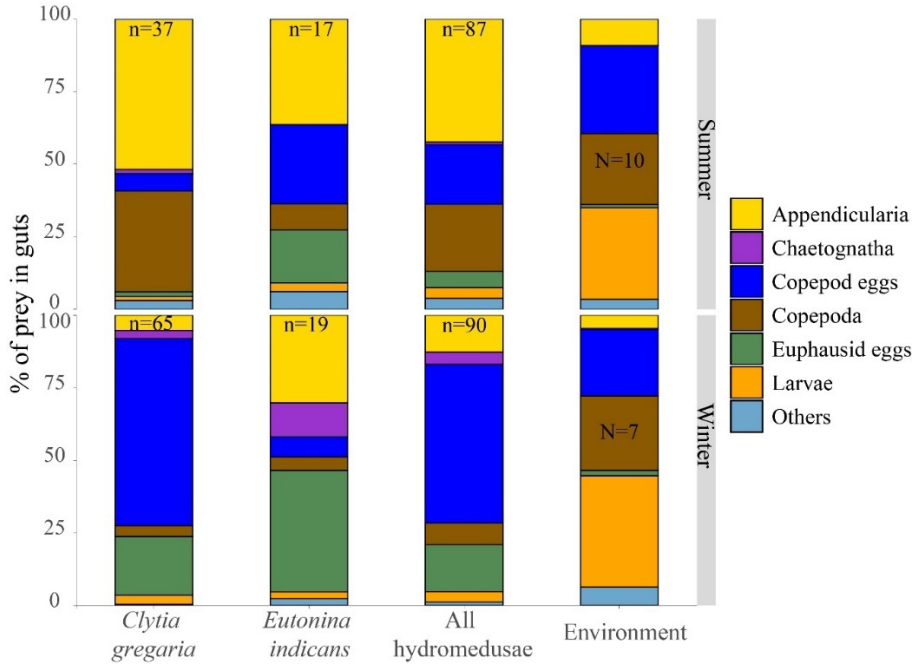

Fig. 2. Percentage of each prey type in the guts of *C. gregaria*, *E. indicans,* all hydromedusae and prey in the environment during summers of 2018 and 2019 and winter of 2019 in the Northern California Current. N= number of ring net samples analyzed, n=number of individuals with gut contents.

2.4. Determination of hydromedusan prey selectivity and ingestion rates

Gut content data for *C. gregaria* and *E. indicans* were pooled for each station and sampling date. Prey selectivity occurring in each station and season was quantified using Pearre's (1982) selectivity index, C:

$$C = \pm\sqrt{\frac{\chi^2}{n}} \quad (1)$$

where,

$$\chi^2 = \frac{n(a_d b_e - b_d a_e)^2}{abde} \quad (2)$$

with "*a*" as the prey species of interest inside the guts (a_d) and plankton (a_e), "*b*" as all other species in diet (b_d) or plankton (b_e), "*d*" and "*e*" are the total prey in diet and plankton, respectively, and "*n*" is the total number of prey in guts and zooplankton subsample. *C* is dimensionless and ranges from -1 to +1, with zero values representing no selection, positive values representing positive selection, and negative values representing negative selection.

Theoretical ingestion rates for individual hydromedusae (IR, $\frac{prey\ consumed}{day}$) were calculated as:

$$IR = \frac{G}{DT} \times 24$$

Where *G* is the corrected number of prey in guts ($G = a_{di}$, see above) and *DT* is prey digestion time (Table I). To address whether seasons modify medusan trophic impact, we used previously published values of prey carbon content (Table I) and added all the carbon contained in each hydromedusa to calculate the individual daily carbon ingestion rate. Due to unequal sample sizes and non-normality of the data, a Kruskal-Wallis (KW) test was used to compare the ranked average daily carbon ingestion rate for each hydromedusan species between seasons. The data distribution was analyzed with the "fitdistrplus" package (Delignette-Muller and Dutang, 2019) in R (ver. 4.0.3).

Table I. Summary of the sampling stations in the Northern California Current, sampled during summers of 2018, 2019 and winter of 2019 (locations provided using a decimal coordinate system).

Transect	Station number	Latitude	Longitude
Newport line	1	44.65207 N	124.294 W

Newport line	2	44.65232 N	124.41W
Newport line	3	44.65177 N	124.648 W
Newport line	4	44.6519 N	124.893 W
Newport line	5	44.65225 N	125.115 W
Trinidad line	1	41.05834 N	124.272 W
Trinidad line	2	41.05798 N	124.346 W
Trinidad line	3	41.05867 N	124.434 W
Trinidad line	4	41.0583 N	124.588 W
Trinidad line	5	41.05784 N	124.753 W

3. RESULTS

3.1. Hydromedusan predators and their prey in the NCC

Eleven species of hydromedusae were collected during the three cruises. From 416 medusae dissected for gut contents, 181 collected individuals had prey in their guts. Only three individuals (one *Clytia gregaria* and two *Eutonina indicans*) were collected in summer 2018. A total of 632 prey items were identified (after digestion time corrections); during winter there was an average of 2.26±0.16(±SE) prey in each medusan gut, and during summer there was an average of 1.90±0.17 prey in each medusan gut. Nine hydromedusae (six *C. gregaria*, one *E. indicans* and two *Liriope tetraphylla*) had very digested gut contents that were not possible to identify, thus we excluded these individuals from subsequent analyses. Only *Proboscidactyla flavicirrata, C. gregaria, E. indicans* and *L. tetraphylla* were collected during both winter and summer. *Aegina citrea* was only collected during winter, and *Bougainvillia* sp., *Corymorpha* sp., *Leuckartiara*

sp., *Sibogita* sp., *Mitrocoma cellularia*, and *Solmissus incisa* were collected only during summer.

The hydromedusan species collected in both winter and summer consumed copepods, appendicularians, and invertebrate eggs (detailed prey taxa presented in Table S2, percentage of prey ingested in Table S3). Ingested appendicularians were from the genus *Oikopleura*, copepod prey included the genera *Centropages*, *Acartia*, *Pseudocalanus*, and *Oithona.* Eggs were classified according to size and presence of these items in the ring net tows as either euphausiid eggs (~500 µm diameter, Ambriz-Arreola et al., 2015; Zeman et al., 2018) or copepod eggs (50-180 µm diameter, Kiørboe et al., 1985; Runge, 1984; Sabatini and Kiørboe, 1994). Invertebrate larvae included mostly nauplii, zoea, veligers, polychaetes, and bryozoans. "Others" included hydromedusae, siphonophores, cladocerans and foraminifera. All four orders of hydromedusae found in this study consumed copepods and appendicularians. Anthoathecata and Limnomedusae also consumed invertebrate larvae. Larvae were not found in the guts of Leptomedusae and Narcomedusae.

3.2. Seasonal ambient prey availability

Prey community composition was similar in both seasons (PERMANOVA $F=1.8228$, $p=0.144$), but some prey abundances were higher during summer compared to winter (Table II). Significant increases in abundances during summer occurred for appendicularians and copepod eggs. Appendicularians increased from $496 \pm 165 \frac{ind.}{m^3}$ (~4.5% of total prey available) during winter, to $1560 \pm 344 \frac{ind.}{m^3}$ (~9% of total prey available) during summer (Welch's $t=2.79$, $p=0.016$).

Table II. Carbon weight and digestion rates used to correct prey counts in the guts.

Prey type	Carbon weight (µg)	Digestion rate (hours)	Temperature (°C)	Sources
Adult copepods (*Acartia* sp.)	3	4	12-14	Harris et al. (1982), Larson (1987), Durbin & Durbin (1992), Suchman et al. (2008)
Copepod eggs	0.1	5.5	12-14	This study
Copepod nauplii	0.1	4***		Larson (1987)
Appendicularia (*Oikopleura* sp.)	0.5	2	12-14	King et al. (1980), Larson (1987)
Chaetognatha	6.64	2*		Canino & Grant (1985) Suchman et al. (2008)
Krill eggs	3.2	5.5**	12-14	This study
Invertebrate larvae	4*	4*	12-14	Uye (1982), Suchman et al. (2008)
Invertebrate larvae (barnacle nauplii)	0.5	4***	12-14	Larson (1987)
Veliger larvae	0.2	6	9.1	Suchman et al. (2008)
Others*	2.3(1.5)	4.4(1.7)	9.1	Suchman et al. (2008)

*average of values for carbon weight and digestion time obtained for polychaetes, molluscs, and gelatinous taxa from Suchman et al. (2008). ** rate extrapolated from copepod eggs digestion rate obtained in this study. *** rate extrapolated from adult copepods digestion rates.

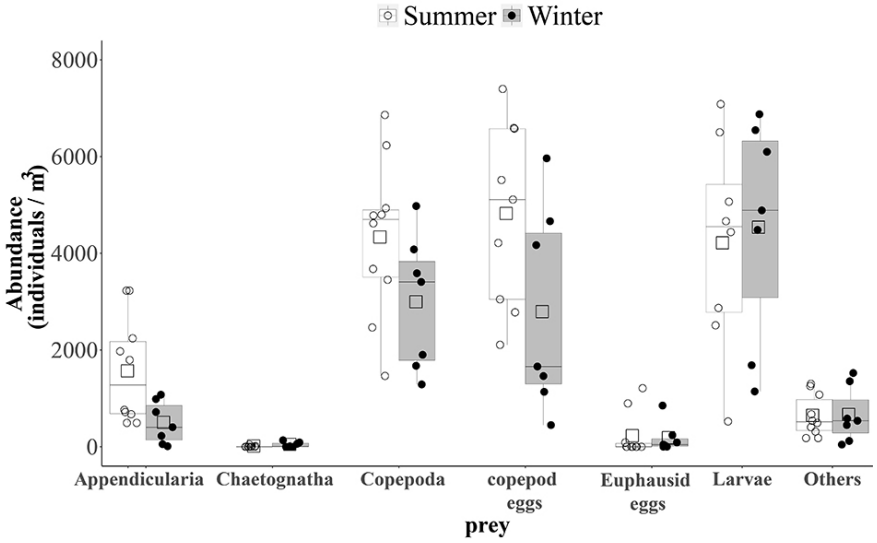

Fig. 3. Major prey groups collected with a 100 µm ring net in Northern California Current surface waters (0-25 m) during winter of 2019 and summer of 2018 and 2019. Open and solid circles represent abundances from a sample for summer and winter, respectively; open squares represent the average abundance for each prey taxa in each season. Bars represent the 25th and 75th quantiles, horizontal line inside the bar represents median, and whiskers represent 95% confidence intervals. Prey composition was similar during both seasons (PERMANOVA F=1.8228, p=0.144).

Copepod eggs increased from 2786 ±798 $\frac{ind.}{m^3}$ (~23% of total prey available) during winter, to 5563 ± 935$\frac{ind.}{m^3}$ (~30.4% of total prey available) during summer (Welch's t=2.26, p=0.030). There was an appreciable increase in copepod abundance from 2988 ± 523 $\frac{ind.}{m^3}$ (~25% of total prey available) during winter, to 4329 ± 514$\frac{ind.}{m^3}$ (~24% of total prey available) during summer (Table II, Fig. 3) but this increase was not significant (Table S4).

3.3. Seasonal changes in prey resource use by hydromedusan predators

Although similar prey were available to hydromedusae during winter and summer, there were seasonal differences in the type of prey ingested by the hydromedusae (PERMANOVA F=10.337, p=0.001, Table II, Table S5, Fig. 4A). More appendicularians and copepods were ingested during summer, and more copepod eggs, euphausiid eggs, and chaetognaths were ingested during winter. These changes in prey resource by the hydromedusan community were likely driven by *C. gregaria*, since this species represented 57% of all the hydromedusae collected. The proportion of prey inside *C. gregaria*'s gut changed substantially between seasons. During winter, ingested prey included copepod eggs (60%), krill eggs (13%), and chaetognaths (6%) (Fig. 2a). During summer, however, most of the ingested prey were appendicularians (mostly from the genus *Oikopleura,* 46%) and adult copepods (32%, Fig. 2b) (PERMANOVA F=17.861, p=0.001, Fig. 4B, Table S5). Prey ingested by *E. indicans* remained similar in both seasons (PERMANOVA F=1.0987, p=0.345, Fig. 4C, Table S5).

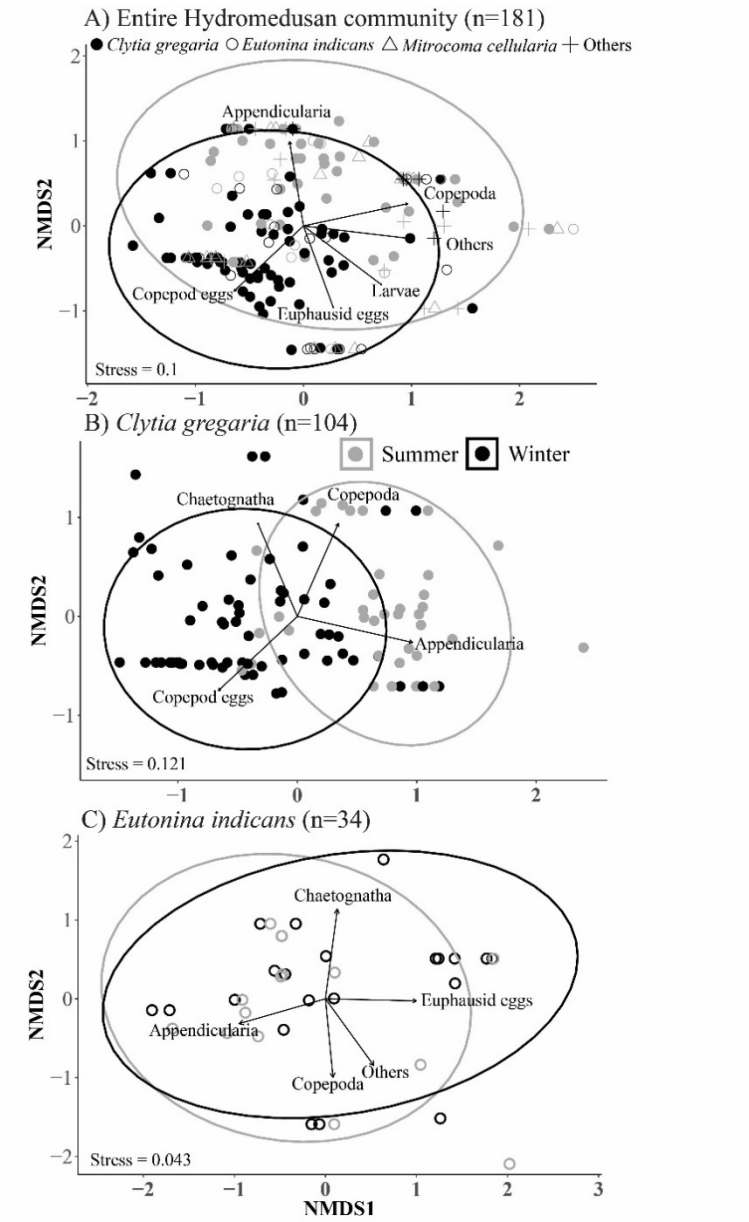

Fig. 4. Non-parametric multidimensional scaling (NMDS) plots with points representing individual medusae for A) all hydromedusae collected, B) *Clytia gregaria* and C) *Eutonina indicans*. Arrows represent the direction along the axes where the prey counts for each taxon in the guts increase. Ellipses indicate 95% confidence intervals.

3.4. Prey selectivity of sympatric hydromedusae

Prey selection patterns, indicated by Pearre's *C* selectivity indices, were similar between *C. gregaria* and *E. indicans* for most prey irrespective of seasons: there was positive selection for appendicularians and chaetognaths, no selection for copepods, and negative selection for invertebrate larvae (Fig. 5, Table III). However, selection for copepod eggs varied seasonally and was 5-9 times greater during winter (0.25 ±0.08 for *C. gregaria* and 0.43 ±0.1 for *E. indicans*) than summer (-0.04 ±0.04 for *C. gregaria* and -0.04 ±0.07 for *E indicans*, Fig. 5, Table III).

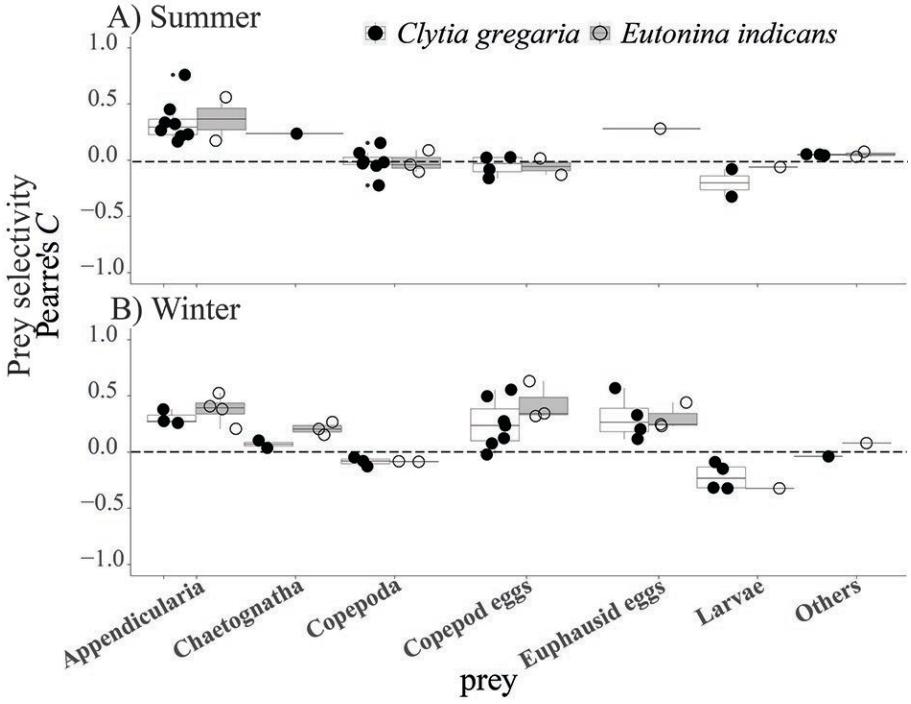

Fig. 5. Average prey selectivity (Pearre's C) values for eight major prey categories encountered in *C. gregaria* and *E. indicans* collected in the Northern California Current for A) summer and B) winter. Individual data points are overlaid on box, Bars represent the 25th and 75th quantiles, horizontal line inside the bar represents median and whiskers represent 95% confidence intervals.

Table III. Average (± standard error) corrected prey counts in *Clytia gregaria* and *Eutonina indicans* guts and prey abundances in the environment. Two averages are presented for ingested prey: (1) Average prey ingested by individual medusae (no. of individuals in parentheses next to each value) and (2) average prey ingested by station (underlined values, N= no. of stations sampled, top of each column).

Prey category	Summer			Winter		
	C. gregaria N=8	*E. indicans* N=4	Environment N=10 $\left(\frac{ind.}{m^3}\right)$	*C. gregaria* N=7	*E. indicans* N=4	Environment N=7 $\left(\frac{ind.}{m^3}\right)$
Appendicularia	2.9 ± 0.6 (26) <u>11.2 ± 5.2</u>	2.5 ± 0.7 (7) <u>4.1 ± 2.4</u>	1560 ± 344	2 ± 0.2 (18) <u>4.9 ± 2.6</u>	1.2 ± 0.3 (8) <u>5.5 ± 2</u>	496 ± 165
Chaetognatha	1 (1) <u>0.2 ±0.2</u>	0	6 ± 4	1.4 ± 0.2 (9) <u>1.2 ± 0.5</u>	0.9 ± 0.5 (3) <u>1 ± 0.4</u>	42 ±20
Copepod eggs	2.6 ± 0.7 (9) <u>2.9 ± 1.5</u>	2.3 ± 0.6 (9) <u>1.2 ± 1.1</u>	5563 ± 935	3.2 ± 0.3 (53) <u>19.9 ± 6.0</u>	3.3 ± 1.0 (9) <u>10.6 ± 4.1</u>	2786 ±798
Copepoda	1.8 ± 0.4 (22) <u>4.4 ± 2.4</u>	0.8 ± 0.3 (3) <u>0.8 ± 0.3</u>	4329 ± 514	1.6 ± 0.2 (10) <u>1.6 ± 1</u>	<u>0.8 ± 0.2 (3)</u> <u>0.4 ± 0.3</u>	2988 ± 523
Euphausid eggs	0.7 ± 0.1 (2) <u>0.1 ± 0.1</u>	1.9 ± 1.4 (3) <u>1.3 ± 1.3</u>	220 ±141	2.7 ± 0.6 (19) <u>7.1 ± 3.0</u>	<u>0.9 ± 0.2 (10)</u> <u>3.0 ± 1.0</u>	179 ± 116
Larvae	1.1 ± 0.02 (2) <u>0.2 ± 0.1</u>	1 (1) <u>0.3 ± 0.1</u>	4038 ±1277	1.6 ± 0.4 (7) <u>1.6 ± 0.8</u>	0.6 ± 0.1 (2) <u>0.2 ± 0.2</u>	4532 ± 869
Others	0.9 ±0.3 (4) <u>0.3 ± 0.2</u>	1.6 ± 0.6 <u>0.5 ± 0.3</u>	641 ± 134	1.8 ± 0.8 (2) <u>0.2 ± 0.2</u>	1.5 (1) <u>0.2 ± 0.2</u>	659 ± 216

3.5. Theoretical prey and carbon ingestion rates by hydromedusae in the NCC

Based on calculated ingestion rates, individual hydromedusae theoretically ate between 3-35 prey per day. For all hydromedusae, over both seasons, the highest ingestion rates were on appendicularians which were higher during summer than winter (Table IV). Despite the relative changes in prey ingestion rates by hydromedusae, carbon ingestion rates remained similar during winter and summer for both *C. gregaria* (37.12±6.0 $\frac{\mu g\ C}{ind.\times day}$ in winter, 37.25±6.9 $\frac{\mu g\ C}{ind.\times day}$ in summer; KW X^2 =3.6688, df=1, p=0.554) and *E. indicans* (24.0±7.5 $\frac{\mu g\ C}{ind.\times day}$ in winter, 20.0±8.7 $\frac{\mu g\ C}{ind.\times day}$ in summer; KW X^2 =0.783, df=1, p=0.376, Fig. 6). These carbon ingestion rates represent ~40% of the total body carbon of *C.gregaria* but only 4% of the total body carbon of *E. indicans* (body carbon data obtained from Larson, 1986 and Li et al. unpubl. data).

Table IV. Average Pearre's *C* prey selectivity value averaged across sampling stations (± standard error) for *Clytia gregaria* and *Eutonina indicans*. All gut content data were corrected by digestion time for each prey type. Numbers within parentheses are sample sizes.

Prey type	Hydromedusae species			
	Winter		Summer	
	Clytia gregaria	*Eutonina indicans*	*Clytia gregaria*	*Eutonina indicans*
Appendicularians	0.30±0.04(3)	0.38± 0.06(4)	0.36±0.07(8)	0.38± 0.19(2)
Chaetognatha	0.07± 0.03(2)	0.21± 0.03(3)	0.25(1)	-
Copepod eggs	0.25± 0.08(7)	0.43± 0.10(3)	-0.04± 0.04(4)	-0.04± 0.07(2)
Copepods	-0.09± 0.02(3)	-0.09± 0.002(2)	-0.003± 0.04(7)	-0.005± 0.06(3)
Krill eggs	0.30± 0.10(4)	0.30±0.07(3)	-	0.29(1)
Invertebrate larvae	-0.22± 0.06(4)	-0.32(1)	-0.19± 0.12(2)	-0.05(1)
Others	-0.04(1)	0.08(1)	0.06± 0.003(3)	0.07± 0.02(2)

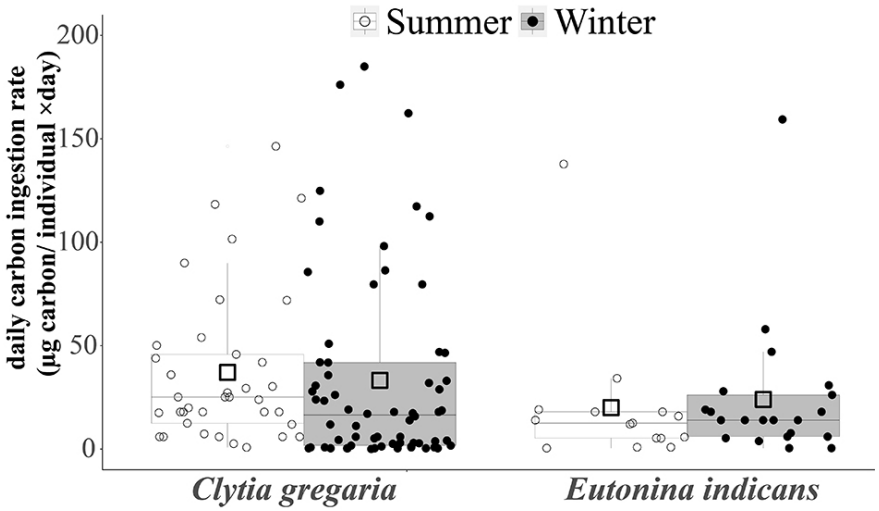

Fig. 6. Daily carbon ingestion rates for individual *C. gregaria* and *E. indicans* in surface waters of the Northern California Current during winter of 2019 and summer of 2018 and 2019. Both *C. gregaria* and *E. indicans* consumed similar amounts of carbon during both seasons (KW X^2 =0.78388, df=1, p=0.376). Individual data points are overlaid on box, Bars represent the 25th and 75th quantiles, horizontal line inside the bar represents median and whiskers represent 95% confidence intervals.

4. DISCUSSION

Cnidarian hydromedusae are ubiquitous members of plankton communities in Eastern Boundary Currents (EBCs) such as the Humboldt Current (Rodriguez et al., 2017), the Canary Current (Berraho et al., 2015) and the Benguela Current (Pagés et al., 1992; Buecher and Gibbons, 2003). However, very little attention has be given to hydromedusan predation in these systems. Here, we provide the first insight into predation by small hydromedusae in the Northern California Current (NCC). The hydromedusan genera found in this study are the same as the ones found in other plankton communities (Pagés et al., 1992; Miglietta et al., 2008; Rodriguez et al. 2017), so this study provides a first approximation of hydromedusan trophic impact in coastal

ecosystems with seasonal upwelling. Despite minimal differences in hydromedusan prey community composition between winter and summer in the NCC, hydromedusan prey ingestion and selection shifted between seasons, from the ingestion of mostly invertebrate eggs during winter to appendicularians and copepods during summer (Fig. 4A).

This shift in prey ingestion is largely driven by the seasonal shift in prey preference by *Clytia gregaria* (Fig.4B), an abundant hydromedusa in the NCC (Francis et al., 2012; Briseño-Avena et al., 2020), and other upwelling systems (Buecher and Gibbons, 2003; Miglietta et al., 2008) This species was collected in much larger quantities (n=117) than *Eutonina indicans* (n=44). *Eutonina indicans* showed no shift in prey ingestion between seasons (Fig. 4C). However, both species had high prey selectivity for appendicularians during both seasons, and enhanced selectivity for copepod and euphausiid eggs during winter (Fig. 5). This high selectivity corresponds to the high ingestion rates obtained for these prey types (Table IV), suggesting that hydromedusae could exert a top-down control on appendicularian and copepod populations, due to the predation on adults and eggs throughout the year, and potentially compete with other planktonic predators for prey.

4.1.Hydromedusan predation impacts in the NCC

Hydromedusae might have limited effects on pelagic food webs due to their small guts and short satiation times (i.e. time to gut fullness), which results in low prey ingestion rates (Colin et al., 2005; Hansson and Kiørboe, 2006). However, seasonal peak abundances of hydromedusae can be as high as those of copepods (the most abundant planktonic taxa) (Hansson et al., 2005) or even higher than copepods in some portions of the NCC (Swieca et al., 2020), and multiple hydromedusan species can co-occur in

pelagic environments (Costello and Colin, 2002). Further, the impact of hydromedusan predation might be species-specific. In Limfjorden, Denmark, a neritic system, the dominant hydromedusae, *Sarsia* sp. and *Rathkea octopunctata*, have prey clearance rates of 0.3 $\frac{liters}{ind.\times day}$ and 0.06 $\frac{liters}{ind.\times day}$ respectively (Hansson et al., 2005). The predation rates of hydromedusae in Limfjorden are lower than those of scyphomedusae and much lower than the theoretical maximum clearance rates for the hydromedusa *C. gregaria* (~29.8$\frac{liters}{ind.\times day}$) (Corrales-Ugalde and Sutherland, 2020). Future research could explore the cumulative impact of the entire hydromedusan community relative to other zooplankton predators in the NCC and other productive ecosystems.

If we consider *Clytia gregaria*'s average abundance off the central Oregon Coast (6.7 ±0.5 $\frac{ind.}{m^3}$, Briseño-Avena et al., 2020), and the daily carbon ingestion rate presented in this study, the theoretical mass of carbon that the hydromedusan community can consume is 0.25 $\frac{mg\ C}{m^3\times day}$, which is three orders of magnitude lower than the amount of carbon an individual scyphomedusa in the NCC was estimated to consume during summer (4-41 $\frac{mg\ C}{ind.\times day}$, Suchman et al., 2008). However, the year-round presence of hydromedusan predators could represent a consistent carbon flux pathway that is present when there are no large scyphomedusae. This carbon consumption rate could further be increased in patches with higher hydromedusan abundance (Swieca et al., 2020).

Based on the theoretical ingestion rates reported in the present study, hydromedusae could be consuming globally 0.98-3.9 $\frac{Pg\ C}{year}$, which is comparable to the 2.4 $\frac{Pg\ C}{year}$ estimated to be consumed globally by epipelagic cnidarians (Luo et al., 2020). These

numbers show that, first, hydromedusae might substantially contribute to the global cnidarian carbon consumption. Second, it is likely that during high hydromedusae abundance and during periods of high productivity in eastern boundary currents, hydromedusan ingestion rates are above the global average ingestion rates by other medusae.

4.2. Seasonal abundance patterns of hydromedusan prey

Hydromedusan prey abundances were similar during winter of 2019 and summer of 2018 and 2019 in the NCC (Fig. 3), which contrasts with the well documented increase in mesozooplankton abundance during summer (Peterson and Miller, 1977). Such similarities in prey abundance between seasons could be the result of the sustained presence of copepods in nearshore and shelf waters during both winter and summer. During winter, the poleward flowing Davidson Current brings warm-water neritic copepods close to shore (Hooff and Peterson, 2006). This copepod species assemblage was reported to be abundant year-round during 2018 and 2019 in the Newport Hydrographic Line, following the positive to near neutral temperature anomalies on Oregon's continental shelf and shelf slope during this period (Thompson et al., 2019). During summer, both warm-water subtropical copepods and subarctic copepod species assemblage were present nearshore (Thompson et al., 2019).

Subarctic copepods are generally larger and have higher energetic value due to their lipid storage, and are associated with high energy transfer efficiency to upper trophic levels when they are consumed by predators (Hooff and Peterson, 2006). This source of high quality food is crucial for the survival of predators with high energetic demands such as larval fishes (Trudel et al., 2005). However, medusozoan jellyfish have

much lower energetic requirements compared to fish (Pitt et al., 2013; Acuña et al., 2011) and might be able to maintain optimal growth and reproductive rates with prey of variable nutritional qualities, but even they might still benefit from nutritious subpolar copepods during summer.

4.3. Trophic position of hydromedusae in the NCC

Hydromedusae in the NCC fed consistently across seasons on primary consumers (appendicularians, copepods and copepod eggs). Seasonal community transitions together with spawning periods of these organisms in the NCC results in these organisms being available for consumption throughout the year. For instance, the predominant crustacean species present during winter are planktonic grazers such as the copepod *Clausocalanus* sp., *Calanus pacificus* and the euphausiid *Euphausia pacifica* (Peterson and Miller, 1977). Both *C. pacificus* and *E. pacifica* produce eggs during winter (Brinton, 1967; Mullin, 1991) and are likely the source of the copepod and invertebrate eggs that the hydromedusae ingested during winter. During summer, several copepod species that were present in our samples (*Paracalanus parvus*, *Oithona* sp.) release or carry eggs (Peterson *et al.,* 1979). In addition, appendicularians (mainly *Oikopleura* sp.) were abundant (Fig. 3). These seasonal shifts between plankton community assemblages ensures availability of food for hydromedusae, which are able to feed on several prey types due to their diverse array of feeding strategies (Mills, 1981 ; Purcell and Mills, 1988; Costello and Colin, 2002; Corrales-Ugalde and Sutherland, 2021).

Given that spatial and temporal overlap of larval fishes and hydromedusae has been documented in the NCC (Swieca et al., 2020), it is relevant to consider how the seasonal shifts in hydromedusan prey preference determine competitive interactions with

fishes. During winter, hydromedusae could compete for prey with the English sole larvae (*Parophrys vetulus*), which feed on appendicularians (Gadomski and Boehlert, 1984), butter sole larvae (*Isopsetta isolepis*), which feed on copepodites (Gadomski and Boehlert, 1984), and sand lances (*Ammodytes hexapterus*), which feed on appendicularians and adult copepods (Hipfner and Galbraith, 2014). During summer, hydromedusae could be competing for prey with sandab larvae (*Citharichthys* spp.) and with northern anchovy (*Engraulis mordax*), both of which feed on copepodites and adult copepods (Schmitt, 1986; Rackowski and Pikitch, 1989). Going forward, studies with better spatial and temporal resolution that focus on dietary niche overlap between hydromedusae and other predators are needed to determine the nature of interspecific predatory interactions in the NCC zooplankton community.

4.4. Spatial variation of feeding interactions and prey selectivity in the NCC

Physical features such as the Columbia River Plume and upwelling fronts determine the patterns of plankton zonation in the NCC (Peterson et al., 1979; Briseño-Avena et al., 2020; Swieca et al., 2020). For instance, certain copepod prey (i.e. *Centropages abdominalis*) that are ingested by Leptomedusae such as *Clytia gregaria* are restricted to nearshore and neritic environments (Peterson and Miller 1977, Corrales-Ugalde and Sutherland, 2020). Euphausiids also show distinct zonation in their distribution: *Thyssanoessa spinifera* is restricted to coastal environments (Smith and Adams, 1988), whereas *Euphausia pacifica* can be abundant in offshore, more oceanic environments and these species rear eggs in different times of the year (Dorman et al., 2005). However, the low spatial resolution of our station layout does not allow for inferences of how location affects hydromedusan prey selectivity, since hydromedusae

were not consistently collected in all stations. The data presented here can inform future studies with *in situ* plankton camera recorders that can accurately determine the fine-scale spatial overlap between predators and prey (Swieca et al., 2020).

4.5. Interannual variability in hydromedusan predation and trophic role in the NCC

Given the limitations imposed by our unequal sample sizes between summer of 2018 compared to 2019, this study was unable to address how interannual variation in NCC oceanography affects hydromedusan predation patterns. Food web modelling of the NCC has concluded that the primary production that passes through the jellyfish functional group is similar across years (Ruzicka et al., 2012). A closer look at the interactions among community members of the NCC zooplankton shows strong negative effects of *Clytia* sp. on invertebrate eggs and larvae during warm periods (Francis et al., 2012). Our gut content data effectively show the preference of *C. gregaria* for copepod and euphausiid eggs during 2019 (Fig. 5), during weak El Niño conditions (Thompson et al., 2019). During winter and summer of 2019, the total number medusae collected (with and without gut contents) were four and three times more (n=209 during winter 2019, n=155 during summer 2019) than summer of 2018 (n=55). This suggest that the negative interaction between invertebrate eggs/larvae and hydromedusae might be driven by an increase in hydromedusan abundance in the NCC during warm periods.

CHAPTER V

CONCLUSIONS

It is imperative to understand the functioning principles of ecological systems to predict the spatial and temporal scales at which ecosystem services will be affected due to global climate change (Scholes 2017). However, ecological studies usually occur at reduced specific scales, and studies that seek to connect different scales are hard to perform (Prairie et al. 2012). By using a standardized mechanistic framework to relate organismal-scale interactions to larger scale processes such as ingestion rates, this work shows how specific behavioral and morphological traits of tentaculate gelatinous predators associate with higher feeding efficiencies (Chapters II and III) and how such traits can be associated to relevant carbon transfer pathways in marine food webs (Chapter IV).

For instance, in chapter I, I showed how the alternation between passive sinking and active feeding behaviors defines the trophic niche of *Clytia gregaria*, allowing this species to capture both passive prey and fast-swimming, flow sensing prey like copepods (Corrales-Ugalde & Sutherland, 2021). This explains the ability of this species to shift prey preferences in the Northern California Current (NCC), from copepod eggs during winter to copepods during summer (Chapter III, Corrales-Ugalde et al. 2021). The combination of these results suggests that swimming behavior of tentaculate predators such as hydromedusae is a key trait that influences the function and structure of pelagic communities and ecosystems (Kiørboe et al. 2018). Including morphology and behavior traits in functional models of large marine

ecosystems will allow for testing of predictions of species interactions in intermediate levels of marine food webs (Fig. 1).

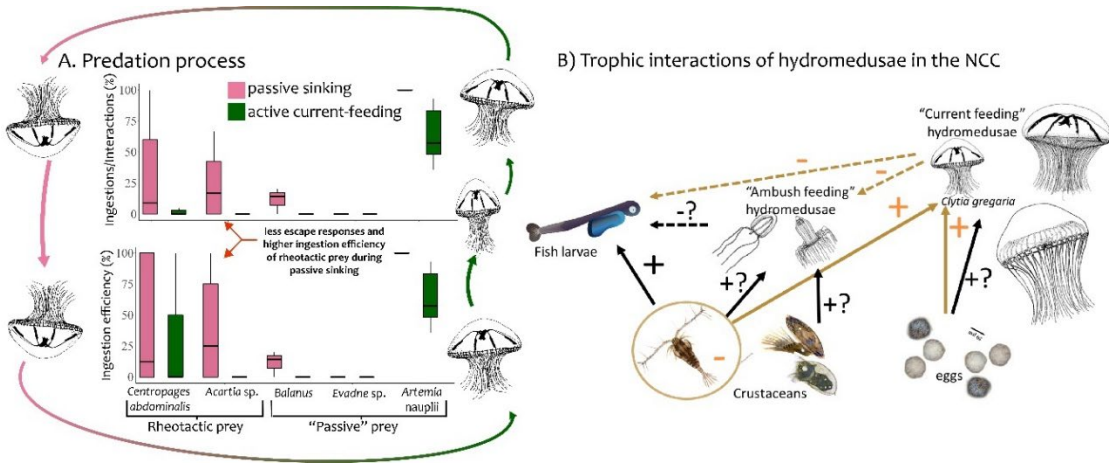

Figure 1. (A)The effects of *Clytia gregaria'*s feeding behavior on the ingestion efficiency of different prey types determines (B) the direct and indirect species interactions that occur between this hydromedusan species and other planktonic organisms (yellow lines) in the Northern California Current. Competitive interactions are represented as dashed lines and consumptive interactions are represented as solid lines.

In addition, this study highlights the relevance of fluid motion as a structuring factor of predator-prey relationships in the plankton. First, it acts as a defining variable of the trophic niches of tentaculate predators, since their feeding behaviors present intrinsic values of fluid deformation rates that might be above or below the mechanical sensing capabilities of their prey (Chapter II, Corrales-Ugalde & Sutherland 2021). Second, low levels of ambient turbulence can increase prey motility while not affecting the patterns of feeding behavior and tentacle deployment of hydromedusae, effectively increasing the encounter rates between these predators and their prey (Chapter III, Fig. 2). This might explain the discrepancy of theoretical prey ingestion rates calculated from settings with no flow (i.e. Chapter II), where predicted

ingestion rates are much higher compared to ingestion rates derived from gut content analysis of wild caught medusae (Hansson et al. 2005).

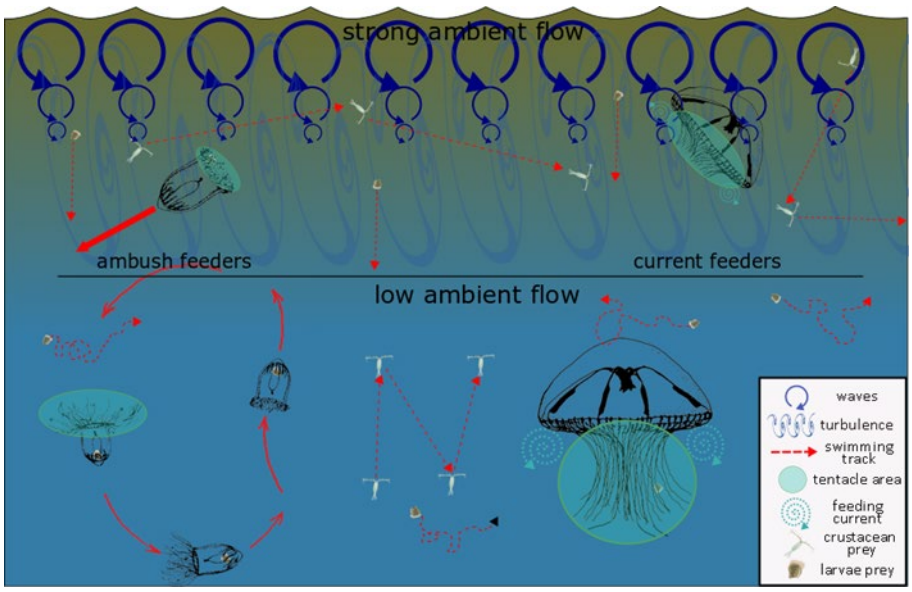

Figure 2. Environmental fluid motion can influence medusan feeding mechanics and alter their feeding success by decreasing the medusan tentacle area, the volume entrained in the medusan feeding currents, the path tortuosity of predator and prey, and the swimming velocity of the prey.

This dissertation also broadens our knowledge on the trophic impact of hydromedusae. Although hydromedusae can invade coastal ecosystems (Morais et al. 2017), have high and constant food assimilation efficiencies (Marshalonis & Pinckney 2008) and can influence zooplankton population dynamics (Daan 1989), their trophic dynamics remain understudied compared to larger, conspicuous scyphomedusae (Suchman et al., 2008; Ruzicka et al., 2012, Zeman et al., 2016; Hays et al., 2018). Chapter IV provides baseline data on hydromedusan diets in coastal upwelling systems, which can be extrapolated to other parts of the world's oceans with similar hydromedusan taxa (Pagés et al., 1992; Miglietta et al., 2008; Rodriguez et al., 2017).

Though hydromedusan predation may represent a smaller portion of energy transfer through the food web compared to larger scyphomedusan predators, their consistent presence and predation impact across seasons may lead to large and context-dependent interactions with their prey and other planktonic predators. Thus, there is deep ecological meaning in the study of inconspicuous and underappreciated organisms, beyond the absolute joy of knowing that us humans share the world with such beautiful and fascinating organisms.

"Life -all life- is in the service of life… The entire landscape comes alive, filled with relationships and relationships within relationships"-Frank Herbert

APPENDIX A: SUPPLEMENTAL INFORMATION FOR CHAPTER II

Statistical tests

Kurtosis and skewness were estimated by bootstrapping the data distribution 1000 times. The ingestion efficiency data distribution had a kurtosis of 1.89 and a skewness of 0.78, whereas the data distribution of the no. interactions/no. ingestions had a kurtosis of 3.43 and a skewness of 1.35. Normally distributed data have a kurtosis of 3.00 and a skewness of 0 (Delignette-Muller & Dutang 2019). This prevented the use of Factorial Analysis of Variance to determine non-random differences among efficiencies of each predation step for each prey species, and for each *C. gregaria*'s feeding behavior (passive sinking vs. swimming) (*predation efficiencies = prey identity* × *predator behavior*). To the best of our knowledge, there is no equivalent non parametric test that allows for comparison of the interaction among predictor variables (prey type × predator behavior).

Maximum deformation rate calculations:

In each node of the velocity vector matrix (defined by the encounter zone of the medusa=1.5 ESD^2), the strain rates $\frac{\partial u}{\partial x}$, $\frac{\partial u}{\partial y}$, $\frac{\partial v}{\partial x}$, $\frac{\partial v}{\partial y}$ were calculated, i.e:

$$\begin{bmatrix} \frac{\partial u}{\partial x} & \frac{\partial u}{\partial y} \\ \frac{\partial v}{\partial x} & \frac{\partial v}{\partial y} \end{bmatrix}$$

The normal strains (ϵ) were then calculated for each node of the vector matrix:

$$\epsilon_{max}, \epsilon_{min} = \frac{\frac{\partial u}{\partial x} + \frac{\partial v}{\partial y}}{2} \pm \sqrt{\left(\frac{\frac{\partial u}{\partial x} - \frac{\partial v}{\partial y}}{2}\right)^2 + \left(\frac{\frac{\partial u}{\partial y} + \frac{\partial v}{\partial x}}{2}\right)^2}$$

as well as the maximum shear:

$$\gamma_{max} = \sqrt{\left(\frac{\frac{\partial u}{\partial x} - \frac{\partial v}{\partial y}}{2}\right)^2 + \left(\frac{\frac{\partial u}{\partial y} + \frac{\partial v}{\partial x}}{2}\right)^2}$$

The **maximum deformation rate** was then defined following Kiørboe &Visser (1999) as:

$$\Delta = MAX(|\epsilon_{max}|, |\epsilon_{min}|, |\gamma_{max}|)$$

The Δ (s^{-1}) was then used as a response variable in the comparisons of fluid signals produced by the hydromedusae's swimming behaviors

Supplemental Table 1: Bonferroni-Dunn comparisons between prey percentage of *C. gregaria*'s gut content. Rank sums between groups are different when $p \leq 0.05/2$.

Prey pairs	Dunn´s *z*	p-value
Copepods-Copepod eggs	2.73	0.0318
Copepods-*Balanus* nauplii	-3.92	**0.0004**
Copepods-*Evadne*	3.95	**0.0004**
Copepods- Invertebrate larvae	3.83	**0.0006**
Copepod eggs- *Balanus* nauplii	6.65	**<0.0001**
Copepod eggs- *Evadne*	6.68	**<0.0001**
Copepod eggs- Invertebrate larvae	6.56	**<0.0001**
Balanus nauplii- *Evadne*	0.02	1.000
Balanus nauplii- Invertebrate larvae	0.09	1.000
Evadne -Invertebrate larvae	-0.12	1.000

Supplemental Table 2: Results of the post-hoc Tukey test for multiple comparisons of mean maximum deformation rate (Δ) produced by the active swimming behavior of three Leptomedusa species (See figure 3 in main text) and the steps in the active swimming cycle (Supplemental figure 4). Significant differences are highlighted in bold.

Species pairs	T value	p-value
Clytia- Aequorea	-2.700	**0.0242**
Mitrocoma - Aequorea	-0.345	0.9967
Mitrocoma - Clytia	2.496	**0.0404**
Swimming cycles		
Bell contraction-contracted	-2.462	0.0772
Bell relaxation-contraction	0.947	0.7798
Bell relaxed-contraction	-1.360	0.5292
Bell relaxation-contraction	3.408	**0.0066**
Bell relaxed-contraction	1.101	0.6901
Bell relaxed- relaxation	-2.307	0.1086

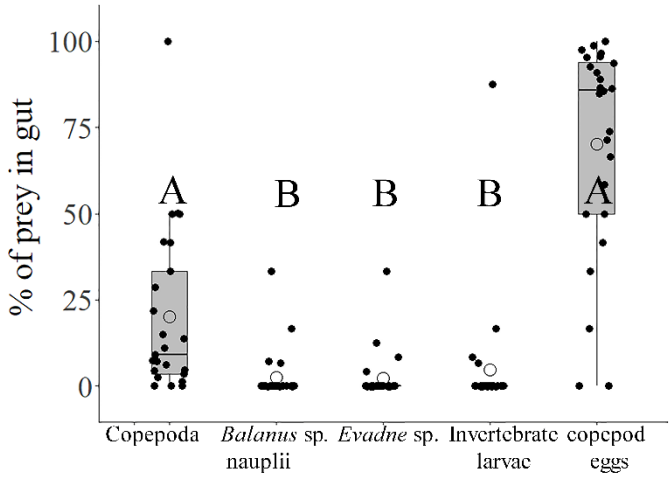

Supplemental Figure 1. Gut content composition of *C. gregaria* (N= 26) collected off Charleston, Oregon in June 2018. Solid circles represent individual data points, open circles represent mean percentages, horizontal lines represent medians, grey boxes represent the 25th and 75th quartiles, and whiskers represent 95% confidence intervals. Letters represent significant differences across rank means (Bonferroni-Dunn test, supplemental Table 1) (Dinno 2016; Dunn 1961). Percentages of copepods include the species *Acartia* sp. (7.22±4.36%, mean±standard error), *Centropages abdominalis* (10.1±3.31%) and *Pseudocalanus* sp. (1.97±0.67%).

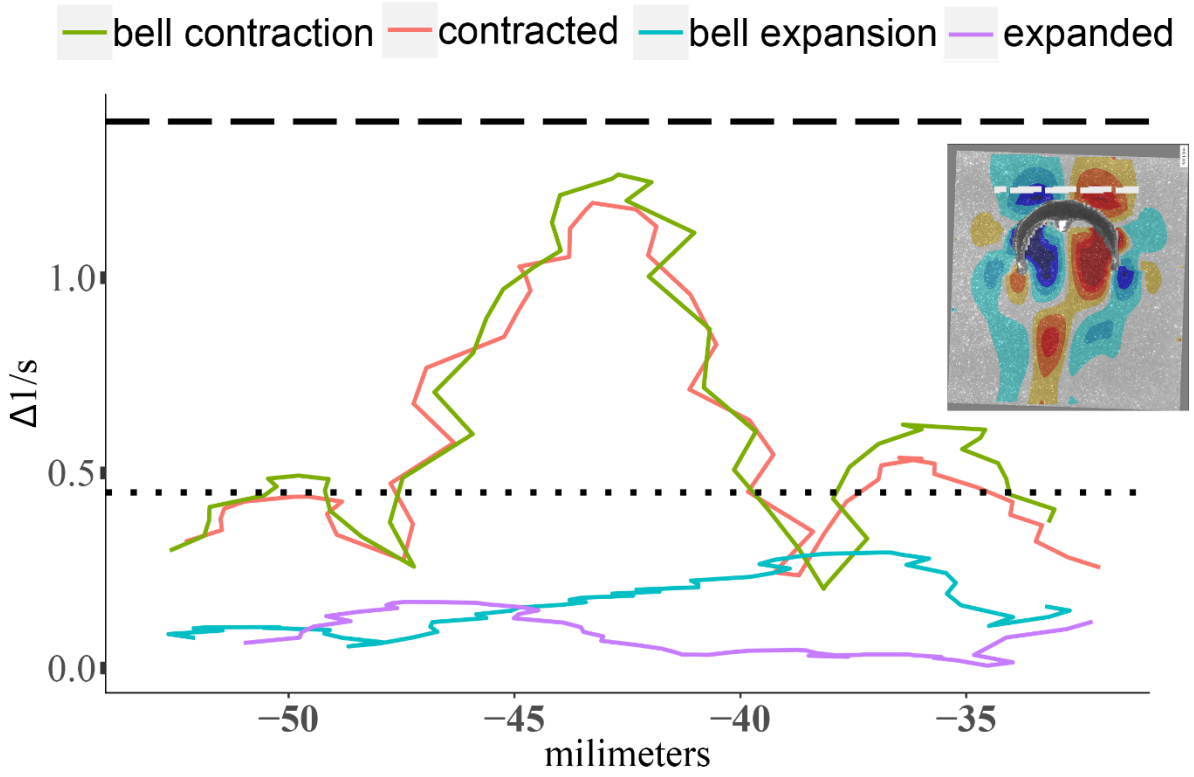

Supplemental Figure 2. Maximum deformation rate (Δ) measured across a transect equal to the bell diameter along the aboral surface of *C. gregaria* (white dashed line in inset) for each step of the swimming cycle. Dotted lines represent the detection threshold of *Acartia* sp. (~0.45 s^{-1}) and dashed lines represent the detection threshold of *Centropages* sp. (~1.4 s^{-1}).

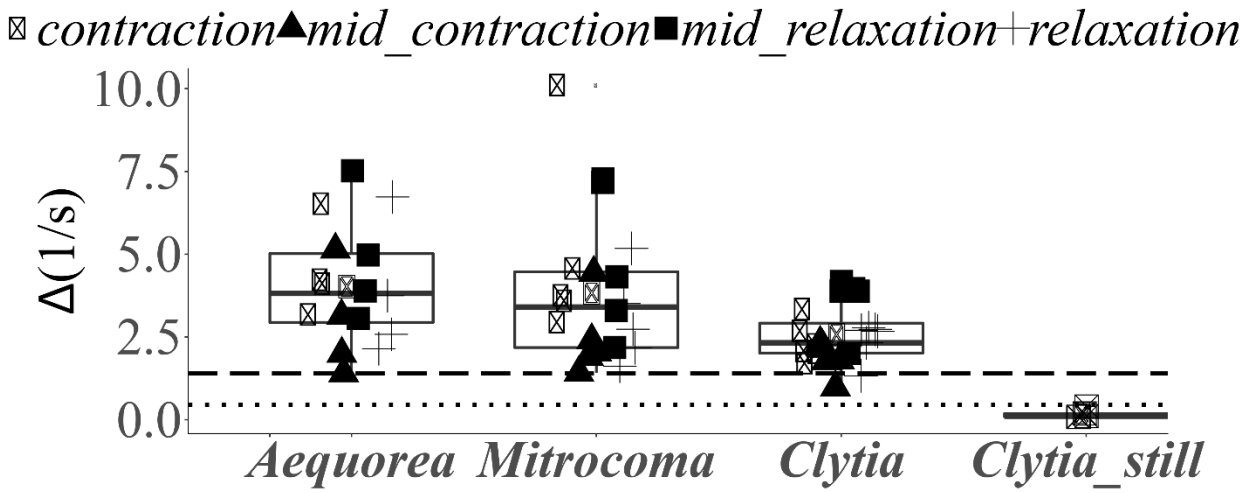

Supplemental Figure 3. Comparison of the maximum deformation rate (Δ) produced in the encounter zone during active swimming in *Aequorea victoria*, *Mitrocoma cellularia* and *Clytia gregaria*, and labeled for each step of the swimming cycle. There was no interaction between the hydromedusae species and the swimming cycle (two-way ANOVA, $F(6,52) = 0.559$, $p = 0.7608$). Dotted lines represent the detection threshold of *Acartia* sp. (~0.45 s^{-1}) and dashed lines represent the detection threshold of *Centropages* sp. (~1.4 s^{-1}).

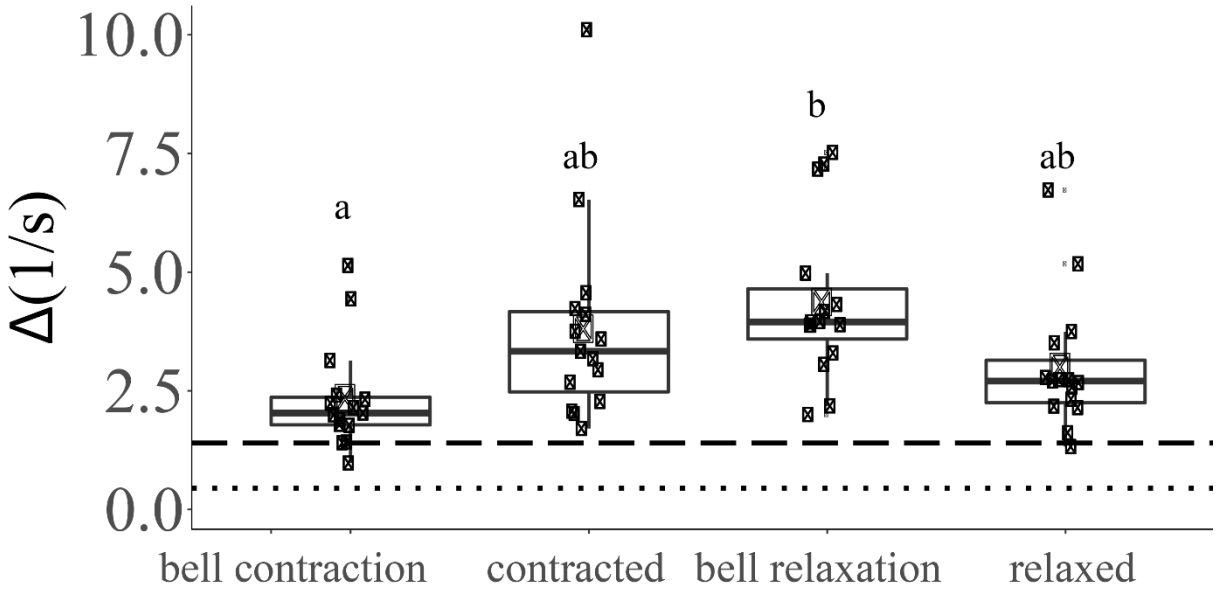

Supplemental Figure 4. Comparison across species of the maximum deformation rate (Δ) produced in the encounter zone during the different steps in the swimming cycle. There were significant differences in the mean Δ between the swim cycle steps (two-way ANOVA, $F(6,52) = 5.008$, $p = 0.0042$). Dotted lines represent the detection threshold of *Acartia* sp. (~0.45 s^{-1}) and dashed lines represent the detection threshold of *Centropages* sp. (~1.4 s^{-1}). Letters above boxplots represent the results of the post-hoc Tukey test (Suppl. Table 2).

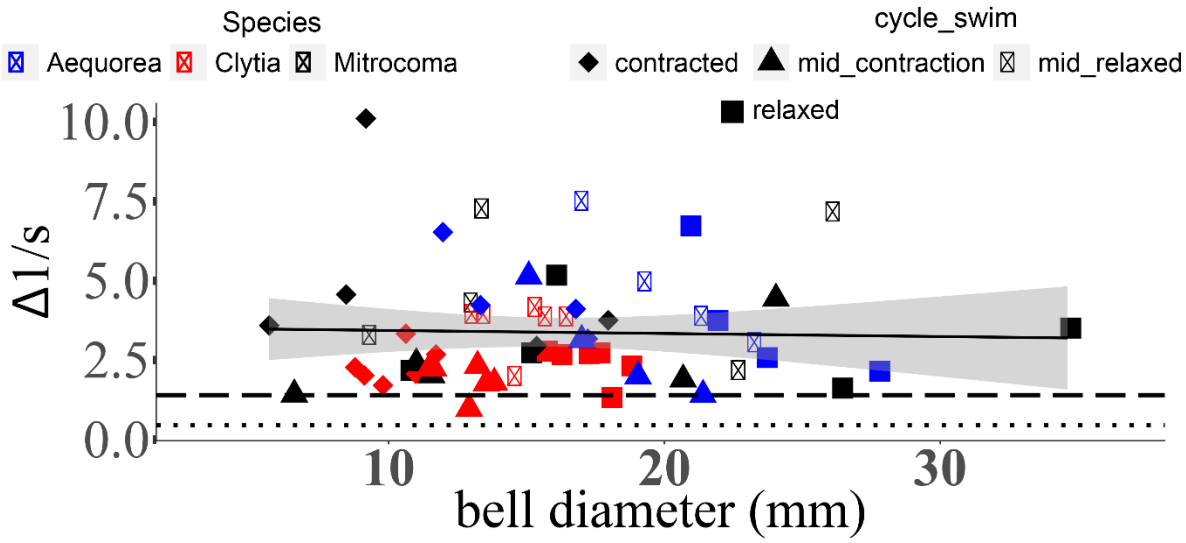

Supplemental Figure 5. Maximum deformation rate (Δ) in the encounter zone produced during active swimming as a function of hydromedusan bell diameter. Solid line represents the result of a linear regression, and the grey area represents the 95% confidence interval for the linear fit (R^2= -0.01631, F(1,58)=0.05311, p=0.8185). Dotted lines represent the detection threshold of *Acartia* sp. (~0.45 s^{-1}) and dashed lines represent the detection threshold of *Centropages* sp. (~1.4 s^{-1}).

APPENDIX B: SUPPLEMENTAL INFORMATION FOR CHAPTER IV

Table S1. Summary of the sampling stations in the Northern California Current, sampled during summers of 2018, 2019 and winter of 2019 (locations provided using a decimal coordinate system).

Transect	Station number	Latitude	Longitude
Newport line	1	44.65207 N	124.294 W
Newport line	2	44.65232 N	124.41W
Newport line	3	44.65177 N	124.648 W
Newport line	4	44.6519 N	124.893 W
Newport line	5	44.65225 N	125.115 W
Trinidad line	1	41.05834 N	124.272 W
Trinidad line	2	41.05798 N	124.346 W
Trinidad line	3	41.05867 N	124.434 W
Trinidad line	4	41.0583 N	124.588 W
Trinidad line	5	41.05784 N	124.753 W

Table S2. Hydromedusan species collected from the MOCNESS tows (0-25 m), and the prey types ingested by each species. n= number of individuals collected

Order	Species	Season	Transect	Stations	Prey found
Anthoatecata					
	Bougainvillia sp. (n=1)	Summer	Newport	3	Appendicularians, copepod eggs
	Corymorpha sp. (n=1)	Summer	Newport	1	Copepods: *Acartia* sp.
	Leuckartiara sp. (n=3)	Summer	Trinidad	1,3	Calanoid copepods, Invertebrate eggs and zoea larvae
	Proboscidactyla flavicirrata (n=6)	Winter, Summer	Newport	1,3,5	Appendicularians, invertebrate eggs, veliger larvae
	Sibogita sp. (n=1)	Summer	Trinidad	3	Zoea larva
Leptomedusae					
	Clytia gregaria (**n=103**)	Winter, Summer	Newport, Trinidad	1,2,3,4,5	Appendicularians, calanoid copepods, chaetognaths, invertebrate eggs
	Eutonina indicans (**n=36**)	Winter, Summer	Newport, Trinidad	1,3,4	Appendicularians, calanoid copepods, chaetognaths, invertebrate eggs
	Mitrocoma cellularia (n=20)	Summer	Newport	1,3,5	Appendicularians, calanoid copepods, chaetognaths, invertebrate eggs
Limnomedusae					
	Liriope tetraphylla (n=4)	Winter, Summer	Newport, Trinidad	5	Calanoid copepods, copepod eggs, invertebrate larvae (Bryozoa)
Narcomedusae					
	Aegina citrea (n=2)	Winter	Trinidad	5	Copepods: *Oncaea* sp., *Pseudocalanus* sp.
	Solmissus incisa (n=1)	Summer	Newport	5	Appendicularia (Oikopleura)

Table S3. Average percentage contribution of the major prey categories to the gut content composition of each hydromedusan predator. For *C. gregaria* and *E. indicans*, percentages are presented for Winter (W) and Summer (S).

	Appendicularia	Chaetognatha	Copepod eggs	Copepoda	Euphausid eggs	Larvae	Others
Bougainvillia sp.	77.8%	-	22.2%	-	-	-	-
Corymorpha sp.	-	-	-	100%	-	-	-
Leuckartiara sp.	19.4%	-	-	19.6%	35.7%	25.3%	-
Sibogita sp.	-	-	-	-	-	100	-
Clytia gregaria	51.8% (S) 5.2%(W)	1.5%(S) 2.8%(W)	5.9%(S) 64.6%(W)	34.8%(S) 3.6%(W)	1.5%(S) 20.2%(W)	1.5%(S) 3.2%(W)	3.0%(S) 0.4%(W)
Eutonina indicans	36.4%(S) 30.2%(W)	-(S) 11.6%(W)	27.2%(S) 7.0%(W)	9.1%(S) 4.6%(W)	18.2%(S) 41.9%(W)	3.0%(S) 2.3%(W)	6.1%(S) 2.3%(W)
Mitrocoma cellularia	38.3%	4.6%	16.7%	17.0%	10%	3.3%	6.7%
Liriope tetraphyla	-	-	33.3%	50%	-	16.7%	-
Aegina sp.	-	-	-	100	-	-	-
Solmissus sp.	100	-	-	-	-	-	-

Table S4. Welch's t-test results for prey abundance comparisons between summer (July 3-12, 2018 and July 14-27, 2019) and winter (March 2-14, 2019). Significant differences are highlighted with asterisks.

Prey Category	t-value	d.f.	p
Appendicularia	2.7888	12.601	0.01574*
Chaetognatha	1.7135	6.6034	0.1329
Copepods	1.8283	14.298	0.08844
Copepod eggs	2.259	14.971	0.03923*
Euphausid eggs	0.22278	14.999	0.8267
Invertebrate larvae	0.84391	14.576	0.4124
Others	0.069595	10.482	0.9458

Table S5. PERMANOVA results based on Bray Curtis similarity matrix with a number of 999 permutations.

Prey found in:	Independent variable	d.f.	Mean squares
Environment $\left(\frac{ind.}{m^3}\right)$	Season	1	0.14934
	Residual	15	0.05944
Hydromedusan community$\left(\frac{prey}{ind.}\right)$ $(corrected)$	Season	1	3.542
	Residual	174	0.34265
$Clytia\ gregaria\left(\frac{prey}{ind.}\right)$ $(corrected)$	Season	1	5.05
	Residual	100	0.28273
Eutonina indicans$\left(\frac{prey}{ind.}\right)$ $(corrected)$	Season	1	0.4088
	Residual	34	0.3720

REFERENCES CITED

Chapter II

Acuña, J.L., A. Lopez-Urrutia, and S. Colin. 2011. Faking giants: the evolution of high prey clearance rates in jellyfishes. Science 333: 1627-1629.

Bradley, C.J., J.R. Strickler, E.J. Buskey, and P.H. Lenz. 2013. Swimming and escape behavior in two species of calanoid copepods from nauplius to adult. J. Plankton Res. 35(1):49-65

Boero, F., J. Bouillon, C. Gravili, M.P. Miglietta, T. Parsons, and S. Piraino. 2008. Gelatinous plankton: irregularities rule the world (sometimes). Mar. Ecol. Prog. Ser. 356: 299-310

Burdick, D.S., D.K. Hartline, and P.H. Lenz. 2007. Escape strategies in co-occurring calanoid copepods. Limnol.Oceanogr. 52:2373–2385

Buskey, E.J., P.H. Lenz, D.K. Hartline. 2002. Escape behavior of planktonic copepods in response to hydrodynamic disturbances: high speed video analyses. Mar. Ecol. Prog. Ser. 235:135-146

Colin, S.P., J.H. Costello, L.J. Hansson, J. Titelman, and J.O. Dabiri. 2010. Stealth predation and the predatory success of the invasive ctenophore *Mnemiopsis leidyi*. Proc. Nat. Ac. Sci. 107 (40):17223-17227.

Colin, S.P., J.H. Costello, and E. Klos. 2003. *In situ* swimming and feeding behavior of eight co-occuring hydromedusae. Mar. Ecol. Prog. Ser. 253:305-309.

Colin, S.P., J.H. Costello, W.M. Graham, and J. Higgins III. 2005. Omnivory by the small cosmopolitan hydromedusa *Aglaura hemistoma.* Limnol. Oceanogr. 50(4):1264-1268

Colin, S.P., R. MacPherson, B. Gemmell, J.H. Costello, K. R. Sutherland, and C. Jaspers. 2015. Elevating the predatory effect: sensory-scanning foraging strategy by the lobate ctenophore *Mnemiopsis leidyi.* Limnol. Oceanogr.60: 100-109.

Corrales-Ugalde, M., S.P. Colin, and K.R. Sutherland. 2017. Nematocyst distribution corresponds to prey capture location in hydromedusae with different predation modes. Mar. Ecol. Prog. Ser. 568:101-110.

Costello, J.H., and S.P. Colin. 2002. Prey resource use by coexisting hydromedusae from Friday Harbor, Washington. Limnol. Oceanogr. 47(4): 934-942

Costello, J.H., S.P. Colin, and J.O. Dabiri. 2008. Medusan morphospace: Phylogenetic constraints, biomechanical solutions, and ecological consequences. Invert. Biol. 127(3): 265–290.

Daan, R. 1989. Factors controlling the summer development of copepod populations in the southern bight of the North Sea. Neth. J. Sea Res. 23(3): 305-322.

Dabiri, J.O., S.P. Colin, J.H. Costello, and M. Gharib. 2005. Flow patterns generated by oblate medusan jellyfish: field measurements and laboratory analyses. J. Exp. Biol. 208: 1357-1265

Dabiri, J.O., S.P. Colin, K. Katija, and J.H. Costello. 2010. A wake-based correlate of swimming performance and foraging behavior in seven co-occurring jellyfish species. J. Exp. Biol. 213:1217-1225.

Delignette-Muller, M.L., and C. Dutang. 2019. Help to fit of a parametric distribution to non-censored or censored data version 1.014 https://CRAN.R-project.org/package=fitdistrplus.

Dinno, A. 2016. Dunn.test: Dunn´s test of multiple comparisons using rank sums. R package version 1.3.2 http:// CRAN.R-project.org/package=dunn.test.

Dunn, O.J. 1964. Multiple comparisons using rank sums. Technometrics 6(3): 241-252.

Durbin, E.G., and A.G. Durbin. 1992. Effects of temperature and food abundance on grazing and short-term weight change in the marine copepod *Acartia hudsonica*. Limnol. Oceanogr. 37(2): 361-378.

Fields, D.M., and J. Yen. 1997. The escape behavior of marine copepods in response to a quantifiable fluid mechanical disturbance. J. Plankton Res. 19(9): 1289-1304.
Ford, M.D., J.H. Costello, K.D. Heidelberg, and J.D. Purcell. 1997. Swimming and feeding by the scyphomedusa *Chrysaora quinquecirrha*. Mar. Biol. 129:355-362.

Garaventa, F., C. Gambardella, A. Di Fino, M. Pittore, and M. Faimali. 2010. Swimming speed alteration of *Artemia* sp. and *Brachionus plicatilis* as a sub-lethal behavioural end-point for ecotoxicological surveys. Ecotoxicol. 19(3): 512-519.

Gardner, G.A., and I. Szabo. 1982. British Columbia pelagic marine copepoda: an identification manual and annotated bibliography. Can. Spec. Pub. Fish. Aquatic Sci. 62: 536 pp.

Gemmell, B.J., J. Sheng, and E.J. Buskey. 2013. Morphology of seahorse head hydrodynamically aids in capture of evasive prey. Nature Comm. 4:2840, doi: 10.1038/ncomms3840

Gemmell, B.J., D.R. Troolin, J.H. Costello, S.P. Colin, and R.A. Satterlie. 2015. Control of vortex rings for manoeuvrability. J. R. Soc. Interface 12:20150389
Gerritsen, J, and J.R. Strickler. 1977. Encounter probabilities and community structure in zooplankton: a mathematical model. J. Fish. Res. Board Can. 34:73-82.

Gravili, C., P. D'Ambrosio, C. Di Camillo, G. Renna, J. Bouillon , and F. Boero.2008. *Clytia hummelincki* (Hydroidomedusae: Leptomedusae) in the Mediterranean Sea. J. Mar. Biol. Assoc. UK. 88(8): 1547-1553.

Hansson, L.J., and T. Kiørboe. 2006. Prey-specific encounter rates and handling efficiencies as causes of prey selectivity in ambush-feeding hydromedusae. Limnol. Oceanogr. 51(4):1849–1858.

Hartline, D.K., P. Lenz, and C.M. Herren. 1996. Physiological and behavioral studies of escape responses in calanoid copepods. Mar. Fresh. Behav. Physiol. 27(2-3): 199-212.

Holling, C.S. 1959. The components of predation as revealed by a study of small mammal predation of the European pine sawfly. Can. Entomol. 91:293-320.

Katija, K., W.T. Beaulieu, C. Regula, S.P. Colin, J.H. Costello, and J.O. Dabiri. 2011. Quantification of flows generated by the hydromedusa *Aequorea victoria*: A Lagrangian coherent structure analysis. Mar. Ecol. Prog. Ser. 435:111–123

Kiørboe, T. 2008. A mechanistic approach to plankton ecology. 1st ed. Princeton University Press.

Kiørboe, T., E. Saiz, and A Vizzer. 1999. Hydrodynamic signal perception in the copepod *Acartia tonsa*. Mar. Ecol. Prog. Ser. 179: 97-111.

Kiørboe, T., F. Møhlenberg, and Hamburger K. 1985. Bioenergetics of the planktonic copepod *Acartia tonsa*: relation between feeding, egg production and respiration, and composition of specific dynamic action. Mar. Ecol. Prog. Ser. 26:85-97.

Kiørboe, T., H. Jiang, R.J. Gonçalves, L.T. Nielsen, and N. Wadhwa. 2014. Flow disturbances generated by feeding and swimming zooplankton. Proc. Nat. Ac. Sci. 32: 11738-11743.

Larson, R.J. 1987. Daily ration and predation impact by medusae and ctenophores in Saanich Inlet, B.C., Canada. Neth. J. Sea Res. 21:35-44

Lenz, P.H., and J. Yen. 1993. Distal setal mechanoreceptors of the first antennae of marine copepods. Bull. Mar. Sci. 53(1):170-179

Lenz, P.H., T.M. Weatherby, W. Weber, and K.K. Wong. 1996. Sensory specialization along the first antenna of a calanoid copepod, *Pleuromamma xiphias.* Mar. Freshw. Behav. Physiol. 27(2-3): 213-221

Lucas, C.H., D.W. Williams, J.A. Williams, and M. Sheader. 1995. Seasonal dynamics and production of the hydromedusan *Clytia hemisphaerica* (Hydromedusa: Leptomedusa) in Southampton water. Estuaries 18(2): 362-372

Madin, L. 1988. Feeding behaviour of tentaculate predators: In situ observations and a conceptual model. Bull. Mar. Sci. 43(3): 413–429.

Marshalonis, D., and J.L. Pinckney. 2008. Grazing and assimilation rate estimates of hydromedusae from a temperate tidal creek system. Hydrobiologia 606:203-211

Matsakis, S., and R.J. Conover. 1991. Abundance and feeding of medusae and their potential impact as predators on other zooplankton in Bedford Basin (Nova Scotia) Canada, durign spring. Can. J. Fish. Aquat. Sci. 48: 1419-1430

Mauchline, J. 1999. The biology of calanoid copepods. 1st ed. Academic Press.

Mills, C.E. 1981. Diversity of swimming behaviors in hydromedusae as related to feeding and utilization of space. Mar. Biol. 64: 185-189.

Mills, C.E. 1995. Medusae, siphonophores and ctenophores as planktivorous predators in changing global ecosystems. ICES J. Mar. Sci. 52: 575-581.

Mills, C.E. 2001. Jellyfish blooms: are populations increasing globally in response to changing ocean conditions? Hydrobiologia 451:55-68

Morais, P., E. Dias, J. Cruz, P. Chainho, M.M. Angelico, J.L. Costa, A.B. Barbosa, and M.A. Teodosio. 2017. Allochthonous-derived organic matter subsidizes the food sources of estuarine jellyfishes. J. Plankton Res. 39(6):870-877 doi: 10.1093/plankt/fbx049.

Morgan C.A., W.T. Peterson, and R.L. Emmett. 2003. Onshore-offshore variations in copepod community structure off the Oregon coast during the summer upwelling season. Mar. Ecol. Prog. Ser. 249:223-236

Ohman, M.A. 2019. A sea of tentacles: optically discernible traits resolved from planktonic organisms *in situ*. ICES J. Mar. Sci. 76(7): 1959-1972

Pastorok, R.A.1981. Prey vulnerability and size selection by *Chaoborus* larvae. Ecology 62:1311-1324.

Peng, J., and J.O.Dabiri. 2009. Transport of inertial particles by Lagrangian coherent structures: application to predator-prey interaction in jellyfish feeding. J. Fluid Mech. 623:75-84.

Peterson, W.T., C.B. Miller, and A. Hutchinson. 1979. Zonation and maintenance of copepod popuations in the Oregon upwelling zone. Deep-Sea Res. 26:467-494

Purcell, J.E. 1992. Effects of predation by the scyphomedusan *Chrysaora quinquecirrha* on zooplankton populations in Chesapeake Bay, USA. Mar. Ecol. Prog. Ser. 87:65-76

Purcell, J.E. 1997. Pelagic cnidarians and ctenophores as predators: Selective predation, feeding rates and effects on prey selection. Ann. Inst. Oceanogr. 73:125-137.

Purcell, J.E. 2017. Successes and challenges in jellyfish ecology: examples from *Aequorea* spp. Mar. Ecol. Prog. Ser. 591:7-27.

Purcell, J.E. 2009. Extension of methods for jellyfish and ctenophore trophic ecology to large-scale research. Hydrobiol. 616: 23-50

Purcell, J.E., and C.E. Mills.1988. The correlation between nematocyst types and diets in pelagic hydrozoa. In D.A. Hessinger and H.M Lenoff HM [eds.], The biology of nematocysts. Academic Press.

Regula, C., S.P. Colin, J.K. Costello, and H. Kordula. 2009. Prey selection mechanism of ambush-foraging hydromedusae. Mar. Ecol. Prog. Ser. 374:135-144.

Robinson, H.E., J. R. Strickler, M.J. Henderson, D.K. Hartline, and P.H. Lenz. 2019. Predation strategies of larval clownfish capturing evasive copepod prey. Mar. Ecol. Prog. Ser. 614:125-146

Robison, R. 2004. Deep pelagic biology. J. Exp. Mar. Biol. Ecol. 300:253-272.

Robinson, K.L., J.J. Ruzicka, M.B. Decker, R.D. Brodeur , F.J. Hernandez, J. Qiñones, E.M. Acha, S.I. Uye, H. Mianzan, and W.M. Graham. 2014. Jellyfish, forage fish, and the world's major fisheries. Oceanography 27(4): 104-115.

Roughgarden, J. 1998. A primer of ecological theory. 1st ed. Prentice-Hall, Inc.

Schaafsma, F.L., Y. Cherel, H. Flores, J.A. van Franeker, M.A. Lea, B. Raymond, and A.P. van de Putte AP. 2018. Review: the energetic value of zooplankton and nekton species of the Southern Ocean. Mar. Biol. 165: 129.

Shiganova, T.A. 1998. Invasion of the Black Sea by the ctenophore *Mnemiopsis leidyi* and recent changes in pelagic community structure. Fish. Oceanogr. 7(3-4): 305-310.

Song, Y., P. Wang, G. Li, and D. Zhou. 2014. Relationships between functional diversity and ecosystem functioning: a review. Acta Ecol. Sin. 34:85-91

Suarez-Morales, E., L. Segura-Puertas, and R. Gasca. 1999. Medusan (Cnidaria) assemblages of the Caribbean coast of Mexico. J. Coastal Res. 15(1): 140-147.

Suchman C.L. 2000. Escape behavior of *Acartia hudsonica* copepods during interactions with scyphomedusae. J. Plankton Res. 22(12): 2307-2323

Suchman, C.L., and B.K. Sullivan. 1998. Vulnerability of the copepod *Acartia tonsa* to predation by the scyphomedusa *Chrysaora quinquecirrha*: effects of prey size and behavior. Mar. Biol. 132:237-245

Suchman, C.L., and B.K. Sullivan. 2000. Effect of prey size on vulnerability of copepods to predation by the scyphomedusae *Aurelia aurita* and *Cyanea* sp. J. Plankton Res. 22(12):2289-2306

Thorington G.U., and D.A. Hessinger. (1996). Efferent mechanisms of discharging cnidae: I. Measurements of intrinsic adherence of cnidae discharged from tentacles of the sea anemone, *Aiptasia pallida.* Biol. Bull. 190:125-138

Waggett, R.J., and E. Buskey. (2007) Copepod escape behavior in non-turbulent and turbulent hydrodynamic regimes. Mar. Ecol. Prog. Ser. 334: 193-198.

Wagner, Z., J.H. Costello, and S.P. Colin. (2020) Fluid and predator-prey interactions of scyphomedusae fed calanoid copepods. Fluids. 5:60. doi:10.3390/fluids5020060

Yen, Y., P. H. Lenz, D.V. Gassie, and D. K. Hartline. 1992. Mechanoreception in marine copepods: electrophysiological studies on the first antennae. J. Plankton Res. 14(4): 495-512

Zapata, F., F. Goetz, S. Smith, M. Howison, S. Siebert, S. Church, S. Sanders, C. Ames, C. McFadden, S. France, M. Daly, A.G. Collins, S.H.D. Haddock, C.W. Dunn, and P. Cartwright. 2015. Phylogenomic analyses support traditional relationships within Cnidaria. PLOS One. 10(10): 1-13.

Chapter III

Acuna, J. L., A. Lopez-Urrutia, and S. Colin. 2011. Faking Giants: The Evolution of High Prey Clearance Rates in Jellyfishes. Science 333: 1627–1629. doi:10.1126/science.1205134

Amoroso, R. O., and D. A. Gagliardini. 2010. Inferring Complex Hydrographic Processes Using Remote-Sensed Images: Turbulent Fluxes in the Patagonian Gulfs and Implications for Scallop Metapopulation Dynamics. J. Coastal Res. 262: 320–332. doi:10.2112/08-1095.1

Arai, M.N. 1992. Active and passive factors affecting aggregations of hydromedusae: a review. Sci. Mar. 56(2-3):99-108

Bouillon J, Gravili C, Pages F, Gili JM, Boero F. 2006. An introduction to Hydrozoa. Memoires du Museum national d'Histoire naturelle 194: 1-591.

Chiaverano, L., W. Graham, and J. Costello. 2015. Parasites alter behavior, reproductive output, and growth patterns of Aurelia medusae in a marine lake. Mar. Ecol. Prog. Ser. 540: 87–98. doi:10.3354/meps11513

Colin, S. P., J. H. Costello, W. M. Graham, and J. I. Higgins. 2005. Omnivory by the small cosmopolitan hydromedusa *Aglaura hemistoma*. Limnol. Oceanogr. 50: 1264–1268. doi:10.4319/lo.2005.50.4.1264

Corrales-Ugalde, M., S. Colin, and K. Sutherland. 2017. Nematocyst distribution corresponds to prey capture location in hydromedusae with different predation modes. Mar. Ecol. Prog. Ser. 568: 101–110. doi:10.3354/meps12059

Corrales-Ugalde, M., S. Sponaugle, R. K. Cowen, and K. R. Sutherland. 2021. Seasonal hydromedusan feeding patterns in an Eastern Boundary Current show consistent predation on primary consumers. J. Plankton Res. 43: 712–724. doi:10.1093/plankt/fbab059

Corrales-Ugalde, M., and K. R. Sutherland. 2021. Fluid mechanics of feeding determine the trophic niche of the hydromedusa *Clytia gregaria*. Limnol. Oceanogr. **66**: 939–953. doi:10.1002/lno.11653

Daan, R. 1989. Factors controlling the summer development of copepod populations in the southern bight of the North Sea. Neth. Jour. Sea Res. 23: 305–322. doi:10.1016/0077-7579(89)90051-3

Francis, T. B., M. D. Scheuerell, R. D. Brodeur, P. S. Levin, J. J. Ruzicka, N. Tolimieri, and W. T. Peterson. 2012. Climate shifts the interaction web of a marine plankton community. Glob. Change Biol. 18: 2498–2508. doi:10.1111/j.1365-2486.2012.02702.x

Fuchs, H. L., A. J. Christman, G. P. Gerbi, E. J. Hunter, and F. J. Diez. 2015. Directional flow sensing by passively stable larvae. J. Exp. Biol. 218: 2782–2792. doi:10.1242/jeb.125096

Fuchs, H. L., and G. P. Gerbi. 2016. Seascape-level variation in turbulence- and wave-generated hydrodynamic signals experienced by plankton. Prog. Oceanogr.141: 109–129. doi:10.1016/j.pocean.2015.12.010

Fuchs, H. L., G. P. Gerbi, E. J. Hunter, A. J. Christman, and F. J. Diez. 2015b. Hydrodynamic sensing and behavior by oyster larvae in turbulence and waves. J. Exp. Biol. 218(9):1419-1432

Hansson, L. J., and T. Kiørboe. 2006. Prey-specific encounter rates and handling efficiencies as causes of prey selectivity in ambush-feeding hydromedusae. Limnol. Oceanogr. 51: 1849–1858. doi:10.4319/lo.2006.51.4.1849

Hansson, L., O. Moeslund, T. Kiørboe, and H. Riisgård. 2005. Clearance rates of jellyfish and their potential predation impact on zooplankton and fish larvae in a neritic ecosystem (Limfjorden, Denmark). Mar. Ecol. Prog. Ser. 304: 117–131. doi:10.3354/meps304117

Hays, G. C., T. K. Doyle, and J. D. R. Houghton. 2018. A Paradigm Shift in the Trophic Importance of Jellyfish? Trends Ecol. Evol. 33: 874–884. doi:10.1016/j.tree.2018.09.001

Horridge, G. A. 1969. Statocysts of medusae and evolution of stereocilia. Cell Tissue Res. 1: 341–353. doi:10.1016/S0040-8166(69)80029-7

Hwang, J.-S., J. H. Costello, and J. R. Strickler. 1994. Copepod grazing in turbulent flow: elevated foraging behavior and habituation of escape responses. J Plankton Res. 16: 421–431. doi:10.1093/plankt/16.5.421

Jaspers, C., J. H. Costello, K. R. Sutherland, B. Gemmell, K. N. Lucas, J. Tackett, K. Dodge, and S. P. Colin. 2018. Resilience in moving water: Effects of turbulence on the predatory impact of the lobate ctenophore *Mnemiopsis leidyi*. Limnol. Oceanogr. 63: 445–458. doi:10.1002/lno.10642

de Jong, J., L. Cao, S. H. Woodward, J. P. L. C. Salazar, L. R. Collins, and H. Meng. 2009. Dissipation rate estimation from PIV in zero-mean isotropic turbulence. Exp. Fluids. 46: 499–515. doi:10.1007/s00348-008-0576-3

Katija, K., W. Beaulieu, C. Regula, S. Colin, J. Costello, and J. Dabiri. 2011. Quantification of flows generated by the hydromedusa Aequorea victoria: a Lagrangian coherent structure analysis. Mar. Ecol. Prog. Ser. 435: 111–123. doi:10.3354/meps09212

Katija, K., and J. O. Dabiri. 2008. In situ field measurements of aquatic animal-fluid interactions using a Self-Contained Underwater Velocimetry Apparatus (SCUVA): In situ field measurements using SCUVA. Limnol. Oceanogr. Methods **6**: 162–171. doi:10.4319/lom.2008.6.162

Khangaonkar, T., Z. Yang, T. Kim, and M. Roberts. 2011. Tidally averaged circulation in Puget Sound sub-basins: Comparison of historical data, analytical model, and numerical model. Estuar. Coast. Shelf Sci. 93: 305–319. doi:10.1016/j.ecss.2011.04.016

Kiørboe, T. 2008. A mechanistic approach to plankton ecology. 1st ed. Princeton University Press

Kritzer, J.P. and Sale, P.F. (eds.), 2006. Marine Metapopulations. Burlington, Massachusetts: Elsevier Academic Press.

Laval, P. 1980. Hyperiid amphipods as crustacean parasitoids associated with gelatinous zooplankton. Oceanogr. Mar. Biol. Ann. Rev. 18: 11-56

Mackie, G. O. 1980. Slow Swimming and Cyclical "Fishing" Behavior in *Aglantha Digitale* (Hydromedusae: Trachylina). Can. J. Fish. Aquat. Sci. 37: 1550–1556. doi:10.1139/f80-200

Marliave, J. B., and C. E. Mills. 1993. Piggyback riding by pandalid shrimp larvae on hydromedusae. Can. J. Zool. 71: 257–263. doi:10.1139/z93-037

Marshalonis, D., and J. L. Pinckney. 2008. Grazing and assimilation rate estimates of hydromedusae from a temperate tidal creek system. Hydrobiol. 606: 203–211. doi:10.1007/s10750-008-9334-z

Matsakis, S., and R. J. Conover. 1991. Abundance and Feeding of Medusae and their Potential Impact as Predators on Other Zooplankton in Bedford Basin (Nova Scotia, Canada) during Spring. Can. J. Fish. Aquat. Sci. 48: 1419–1430. doi:10.1139/f91-169

Michalec, F.-G., S. Souissi, and M. Holzner. 2015. Turbulence triggers vigorous swimming but hinders motion strategy in planktonic copepods. J. R. Soc. Interface. 12: 20150158. doi:10.1098/rsif.2015.0158

Mills C.E. 1981. Diversity of swimming behaviors in hydromedusae as related to feeding and utilization of space. Mar. Biol. 64:185-189

Ohtsuka, S., K. Koike, D. Lindsay, and others. 2009. Symbionts of marine medusae and ctenophores. Plankton Benthos Res. 4: 1–13. doi:10.3800/pbr.4.1

Pimm, S. L. 1981. Food webs. 1st ed. Chapman and Hall

Purcell, J. 2018. Successes and challenges in jellyfish ecology: examples from Aequorea spp. Mar. Ecol. Prog. Ser. 591: 7–27. doi:10.3354/meps12213

Rakow, K. C., and W. M. Graham. 2006. Orientation and swimming mechanics by the scyphomedusa Aurelia sp. in shear flow. Limnol. Oceanogr. 51: 1097–1106. doi:10.4319/lo.2006.51.2.1097

Rothschild, B. J., and T. R. Osborn. 1988. Small-scale turbulence and plankton contact rates. J. Plankton Res. 10: 465–474. doi:10.1093/plankt/10.3.465

Ruzicka, J. J., R. D. Brodeur, R. L. Emmett, J. H. Steele, J. E. Zamon, C. A. Morgan, A. C. Thomas, and T. C. Wainwright. 2012. Interannual variability in the Northern California Current food web structure: Changes in energy flow pathways and the role of forage fish, euphausiids, and jellyfish. Progr. Oceanogr. 102: 19–41. doi:10.1016/j.pocean.2012.02.002

Ruzicka, J. J., E. A. Daly, and R. D. Brodeur. 2016. Evidence that summer jellyfish blooms impact Pacific Northwest salmon production D.P.C. Peters [ed.]. Ecosphere 7(4):e01324 doi:10.1002/ecs2.1324

Saiz, E., and M. Alcaraz. 1992. Free-swimming behaviour of Acartia clausi (Copepoda: Calanoida) under turbulent water movement. Mar. Ecol. Prog. Ser. 80: 229–236. doi:10.3354/meps080229

Singla, C.L. 1983. Fine structure of the sensory receptors of *Aglantha digitale* (Hydromedusae:Trachylina). Cell Tiss. Res. 231:415-425

Sutherland, D. A., P. MacCready, N. S. Banas, and L. F. Smedstad. 2011. A Model Study of the Salish Sea Estuarine Circulation*. Jour. Phys. Oceanogr. **41**: 1125–1143. doi:10.1175/2011JPO4540.1

Sutherland, K. R., J. H. Costello, S. P. Colin, and J. O. Dabiri. 2014. Ambient fluid motions influence swimming and feeding by the ctenophore Mnemiopsis leidyi. J. Plankton Res. 36: 1310–1322. doi:10.1093/plankt/fbu051

Tanaka, T., and J. K. Eaton. 2007. A correction method for measuring turbulence kinetic energy dissipation rate by PIV: Validated by random Oseen vortices synthetic image test. Exp. Fluids 42: 893–902. doi:10.1007/s00348-007-0298-y

Thompson T.E. 1981. Oceanography of the British Columbia Coast Can. Spec. Publ. Fish. Aquat. Sci. 56:1–291

Vader, W. 1972. Associations between gammarid and caprellid amphipods and medusae. Sarsia 50: 51–56. doi:10.1080/00364827.1972.10411217

Yang, Z., T. Wang, R. Branch, Z. Xiao, and M. Deb. 2021. Tidal stream energy resource characterization in the Salish Sea. Renew. Energy 172: 188–208. doi:10.1016/j.renene.2021.03.028

Zamon, J. 2002. Tidal changes in copepod abundance and maintenance of a summer Coscinodiscus bloom in the southern San Juan Channel, San Juan Islands, USA. Mar. Ecol. Prog. Ser. 226: 193–210. doi:10.3354/meps226193

Zamon, J. E. 2001. Seal predation on salmon and forage fish schools as a function of tidal currents in the San Juan Islands, Washington, USA: Seal predation on salmon and forage fish. Fish. Oceanogr. 10: 353–366. doi:10.1046/j.1365-2419.2001.00180.x

Chapter IV

Acuña, J. L., Lopez-Urrutia, A., and Colin, S. (2011) Faking giants: the evolution of high prey clearance rates in jellyfishes. *Science*, **333**, 1627–1629.

Ambriz-Arreola, I., Gómez-Gutiérrez, J., Franco-Gordo, M., and Kozak, E. (2015) Reproductive biology, embryo and early larval morphology, and development rates of krill (*Euphausia lamelligera* and *Euphausia distinguenda*), endemic to the Eastern Tropical Pacific. *Sex. Early. Dev. Aquat. Org.*, **1**, 143–161.

Berraho, A., Somoue, L., Hernández-León, S. and Valdés, L. (2015). Zooplankton in the Canary Current Large Marine Ecosystem. In Valdés, L. and Déniz-González I.(eds). *Oceanographic and biological features in the Canary Current Large Marine Ecosystem*. IOC Technical Series, No. 115, pp. 183-195

Bi, H., Peterson, W. T., and Strub, P. T. (2011) Transport and coastal zooplankton communities in the northern California Current system. *Geophys. Res. Lett.*, **38**, L12607

Brinton, E. (1976). Population biology of *Euphausia pacifica* off Southern California. *Fish. Bull.*, **74**(4), 733-762.

Briseño-Avena, C., Schmid M. S., Swieca K., Sponaugle S., Brodeur, R.D. and Cowen, R. K. (2020). Three-dimensional cross-shelf zooplankton distributions off the Central Oregon Coast during anomalous oceanographic conditions. *Prog. Oceanogr.* **188**, 102436

Brodeur, R. D. and Pearcy, W. G. (1992) Effects of environmental variability on trophic interactions and food web structure in a pelagic upwelling ecosystem. *Mar. Ecol. Progr. Ser.*, **84**, 101–119.

Buecher, E. and Gibbons, M.J. (2003). Observations on the diel vertical distribution of hydromedusae in the Southern Benguela. *Afr. J. Mar. Sci.*, **25**, 231-238

Canino, M. F. and Grant, G. C. (1985) The feeding and diet of *Sagitta tenuis* (Chaetognatha) in the Lower Chesapeake Bay. *J Plankton Res*, **7**, 175–188.

Colin, S. P., Costello, J. H., Graham, W. M., and Higgins, J. I. (2005) Omnivory by the small cosmopolitan hydromedusa *Aglaura hemistoma*. *Limnol. Oceanogr.*, **50**, 1264–1268.

Corrales-Ugalde, M. and Sutherland, K. R. (2021) Fluid mechanics of feeding determine the trophic niche of the hydromedusa *Clytia gregaria. Limnol. Oceanogr.*, **66**, 939–953.

Costello, J. H. and Colin, S. P. (2002) Prey resource use by coexistent hydromedusae from Friday Harbor, Washington. *Limnol. Oceanogr.*, **47**, 934–942.

Costello, J. H., Colin, S. P., and Dabiri, J. O. (2008) Medusan morphospace: phylogenetic constraints, biomechanical solutions, and ecological consequences. *Invert. Biol.*, **127**, 265–290.

Daan, R. (1989) Factors controlling the summer development of copepod populations in the southern bight of the North Sea. *Neth. Jour. Sea Res.*, **23**, 305–322.

Delignette-Muller, M.L., and Dutang, C. (2015). "fitdistrplus": an R package for fitting distributions. *J. Stat. Soft.* **64**(4), 1-34.

Dorman, J., Bollens, S., and Slaughter, A. (2005) Population biology of euphausiids off northern California and effects of short time-scale wind events on *Euphausia pacifica*. *Mar. Ecol. Prog. Ser.*, **288**, 183–198.

Francis, T. B., Scheuerell, M. D., Brodeur, R. D., Levin, P. S., Ruzicka, J. J., Tolimieri, N., and Peterson, W. T. (2012) Climate shifts the interaction web of a marine plankton community. *Glob. Change Biol.*, **18**, 2498–2508.

Gadomski D.M., and Boehlert G.W. (1984). Feeding ecology of pelagic larvae of English sole *Parophrys vetulus* and butter sole *Isopsetta isolepis* off the Oregon coast. *Mar. Ecol. Prog. Ser.* **21**, 1-12.

Guigand, C. M., Cowen, R. K., Llopiz, J. K., and Richardson, D. E. (2005) A Coupled Asymmetrical Multiple Opening Closing Net with Environmental Sampling System. *Mar Technol. Soc. J.*, **39**, 22–24.

Hansson, L. J. and Kiørboe, T. (2006) Prey-specific encounter rates and handling efficiencies as causes of prey selectivity in ambush-feeding hydromedusae. *Limnol. Oceanogr.*, **51**, 1849–1858.

Hansson, L., Moeslund, O., Kiørboe, T., and Riisgård, H. (2005) Clearance rates of jellyfish and their potential predation impact on zooplankton and fish larvae in a neritic ecosystem (Limfjorden, Denmark). *Mar. Ecol. Prog. Ser.*, **304**, 117–131.

Hays, G. C., Doyle, T. K., and Houghton, J. D. R. (2018) A Paradigm Shift in the Trophic Importance of Jellyfish? *Trends Ecol. Evol.*, **33**, 874–884.

Hipfner, J.M., and Galbraith, M. (2014). Diet of the Pacific Sand Lance (*Ammodytes hexapterus*) in the Salish Sea, British Columbia, in the 1960s. *Can. Field. Nat.* **128**(1), 1-6

Hooff, R. C. and Peterson, W. T. (2006) Copepod biodiversity as an indicator of changes in ocean and climate conditions of the northern California Current ecosystem. *Limnol. Oceanogr.*, **51**, 2607–2620.

Hosia, A. and Båmstedt, U. (2007) Seasonal changes in the gelatinous zooplankton community and hydromedusa abundances in Korsfjord and Fanafjord, western Norway. *Mar. Ecol. Prog. Ser.*, **351**, 113–127.

Kiørboe, T., Møhlenberg, F., and Hamburger, K. (1985) Bioenergetics of the planktonic copepod *Acartia tonsa*: relation between feeding, egg production and respiration, and composition of specific dynamic action. *Mar. Ecol. Prog. Ser.*, **26**, 85–97.

Larson, R.J. (1986). Seasonal changes in the standing stocks, growth rates, and production rates of gelatinous predators in Saanich Inlet, British Columbia. *Mar. Ecol. Prog. Ser.* **33**, **89-98**

Larson, R. J. (1987) Trophic ecology of planktonic gelatinous predators in Saanich Inlet, British Columbia: diets and prey selection. *J Plankton Res*, **9**, 811–820.

Luo, J.Y., Condon, R.H., Stock, C.A., Duarte, C.M., Lucas, C.H., Pitt, K.A. and Cowen, R.K. (2020). Gelatinous zooplankton-mediated carbon flows in the global oceans: a data-driven modeling study. *Global Biogeochem. Cyles.* **34**,

Luo, J., Grassian, B., Tang, D., Irisson, J., Greer, A., Guigand, C., McClatchie, S., and Cowen, R. (2014) Environmental drivers of the fine-scale distribution of a gelatinous zooplankton community across a mesoscale front. *Mar. Ecol. Prog. Ser.*, **510**, 129–149.

Marques, F., Chainho, P., Costa, J. L., Domingos, I., and Angélico, M. M. (2015) Abundance, seasonal patterns and diet of the non-native jellyfish *Blackfordia virginica* in a Portuguese estuary. *Estuar. Coast. Shelf Sci.*, **167**, 212–219.

Martinussen, M.B., and Bamstedt, U. 2001. Digestion rate in relation to temperature of two gelatinous planktonic predators. *Sarsia,* 86: 21-35.

Matsakis, S. and Conover, R. J. (1991) Abundance and Feeding of Medusae and their Potential Impact as Predators on Other Zooplankton in Bedford Basin (Nova Scotia, Canada) during Spring. *Can. J. Fish. Aquat. Sci.*, **48**, 1419–1430.

Miglietta, M. P., Rossi, M., and Collin, R. (2008) Hydromedusa blooms and upwelling events in the Bay of Panama, Tropical East Pacific. *Jour. Plank. Res.*, **30**, 783–793.

Miller, T., Brodeur, R., Rau, G., and Omori, K. (2010) Prey dominance shapes trophic structure of the northern California Current pelagic food web: evidence from stable isotopes and diet analysis. *Mar. Ecol. Prog. Ser.*, **420**, 15–26.

Mills, C. E. (1981). Diversity of swimming behaviors in hydromedusae as related to feeding and utilization of space. *Mar. Biol.* **64**, 185-189.

Morais, P., Dias, E., Cruz, J., Chainho, P., Angélico, M. M., Costa, J. L., Barbosa, A. B., and Teodósio, M. A. (2017) Allochthonous-derived organic matter subsidizes the food sources of estuarine jellyfish. *Jour. Plank. Res.*, **39**, 870–877.

Mullin, M. M. (1991) Production of eggs by the copepod *Calanus pacificus* in the southern California sector of the California Current System. *CALCOFI Rep.* **32**, 65-90.

Oksanen,J., Blanchet, F.G.,Friendly, M., Kindt, R., Legendre, P., McGlinn, D., Minchin, P.R., O'Hara, R. B., Simpson, G.L., Solymos, P., Stevens, M.H.H., Szoecs, E., and Wagner, H. (2020). “vegan”: Community Ecology Package. R package version 2.5-7.

Pearre, S. (1982). Estimating prey preference by predators: uses of various indices, and a proposal of another based on χ^2. *Can. J. Fish. Aquat. Sci.*, **39**, 914-923

Peterson, W. T. and Miller, C. B. (1977) Seasonal cycle of zooplankton abundance and species composition along the central Oregon coast. *Fish. Bull.* **75**(4):717-724

Peterson, W. T., Miller, C. B. and Hutchinson A. (1979) Zonation and maintenance of copepod populations in the Oregon upwelling zone. *Deep Sea Res.* **26A**, 467-494

Pitt, K. A., Duarte, C. M., Lucas, C. H., Sutherland, K. R., Condon, R. H., Mianzan, H., Purcell, J. E., Robinson, K. L., and Uye, S.-I. (2013) Jellyfish Body Plans Provide Allometric Advantages beyond Low Carbon Content. *PLoS ONE*, **8**, e72683.

Postel, L., Fock, H. and Hagen, W. (2000). Abundance and biomass. In Harris, R.P., Wiebe, P Lenz, J., Skjoldal H.R., and Huntdley, M. (eds). Zooplankton Methodology Manual. ICES. Academic Press. pp.83-192.

Purcell, J. E. and Mills (1988) The correlation between nematocyst types and diets in pelagic hydrozoa. In Hessinger, D. A. and Lenhoff, H. M. *The biology of nematocysts*. Academic Press, pp. 463–485.

Purcell, J. E., Siferd, T. D., and Marliave, J. B. (1987) Vulnerability of larval herring (*Clupea harengus pallasi*) to capture by the jellyfish *Aequorea victoria*. *Mar. Biol.*, **94**, 157–162.

Purcell, J. and Grover, J. (1990) Predation and food limitation as causes of mortality in larval herring at a spawning ground in British Columbia. *Mar. Ecol. Prog. Ser.*, **59**, 55–61.

Rackowski, J.P., and Pikitch, E.K. (1989). Species profiles: life histories and environmental requirements of coastal fishes and invertebrates (Pacific Southwest). Pacific and Speckled sanddabs. *U.S. Fish Wildl. Serv. Biol. Rep.* **82**(11.107). U.S. Army Corps of Engineers, TR EL-82-4 (18 pp).

Regula, C., Colin, S., Costello, J., and Kordula, H. (2009) Prey selection mechanism of ambush-foraging hydromedusae. *Mar. Ecol. Prog. Ser.*, **374**, 135–144.

Rodriguez, C. S., Marques A. C., Mianzan, H.W., Tronolone, V. B., Migotto, A. E. and Genzano, G. N. (2017). Environment and life cycles influence distribution patterns of hydromedusae in austral South America. *Mar. Biol. Res.* **13**(3), 659-670

Runge, C.A. (1984). Egg production of the marine, planktonic copepod *Calanus pacificus* Brodsky: laboratory observations. *J. Exp. Mar. Biol. Ecol.* **74,** 53-66.

Ruzicka, J. J., Brodeur, R. D., Emmett, R. L., Steele, J. H., Zamon, J. E., Morgan, C. A., Thomas, A. C., and Wainwright, T. C. (2012) Interannual variability in the Northern California Current food web structure: Changes in energy flow pathways and the role of forage fish, euphausiids, and jellyfish. *Prog. Oceanogr.*, **102**, 19–41.

Sabatini, M. and Kiørboe, T. (1994) Egg production, growth and development of the cyclopoid copepod *Oithona similis*. *J Plankton Res*, **16**, 1329–1351.

Schmitt, P.D. (1986). Prey size selectivity and feeding rate of larvae of the Northern Anchovy, *Engraulis mordax* Girard. *CALCOFI Rep.* **27,** 153-160

Smith, S. E. and Adams, P. B. (1988) Daytime surface swarms of *Thysanoessa spinifiera* (Euphausiacea) in the Gulf of Farallones, California. *Bull. Mar. Sci.* **42**(1), 76-84

Suchman, C., Daly, E., Keister, J., Peterson, W., and Brodeur, R. (2008) Feeding patterns and predation potential of scyphomedusae in a highly productive upwelling region. *Mar. Ecol. Prog. Ser.*, **358**, 161–172.

Suchman, C. L., Brodeur, R. D., Daly, E. A., and Emmett, R. L. (2012) Large medusae in surface waters of the Northern California Current: variability in relation to environmental conditions. *Hydrobiologia*, **690**, 113–125.

Sullivan, B. K., Suchman, C. L., and Costello, J. H. (1997) Mechanics of prey selection by ephyrae of the scyphomedusa *Aurelia aurita*. *Mar. Biol.*, **130**, 213–222.

Swieca, K., Sponaugle, S., Briseño-Avena, C., Schmid, M., Brodeur, R., and Cowen, R. (2020) Changing with the tides: fine-scale larval fish prey availability and predation pressure near a tidally modulated river plume. *Mar. Ecol. Prog. Ser.*, **650**, 217–238.

Thompson, A.R., Kahru M., Goericke R., Weber, E.D., Watson, W., Schroeder I. D., Bograd S. J., Hazen E. L. et al. (2019). State of the California Current 2018-2019: a novel anchovy regime and a new marine heatwave? *CalCOFI Rep.* **60**, 1-65.

Trudel, M., Tucker, S., Morris, J. F. T., Higgs, D. A., and Welch, D. W. (2005) Indicators of Energetic Status in Juvenile Coho Salmon and Chinook Salmon. *N. Am. J. Fish. Manag.*, **25**, 374–390.

Zeman, S. M., Brodeur, R. D., Daly, E. A., and Sutherland, K. R. (2016) Prey selection patterns of *Chrysaora fuscescens* in the northern California Current. *J. Plankton Res.* **38(6),**1433-1443

Zeman, S. M., Corrales-Ugalde, M., Brodeur, R. D., and Sutherland, K. R. (2018) Trophic ecology of the neustonic cnidarian *Velella velella* in the northern California Current during an extensive bloom year: insights from gut contents and stable isotope analysis. *Mar Biol*, **165**, 150.